# THE INFLUENCE OF HYDROGEN GAS EXPOSURE AND LOW TEMPERATURE ON THE TRIBOLOGICAL CHARACTERISTICS OF TI-6AL-4V

A Thesis

by

RYAN TRAVIS GOLA

Submitted to the Office of Graduate Studies of
Texas A&M University
in partial fulfillment of the requirements for the degree of

MASTER OF SCIENCE

December 2008

Major Subject: Mechanical Engineering

# THE INFLUENCE OF HYDROGEN GAS EXPOSURE AND LOW TEMPERATURE ON THE TRIBOLOGICAL CHARACTERISTICS OF TI-6AL-4V

A Thesis

by

RYAN TRAVIS GOLA

Submitted to the Office of Graduate Studies of
Texas A&M University
in partial fulfillment of the requirements for the degree of

MASTER OF SCIENCE

Approved by:

| | |
|---|---|
| Chair of Committee, | Hong Liang |
| Committee Members, | William Schneider |
| | Xinghang Zhang |
| Head of Department, | Dennis O'Neal |

December 2008

Major Subject: Mechanical Engineering

# ABSTRACT

The Influence of Hydrogen Gas Exposure and Low Temperature on the Tribological Characteristics of Ti-6Al-4V. (December 2008)

Ryan Travis Gola, B.S., Texas A&M University

Chair of Advisory Committee: Dr. Hong Liang

This research studies individual and combined effects of hydrogen gas exposure and low temperature on the tribological characteristics of Ti-6Al-4V. Experimental approaches include test system modification and tribological analysis. An existing ball-on-disk tribometer was modified to allow liquid nitrogen to be constantly injected into an insulated test chamber to enable testing at low temperature. Twelve 3.8 cm diameter Ti-6Al-4V disks were manufactured and polished, then half were exposed to pure hydrogen gas at elevated temperature and pressure and the remaining disks were untreated. The testing was split in to four groups of three disks based on testing temperature and previous hydrogen exposure. A silicon nitride ball was used for all tests. Each group was tested at two normal loads, 10N and 20N, at the same linear speed. Group 1 was unexposed and tested at room temperature, Group 2 was unexposed and tested at low temperature, Group 3 was exposed and tested at room temperature and Group 4 was exposed and tested at low temperature. Average friction coefficients and the specific wear rate were calculated from the test data. Also high-resolution digital microscope imaging was used to observe and characterize the wear mechanisms of the

four groups of samples. Results show that hydrogen exposure facilitated adhesive wear of the surface and that low temperature induced a slip-stick wear mechanism under higher loads, but not at lower loads and regardless of exposure to hydrogen gas. This research opens avenues for future investigation in effects of hydrogen and low temperature embrittlement on the tribological performance of materials. With the increasing interests in hydrogen energy, the present work established a foundation for future study.

# DEDICATION

This thesis is dedicated to my incredible wife, Christina, and to my parents, Joseph and Dorothy Gola.

## ACKNOWLEDGEMENTS

I would like to express my deep appreciation and thanks to the members of my degree committee and the Liang Research Group. I especially thank Ke Wang, Rodrigo Cooper and Grant Fox for their extensive help throughout my research. I also owe Jason Caswell a whole lot more than he will ever know for all of his electrical expertise, time, patience and hard work.

I appreciate the opportunity that Dr. Liang has given me to tailor my research to some of my own interests and I thank her for sharing her insight and perspective in our discussions and for her understanding when there were setbacks and for her encouragement throughout my research. This research was in part sponsored by the National Science Foundation (0535578), the Texas Engineering Experiment Station, and the Department of Mechanical Engineering, Texas A&M University.

I thank my parents for their support throughout all of my life and for setting fantastic examples for me to follow. I thank my mom for teaching me the value of education, encouraging me to explore the world and showing me how to have a sense of adventure, even as an adult. I thank my dad for instilling in me his expectation of hard work and passing along his sage advice while letting me find my own path.

I especially thank my wife, Christina, for her love and unwavering support of my decision to pursue my master's degree. She has been a constant source of encouragement and is the best editor and research resource I could ever ask for. I could not have done any of this without you.

# NOMENCLATURE

| | |
|---|---|
| ASTM | American Society of Testing and Materials |
| BCC | Body Center Cubic |
| C | Celcius |
| cm | Centimeters |
| EHE | Environmental Hydrogen Embrittlement |
| FCC | Face Center Cubic |
| FCT | Face Center Tetragonal |
| $H_2$ | Hydrogen Gas |
| HCP | Hexagonal Close Packed |
| HRE | Hydrogen Reaction Embrittlement |
| IHE | Internal Hydrogen Embrittlement |
| $LH_2$ | Liquid Hydrogen |
| $LN_2$ | Liquid Nitrogen |
| m | Meters |
| m/s | Meters per Second |
| N | Newtons |
| psi | Pounds per Square Inch |
| PTFE | Poly(tetrafluoroethene) |
| RPM | Revolutions per Minute |
| μm | Micrometers |

# TABLE OF CONTENTS

Page

CHAPTER Page

# LIST OF FIGURES

Page

Page

Page

Page

Page

Page

Page

# LIST OF TABLES

Page

# CHAPTER I

# INTRODUCTION

This chapter provides an overview of the current state of tribological testing and current understanding of hydrogen and low temperature effects on material properties. The chapter serves as the background in order to understand the nature of the research.

## 1.1. Thesis Overview

This thesis contains seven chapters. Chapter I provides an overall view of the work and establishes the current state of related research. Chapter II discusses the social and technological factors creating the need for research and states the specific objectives for this research. Chapter III discusses tribotesting in general and analysis techniques, while Chapter IV states specifically the procedures used for the testing conducted during this research. The results are presented in Chapter V and discussed in Chapter VI. Chapter VII presents the major conclusions and Chapter VIII discusses future applications for this research.

## 1.2. Literature Review

Tribology is presently far from an exact science. Although friction and wear are often mentioned and studied together they are not directly linked.[1] The key to predicting a material's wear and frictional response is to understand how numerous variables collectively interact.[2] A material's tribological characteristics are the result of the set of variables present at the surface during frictional contact.[2-4] This collection of variables is called a tribosystem. Variables such as hardness, normal load, surface roughness,

---

This thesis follows the style of *Journal of Applied Physics*.

ambient chemical environment, films and foreign particles on the surfaces, temperature and temperature gradients and others compose a tribosystem.[2-5] Because tribosystems have many variables, the combinations and test results are often difficult to replicate. Bayer emphasizes this in *Mechanical Wear Fundamentals and Testing*, stating that frequently intralaboratory results vary by 20% and interlaboratory results vary by 40% while following the procedures and techniques of the ASTM standards.[4] Even though the exact tribological behavior cannot always be predicted with great precision, general trends can be established. The design and focus of this research was based on previous work studying the effects of low temperature on material properties, the effects of hydrogen on material properties, the effect of low temperature on wear and friction properties, and the effect of liquid hydrogen on wear and friction properties. Also, this research was guided by the absence of information about wear and friction of materials after exposure to hydrogen gas.

### 1.2.1. Temperature Effects on Mechanical Properties

Many studies have documented the changes that low temperatures induce in metallic materials' mechanical and physical properties. The fundamental changes in metals that are typically noted with decreasing temperatures are an increase in hardness, modulus of elasticity, yield strength and ultimate tensile strength, and a decrease in the ductility and toughness.[6] Atomic thermal vibrations decrease with decreasing temperatures, reducing the internal energy of a material and decreasing the average atomic spacing; therefore, increasing the density of atoms and increasing the modulus of elasticity. This decrease in atomic thermal vibrations also hinders dislocation motion.[6]

Therefore, a material's ductility decreases while the yield and ultimate tensile strengths generally increase. When dislocation motion is impeded in a material and stress is applied, the force is transferred primarily to atomic bonds. If the force exerted on a bond exceeds the atomic bond strength, the bond will break, transferring the force to adjacent bonds. When the adjacent bonds break and the process repeats itself this behavior can be represented on the macroscale as crack formation and propagation and described as a decrease in ductility.

### 1.2.2. Low Temperature Tribological Testing

There are several studies regarding low temperature tribological characteristics, however they primarily study austenitic and stainless steels[7-9], polymers[10,11], lubricants[12,13] and coatings[14,15] which have traditionally been used in cryogenic applications and for cryogenic machining.[16-18] In one of the earliest studies, Bisson states that cryogenic environments, more than any other, are sensitive to friction damage.[19] The possible reasons given were that commonly used low-temperature materials had poor tribological properties, cold welding leading to adhesive wear was seen often, liquid lubricants were unusable in cryogenic environments and some solid lubricants, such as graphite, failed to lubricate in inert environments.[19] Metallic materials typically show a direct decrease in the friction coefficient with a decrease in temperature.[9,18,20-22] However, the wear response often does not correlate with a temperature decrease. Low-temperature friction and wear data for other groups of materials, such as ceramics, have been studied where temperature had little effect on the tribological characteristics. Tobler reported that the static friction coefficient for fire-polished Pyrex glass is

relatively constant at about 0.23 for temperatures between 77 and 300 K.[1] Diamond-like carbon films under cryogenic temperatures were reported by Ostrovskaya et al.[14] A quasi-amorphous structured DLC was studied in this report. The tribological study was conducted in $LN_2$ with a pin-on-disk apparatus. DLC was coated on a steel 45 disk or bearing ball of 4 mm diameter containing 15% chromium. The thickness of the DLC coating was 1-2 μm and the polycrystalline formations were from 10 nm to several micrometers. Friction and wear tests were conducted on DLC coated pin and disk at temperature 77 K at a speed of 0.06 m/s, with a Hertzian pressure of 2.3 GPa. Results showed that the friction and wear rate depend on the initial roughness of the DLC disk rather than temperature.[14]

Often the wear response is heavily influenced by the material tested, the chemical environment during testing, and the test parameters including normal load, speed and duration.[9,20,22,23] These factors all contribute to the amount of work hardening, frictional heating, rate of cooling during testing, and phase changes due to temperature and pressure that can have significant effects on the wear response.[8,22]

Machining can be viewed as a magnified process of the abrasive wear of large surface asperities. Therefore, machining is an effective method to evaluate the abrasive behavior associated with embrittlement of a work piece. Hong et al. performed cutting experiments conducted at speeds ranging from 2 to 5 m/s for AISI 1018 and 0.5 to 1.5 m/s for Ti-6Al-4V. These conditions are used in conventional turning operations. When tested in $LN_2$, the friction coefficient was lower than in dry air, room temperature conditions. Both AISI 1018 and Ti-6Al-4V show increased brittleness at low

temperatures. The cold strengthening of the titanium alloy increased the cutting force in cryogenic machining, but lower friction reduced the feed force.[17,18] In cryogenic temperature, the material becomes brittle, so the work piece is less deformed, resulting in a dull angle. Aside from the increased brittleness, the reduced interface temperature in cryogenic conditions reduces the adhesion between the cutting tool and the chip, resulting in low friction force, better product finish and increased tool life.[17]

The wear properties of titanium alloys have been studied at room and low temperatures. Low temperature testing under vacuum conditions have shown an increase in wear rate with an increase in sliding speed at low temperature due to the formation of secondary structures and surface hardening as a result of frictional heating and rapid cooling during testing.[22] A study by Bozet compared wear of Ti-6Al-4V against PCTFE in air, argon gas and liquid nitrogen, showed tribochemcial and abrasive wear due to interactions between chlorine, fluorine, titanium and aluminum.[10] Research by Molinari et al. showed an increase in wear rate with an increase in load at room temperature in air due to oxidative and delamination wear as a result of softening due to frictional heating.[24] Nevertheless, studies have not been conducted that test the influence of load, temperature and hydrogen exposure on Ti-6Al-4V in a comparable chemical environment and pressure.

### 1.2.3. Hydrogen Exposure Effects on Mechanical Properties

Hydrogen can embrittle a material in three primary methods. The first is Internal Hydrogen Embrittlement (IHE) in which hydrogen already present in the material, typically from processing, diffuses and resides in interstitial sites. When hydrogen

concentrations are high enough, the material will form microcracks, which can propagate in the material to the surface; therefore, IHE is often associated with delayed failure. Internal Hydrogen Embrittlement does not require external stresses to form microcracks, propagation can be the result of residual stresses in the material from processing.[25] The second method is Environmental Hydrogen Embrittlement (EHE) where hydrogen in the environment around the material diffuses into the material's microstructure while under stress.[25] The hydrogen atoms diffuse into the areas of highest local stress and impede dislocation motion and reduce the cohesive force of the material at that location.[26] This pinning effect can then lead to crack formation. The third method is Hydrogen Reaction Embrittlement (HRE) where external hydrogen diffuses into the surface layer and reacts with the components of the bulk material lattice forming a hydride or in some cases a gas.[27] The formation of a hydride changes the amount of strain in the lattice, altering the mechanical properties. The result of these property changes is a decrease in ductility. The formation of a gas can lead to the formation of blisters which can propagate to form cracks.[26]

Aside from embrittlement, hydrogen can have other effects on mechanical properties and material performance. Yashiro et al. studied the effects of hydrogen permeation by electrochemical techniques on pitting in stainless steels and showed an increase susceptibility with hydrogen permeation.[28] Jiang et al. studied the negative effects of hydrogen on the wear resistance of titanium in a corrosive media.[29]

### 1.2.4. Titanium Hydrogen Adsorption

In general, hydrogen embrittlement decreases ductility and increases crack extension rates resulting in a decrease in toughness.[25] In titanium and titanium alloys, including Ti-6Al-4V, hydrogen embrittlement results from the formation of brittle hydride phases.[25,30] A reduction in hardness has also been shown to correlate with an increase with hydrogen concentration in Ti-6Al-4V.[31] The research in this thesis focuses on Ti-6Al-4V, a duplex α and β phase alloy where β phase grains are dispersed in a α phase matrix. The α phase has a hexagonal close packed (hcp) crystal structure and the β phase has a body centered cubic (bcc) crystal structure. Hydrogen can be absorbed by both the α and β phase and form a solid solution that results in the expansion of their respective lattices. However, hydrogen does not absorb into each phase equally. Hydrogen will absorb into the β phase at a faster rate due to the bcc crystal structure's open nature allowing hydrogen to more readily diffuse into interstitial sites.[32] Since diffusion into the β phase is easier it effectively absorbs more hydrogen. Since there is more hydrogen in the β phase there is a reaction between the two phases at the boundary; when enough hydrogen is present, cracks typically form at the phase boundary and in the α phase.[32] In titanium there are three types of hydrides ($TiH_x$) that can form: ε, δ and γ. The ε hydride has a face center tetragonal (fct) crystal structure and at higher concentrations of titanium where x is greater than or equal to 1.99. The δ hydride has a face center cubic (fcc) crystal structure and forms when moderate concentrations of hydrogen are present in titanium, where x is between 1.5 and 1.99. The γ hydride has an fct crystal structure and forms at lower concentrations of hydrogen, between 1-3 atomic

percent.[32] Hydrogen can be introduced into a material during processing, by electrochemical methods and by direct exposure to hydrogen gas or liquid. By exposing Ti-6Al-4V to hydrogen gas of various concentrations, temperatures, pressures and hold times, hydrogen will diffuse into the surface in various concentrations depending on the particular exposure variables.[30,33] Hydrogen gas exposure can also produce $TiH_2$ hydrides to the point where visible surface cracks form. Concentrations of hydrogen lower than that required to form hydrides may cause failure when diffused in to a material.[30]

### 1.2.5. Low Temperature and Hydrogen Exposure Effects on Mechanical Properties

Several studies have been performed on austenitic and stainless steels at low temperatures during or after hydrogen exposure. For Cr-Ni-MnN austenitic steels exposed to high-pressure hydrogen gas then tested at various low temperatures, Ma et al. reported an increase in yield and ultimate tensile strengths, a decrease in ductility and fracture toughness. Some reduction in toughness at temperatures below the martensite start temperature was attributed to formation of strain induced martensite.[34] Ogata tensile tested special stainless steel specimens at various low temperatures with high-pressure hydrogen gas trapped in a bore in the specimens during testing. This testing showed little dependence of hydrogen exposure on the yield and ultimate tensile strengths. However his study found that the amount of embrittlement, and a corresponding decrease in the reduction of area and elongation, was dependent on the amount of strain-induced martensite formed at certain low temperature ranges.[35]

### 1.2.6. Tribological Testing of Materials Exposed to Hydrogen at Low Temperature

The effects of hydrogen on the deterioration of austenitic steels during wear at cryogenic temperatures were reported by Pinto et al.[36] Wear tests were conducted on a ball-on-disk sliding tribometer, at 20K temperature and 20MPa pressure. The normal force was 5 and 10 N, with sliding speeds of 0.06 and 0.2 m/s, and sliding distance of 1000 m. The ball was made of aluminum oxide and the disk was austenitic steel. In a hydrogen environment, embrittlement was found. The researchers concluded that material chemical composition has a large effect on wear resistance at low temperature and exposure to liquid hydrogen did induce surface cracking, but did not appear to affect the wear resistance when compared to testing performed in inert chemical environments.[36] Pinto et al. also found that N (nitrogen) in austenitic steels enhanced the stability of the austenitic microstructure and the wear performance at cryogenic temperatures. High N-content, particularly in CrMn steels, induced a ductile to brittle transition in the top surface layer at extremely low temperatures. However, the increased hardness resulted in the improved wear resistance, providing a path to reduce the potential damage of the hydrogen embrittlement. Although stacking fault energies decreased and twinning was encouraged at low temperature, the material wear pattern did not appear affected.

# CHAPTER II

# MOTIVATION AND OBJECTIVES

This chapter describes the current social and technological factors that create the need for this research. The purpose and specific objectives for this research is stated to understand the role that this research will play in application to designs and as a basis for future research.

## 2.1. Hydrogen Energy and Future Products

A transition from an economy that creates its energy from hydrocarbons, including petroleum, coal and natural gas to one that is based on hydrogen, including liquid hydrogen ($LH_2$) and hydrogen gas ($H_2$), has garnered enormous attention in recent years.[37] A hydrogen economy would use hydrogen as fuel for transportation and energy for industries, businesses and homes. The push for a hydrogen economy has been spurred most recently by increased awareness of global climate change and rising energy prices. The purpose of the transition is to establish a reliable energy source that reduces environmental impact and is separated from geo-political issues that can cause fluctuations in energy availability and prices. In recent years, several automakers proved the viability of hydrogen technology by creating prototypes of vehicles powered by hydrogen fuel cells and hydrogen fueled internal combustion engines.[37] These advances, among others, have also given greater attention to developing a feasible infrastructure to supply liquid hydrogen or hydrogen gas safely and reliably, comparable to the existing hydrocarbon infrastructure. One consistent concern in the discussion of hydrogen use is hydrogen embrittlement of storage vessels, pipelines and hydrogen controlling

components. If materials become embrittled from contact with hydrogen they may pose safety risks for the public and functional problems for distributing energy reliably. Therefore, engineers and scientists need a solid understanding of how materials will behave after exposure to hydrogen to ensure the safety and reliability of a new energy system.

In addition to hydrogen embrittlement, extreme low temperatures resulting from the use of liquid hydrogen also present challenges in the design of hydrogen systems. The use of liquid hydrogen has been proposed to efficiently store and transport hydrogen due to the higher density of energy per unit of volume compared to hydrogen gas.[37] Liquid hydrogen vaporizes at -196°C; therefore, vessels, pipelines, valves and other contacting materials must be designed to perform below this temperature. Many materials' tribological properties are different at cryogenic temperatures than at room or elevated temperatures due to changes in microstructure and interatomic distances.[20] More research is needed to understand the influence of low temperatures on components that will be contacting hydrogen in a new hydrogen infrastructure.

The purpose of this research is to determine the influence of low temperature and hydrogen gas exposure on the tribological characteristics of Ti-6Al-4V. Titanium is often used instead of less expensive materials because of its unique combination of high yield and ultimate tensile strength, high corrosion resistance and low density. As the most common commercially available titanium alloy, Ti-6Al-4V is a good candidate for low density, high strength components that can be used in fuel-efficient vehicles and for hydrogen storage and transportation. Titanium is also susceptible to hydrogen

embrittlement, which may affect how titanium components perform after exposure to hydrogen. To better understand how hydrogen gas exposure affects the friction and wear characteristics of Ti-6Al-4V a series of tribological tests were performed on exposed and unexposed commercially available Ti-6Al-4V samples at various loads and at room and low temperatures.

# CHAPTER III

# TRIBOLOGICAL TESTING THEORY

This chapter presents a general understanding of tribological testing and the methods to analyze wear and friction.

## 3.1. Tribological Testing

Tribology is the study of wear and friction resulting from relative motion of contacting bodies.[3] The goal of most tribological testing is to determine values for frictional forces, the amount of wear and the wear mechanism. In order to fully understand the friction and wear values, the parameters used to describe friction and wear must be clearly understood. A clear understanding of the parameters is critical when comparing values from different studies and testing methods.

## 3.2. Friction Parameters

The amount of friction resulting from the contact is typically quantified by the coefficient of friction, $\mu$. This value is dimensionless and is calculated, as shown, by dividing the tangential force, $F_T$, by the normal force, $F_N$, measured during the frictional contact.

$$\mu = F_T / F_N$$

Often, under the same normal force, there is a larger coefficient of friction during the initial period of contact then after a certain period the coefficient of friction reduces

to a steady lower value.[2] The period during which a higher coefficient of friction is found is called the run-in period. The lower coefficient of friction value observed after the run-in period is called the steady state coefficient of friction. The coefficient of friction can be reported in two ways, the average friction coefficient or the steady state friction coefficient. The average friction coefficient includes the run-in period in its average calculation, while the steady state friction coefficient excludes the run-in period and only averages the values measured after steady state values are achieved. Friction coefficient values are best compared at steady state because average friction coefficient values can be artificially high if the value was determined from a shorter test.

### 3.3. Wear Parameters

Wear can be compared using several different parameters. One method is to measure wear in terms of volume or mass loss from one or both bodies in contact. Mass loss may be measured directly or calculated from a volume loss measurement divided by the material density. Volume loss, $V_{loss}$, can be calculated by measuring key parameters of the body and the wear scar or track and determining the amount of material lost through geometric relations.[38] Mass and volume loss parameters are best for comparing testing under identical conditions and variables. Another parameter is the wear rate, which is calculated by dividing the volume or mass loss by the total sliding distance, $d$. To enable comparisons between different test variables, a normalized parameter called the specific wear rate, $w_s$, is calculated as shown by dividing the volume loss by the product of the normal force and sliding distance.[2]

$$w_s = V_{loss} / (F_N d)$$

The specific wear rate takes the variables of normal force and sliding distance into account, making the parameter better to compare tests performed at different normal load and sliding distances when compared only to a value for volume loss or wear rate.

### 3.4. Wear Mechanisms

Wear is the damage to a material due to contact and relative motion to another substance.[4] The type and extent of damage can be due to several mechanisms in which materials typically wear. Wear mechanisms can be classified in several broader groups including: single cycle deformation, repeated cycle deformation, adhesion, abrasion, thermal, oxidation, and Tribofilm.[4]

Single cycle deformation defines a class of wear mechanisms that cause damage from a single contact, such as cracking or plastic deformation. Abrasion and adhesion can fall in this class in certain cases. Repeated cycle deformation is when the damage only occurs after repeated contact, such as fretting and fatigue failure.[4] Delamination and adhesion can be the result of repeated cycle deformation and can fall in this classification. Adhesive mechanisms are characterized by material transfer from one body to another. Typically adhesion is stronger for similar and soluble materials although dissimilar materials such as some metal-ceramic pairs also show adhesion.[2] Abrasion occurs when material is removed from one body by uneven surfaces or hard particles and the material removed does not adhere to the other body. Scratching and microcutting are common examples of abrasion.[4] Three body abrasion occurs when a

hard particle of a composition other than the two contacting bodies causes material removal.[4] Thermal wear occurs due to changes in the material due to frictional heating. High, localized temperatures at the contact points, called the flash temperature, can cause localized melting or phase changes. This type of wear can lead to softening, thermal cracking, and thermoelastic instability.[4] Oxidative wear consists of the removal and regeneration of an oxide layer between bodies. Often this process is also called corrosive or chemical wear and tends to reduce wear compared to situations where the oxide layers cannot form and other wear mechanisms dominate.[4] Tribofilm wear occurs when compacted wear debris or third body particles form a layer between the bodies. A transfer film or layer is a specific occurrence when the composition of the layer is the same as the body it is contacting.[4]

### 3.5. Hertzian Contact Pressure

Areas of high pressure develop at the point of contact between the ball and disk. The bearing area between the ball and disk is very small initially; leading to local areas of very high pressure due to the geometry of the contact where the ball contacts an initially flat disk. In this research, the ball was much harder than the disk therefore the disk deforms slightly to conform to the curvature of the ball. The change in the contact area due to this deformation can be calculated based on the mechanical properties of the two bodies. From the change in contact area, a relation between the geometry and material properties was developed by Hertz to calculate the maximum pressure under the point of contact, this pressure is called the Hertzian contact stress.[39] The maximum pressure, $P_{max}$, is determined by a relation between the normal load, $F$, and the radius of

the contact area, $a$, as shown. For a sphere-on-flat contact of bodies composed of different materials the radius of the contact area, $a$, is determined by the diameter of the sphere, $d$, and the elastic modulus, $E$, and Poisson's ratio, $v$, of each contacting body as shown.[39]

$$P_{max} = \frac{3F}{2\pi a^2}$$

$$a = \left[\frac{3Fd}{8}\left(\frac{1\text{-}v_1^2}{E_1} + \frac{1\text{-}v_2^2}{E_2}\right)\right]^{1/3}$$

### 3.6. Frictional Heating

Heat generated from frictional contact can cause local temperature rises that can affect the tribological response and in some instances are enough to alter the microstructure of the material.[2,4,22] A temperature rise due to frictional contact is called a flash temperature. Frictional heating is calculated by using the proper equation for the particular speed regime and is dependent on the contact geometry and velocity. The Peclet number, $L$, is a dimensionless parameter used to distinguish between the different regimes. The Peclet number is calculated from the product of the linear velocity, $V$, and the radius of contact, $a$, divided by two times the thermal diffusivity of the body analyzed, $D$. For circular contacts with a Peclet numbers between 0.1 and 5, the average temperature rise, $T_{fa}$, and the maximum flash temperature, $T_{fmax}$, are calculated as shown;

$k$ is the thermal conductivity, $\alpha$ and $\beta$ are constants that depend on the value of $L$, $\mu$ is the coefficient of friction, $a$ is the radius of contact area, $F$ is the normal force, $V$ is the linear velocity and $\sigma_y$ is the yield strength of the body analyzed.[2,40]

$$L = Va/2D$$

$$T_{f_a} = 0.25\alpha\frac{\mu FV}{ka}$$

$$T_{f_{max}} = 0.222\beta\frac{\mu V}{k}\left(\sigma_y F\right)^{1/2}$$

For wear conditions with Peclet numbers close to 0.1, the $\alpha$ coefficient is 0.85 and the $\beta$ coefficient is 0.95 in accordance with the methods used by Stachowiak in *Engineering Tribology.*[2]

# CHAPTER IV

# EXPERIMENTAL PROCEDURE

This chapter describes the materials and sample preparation for this research. The testing methods, testing machines and the test plan for this research are also described in detail.

## 4.1. Materials

The disks were manufactured from a commercially available duplex annealed Grade 5 Ti-6Al-4V rod purchased from McMaster-Carr. The two phases of the duplex titanium alloy are the α phase, which has a hexagonal close packed (hcp) crystal structure and the β phase, which has a body centered cubic (bcc) crystal structure. Table 1 lists the elements and composition of Ti-6Al-4V Grade 5 per ASTM standard B348 for titanium and titanium alloys.[41]

Table 1: Composition of Ti-6Al-4V Grade 5.

| Element | % Composition |
|---|---|
| Nitrogen, max | 0.05 |
| Carbon, max | 0.08 |
| Hydrogen, max | 0.015 |
| Iron, max | 0.40 |
| Oxygen, max | 0.20 |
| Aluminum | 5.50-6.75 |
| Vanadium | 3.50-4.50 |
| Residuals, each | 0.10 |
| Residuals, total | 0.40 |
| Titanium | Balance |

The balls tested are 6 mm diameter silicon nitride ($Si_3N_4$) ceramic ball bearings with a Grade 5 roundness purchased from VXB Bearing. The Grade 5 roundness means the spherical roundness is controlled and is assumed to be consistent for each ball used. Silicon nitride was selected because it has a very high hardness compared to the titanium alloy and will theoretically not wear during testing. Also with very stable thermal properties at low temperatures, the mechanical properties of silicon nitride will be assumed to be the same as at room temperature.

### 4.2. Sample Preparation

Hydrogen embrittlement is a known problem in many materials and, each material possess varying degree of susceptibility. In this research, the samples were treated to achieve a detectable amount of hydrogen in the sample, however not enough to form cracks or hydrates that would change the phase or alter the surface roughness of the samples. This allows any changes in results between hydrogen exposed and non-exposed samples to be directly compared without skewing the comparison due to surface feature differences or the effects of different phases. The exposure variables were selected based on hydrogen uptake and permeation information from ASTM standard G148[42] and procedures described in electrochemical testing in ASTM and ASM guidelines for corrosion testing.[43,44] In addition, information from studies of hydrogen adsorption and permeation was used as a basis to select the hydrogen exposure method and duration.[45-50]

Twelve samples were machined from the same Ti-6A-4V rod during a 4 hour time period. Care was taken to ensure sufficient machining fluid, and slow feed rates were used to prevent unintended localized heating of the sample to prevent any

thermally induced microstructure changes. A change in microstructure could potentially affect both hydrogen uptake and mechanical properties resulting in non-characteristic wear. The samples were polished on rotating polishing wheels using a four-step method for each sample. The as-machined surface was first polished with a 240 grit polishing pad, followed with a 400, 800, and 1200 grit pad, respectively, to obtain the final surface finish. After polishing, the samples were cleaned in an ultrasonic bath of acetone for 10 minutes to remove any remaining machining fluid or polishing debris. The samples were then wrapped in KimWipes to prevent exposure to air and to keep from touching any surfaces.

Following the machining and cleaning stage, the samples were divided into two groups, six samples in each group. The first group of six were sent to SET Laboratories in Houston, TX to be exposed to hydrogen. Dr. Saadine Tebbal at SET Laboratories performed the hydrogen exposure at elevated temperatures and pressure in a modified 5-gallon auto clave. The clean samples were secured to a PTFE coated rod running through the center holes and had PTFE coated spacers between each disk. In the autoclave PTFE coated netting was placed along the bottom and sides of the autoclave to prevent sample contact with the interior of the chamber to minimize surface contamination. The samples were placed in the PTFE netting lined autoclave and the chamber was sealed. Figure 1 shows a diagram of the autoclave and sample arrangement during the exposure process. Due to the explosive nature of hydrogen gas the autoclave was pressure tested with nitrogen gas prior to injecting and pressurizing hydrogen gas. To test the chamber the air was evacuated and pure nitrogen gas was pumped into the chamber to 2000 psi to

pressure test the chamber for 48 hours. After the 48-hour test period, the nitrogen was evacuated and pure hydrogen gas was pumped into the sealed chamber. For the hydrogenation stage, pure hydrogen gas was pressurized to 345 psi (1 MPa) and the temperature was elevated to 212° Fahrenheit (100° Celsius) and held for 24 hours. Table 2 lists the conditions during hydrogen exposure.

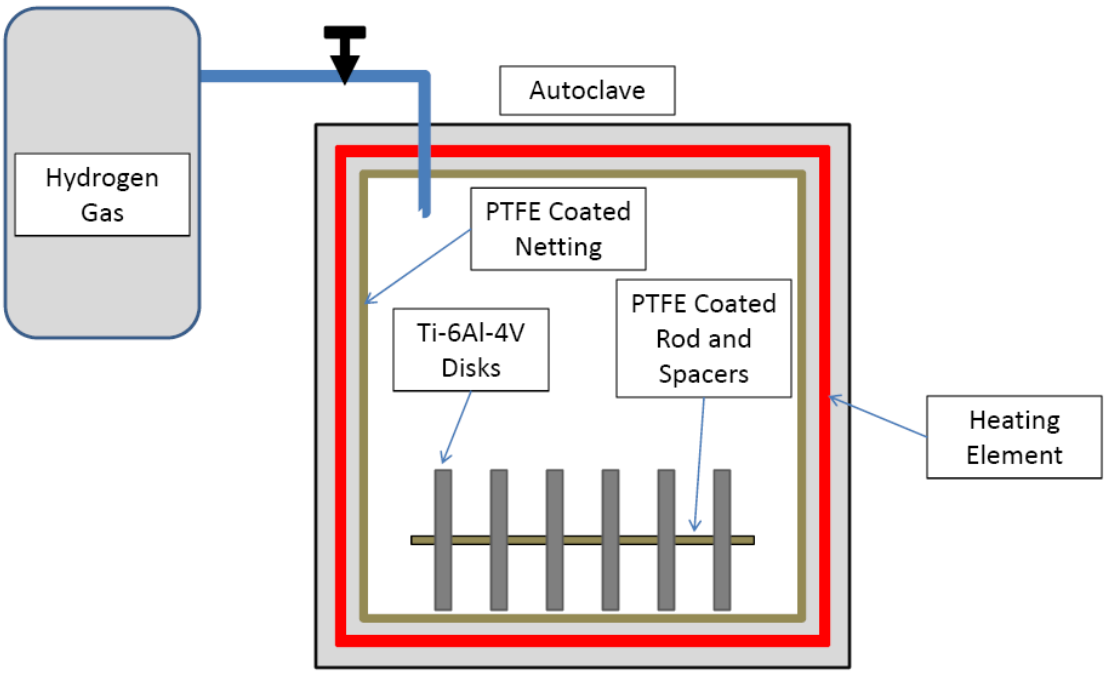


Figure 1: Hydrogen gas exposure system diagram.

Table 2: Hydrogen gas exposure conditions.

| Sample Type | Sample Size (cm) | Quantity | Temp (C) | Pressure (MPa) | Exposure Time (hrs) |
|---|---|---|---|---|---|
| Disk | 3.8 dia x 1.0 thick | 6 | 100 | 1 | 24 |

## 4.3. Testing Methods

### 4.3.1. Visual Surface Analysis and Imaging

Pre-test visual surface analysis was conducted to look for detectable differences between the hydrogen exposed and non-exposed samples. In addition, visual surface analysis was used after testing to examine the wear tracks on the disks and the wear scars on the balls. For this analysis, high-resolution digital imaging was conducted using a Keyence digital microscope, shown in Figure 2. The entire wear tracks of each test were examined and selected image were chosen to record features of interest or show typical wear patterns. Magnification up to 1000 times was used in the surface analysis.

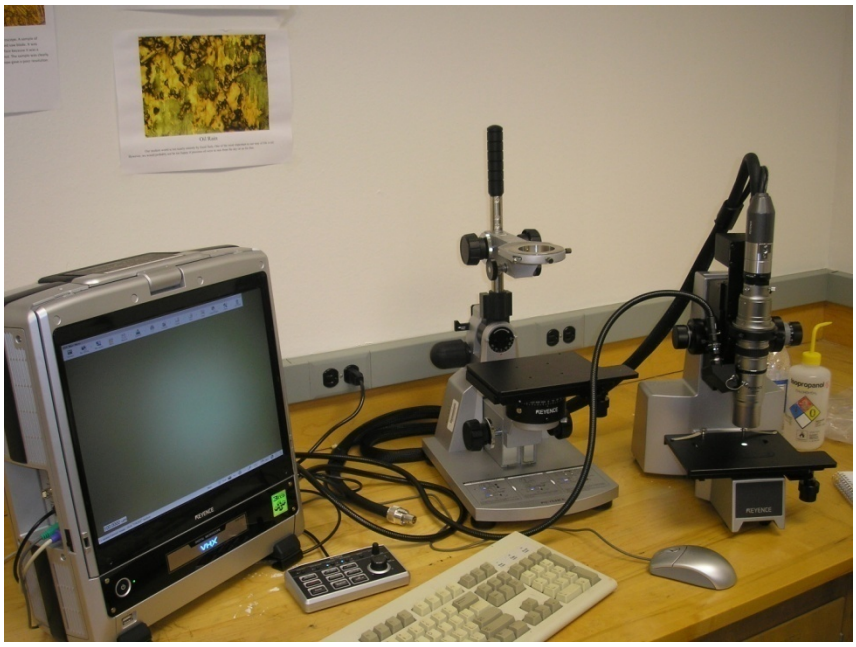

Figure 2: Keyence digital optical microscope.

### 4.3.2. X-Ray Diffraction Analysis

X-ray diffraction (XRD) analysis was performed on the disk surfaces to determine if there was a detectable difference in the lattice between the hydrogen exposed and non-exposed disks. This technique was used to detect the presence of interstitial atoms resulting from hydrogen exposure that change the lattice spacing and therefore alter the diffraction pattern. A Bruker D8 Discover X-Ray Diffractometer was used to perform the analysis over an angular range of 25-85°. Figure 3 shows an image of the XRD machine used for this analysis.

Figure 3: Bruker x-ray diffractometer.

### 4.3.3. Surface Hardness Measurements

Surface hardness measurements using the Rockwell Superficial 15T testing method with a 15 kg normal load on an Instron Series 2000 Automated Rockwell Hardness Tester, shown in Figure 4, were performed on the disk surfaces. Each disk was tested to determine if there was a detectable difference between the hardness values between the hydrogen exposed and non-exposed disks at room temperature and low temperature. Each disk was tested in five locations at the relative temperature in which it was tribologically tested. The five hardness values for each disk are stored in the Instron tester and an average value and standard deviation are output. For low temperature samples, the disk was placed in a Dewar of liquid nitrogen for two minutes then quickly

removed and hardness tested. The low temperature hardness tests were completed quickly so that very little ice was able to form on the surface. The effects of ice formation are considered to be negligible due to the high contact stress and thin ice layer. Hardness testing was performed after the completion of tribological testing for two reasons. The first reason is to prevent surface damage to the disks resulting from the hardness testing that would alter the tribological testing results. Secondly, to prevent thermal cycling of the low temperature tested disks that may affect the microstructure and alter the tribological testing results.


Figure 4: Instron Rockwell hardness tester.

### 4.3.4. Surface Roughness Measurements

Surface roughness measurements were performed on unworn portions of the disk surfaces between the wear tracks after tribological testing to ensure that the disks all had comparable average surface roughness values. The tests were performed after tribological testing to prevent surface damage to the disks resulting from scratches from surface roughness testing that would alter the tribological testing results. A Datatraq 2000 profilometer with diamond tip stylus was used for testing. Three tests were performed around the disk and averaged. Each test was 0.8 mm in length and the surface roughness range was set for ±20 μm.

### 4.3.5. Ball on Disk Testing

#### 4.3.5.1. Test Apparatus

For this research a series of pin on disk wear tests were designed in the intent of ASTM testing standard G99[38] to evaluate the wear and friction performance of hydrogen exposed and unexposed Ti-6Al-4V disks at ambient and low temperatures. An AMTI Pin on Disk Tribometer Model 01 was modified to be used for the testing at low temperatures. The Model 01 was chosen for this testing for several reasons. First, it was originally designed to be used for high temperature tribological testing and therefore had a heavily insulated test chamber with an integrated chemical injection port and a thermocouple that continuously measures the temperature inside the chamber. The K-type thermocouple extends into the chamber and takes a temperature reading about 2 cm above the surface of the disk. Secondly, the Model 01 has a bell jar that encapsulates the entire test chamber, allowing environmental control. The chemical injection port was

used to run 0.25 inch stainless steel tubing from beneath the tribometer into the bell jar enclosed area and directly into the test chamber. The tubing enters the insulated test chamber from the top of the chamber through a port located about 3.5 cm from the ball holder feed through and extends down about 4.5 cm. For low temperature testing, a method to decrease the temperature of the test environment was needed to simulate use with liquid hydrogen. Due to the various safety risks associated with using liquid hydrogen it was not used in this testing. Instead liquid nitrogen ($LN_2$) was used to lower the test chamber temperature to temperatures below -100°C. A cryogenic transfer hose was connected from a low pressure (22 psi) liquid nitrogen container to the chemical injection tubing through a feed through fitting located on the base plate of the tribometer. During low temperature testing this tubing system allowed liquid nitrogen to be sprayed continuously into the insulated test chamber next to the disk on the spindle surface as the test was performed.

In order to enable direct comparison of the results it is important to maintain a similar chemical environment for both the room temperature and low temperature testing. Therefore, during room temperature testing nitrogen gas was continuously injected through the same tubing system. A gas regulator was used to inject the nitrogen gas into the chamber at 22 psi to match the pressure of the liquid nitrogen system.

Figure 5 shows the ball holder and disk moved out of the insulated test chamber prior to testing. During testing, the ball holder and disk are in perpendicular contact with each other and normal load is applied by attaching weights to the transducer housing as shown in Figure 6. When testing begins, the disk rotates and the normal and frictional

forces on the ball are transmitted to strain gauges in the transducer housing where the signals are output to the control box. The relative sliding contact produces wear of both the ball and the disk. After the test, both the pin and the disk are examined to evaluate the amount and type of wear that occurred. Figure 7 shows the bell jar in the lower position during testing and Figure 8 shows an $LN_2$ tank connected to the tribometer prior to testing.

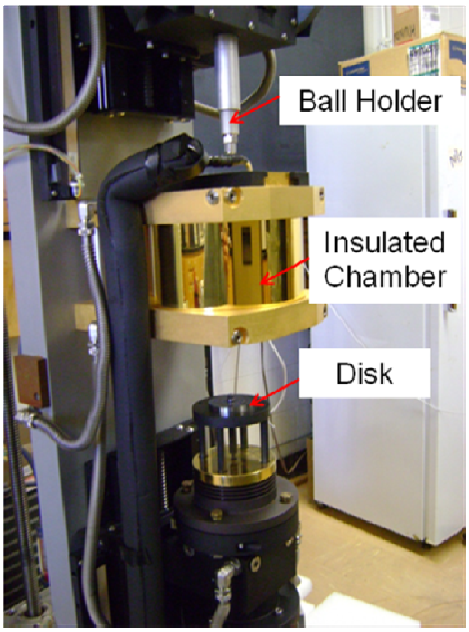


Figure 5: Tribometer with ball and disk removed from insulated chamber.

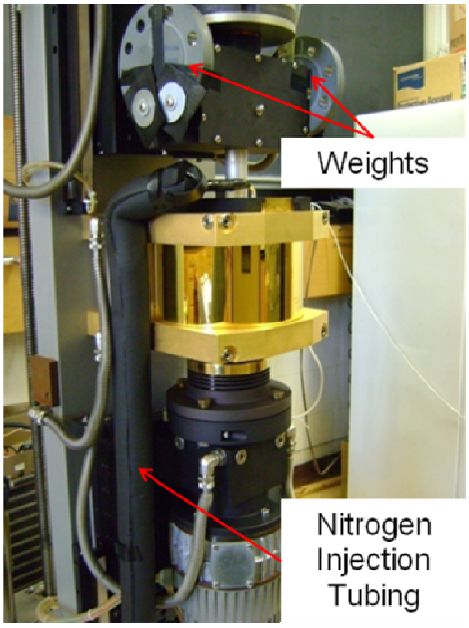


Figure 6: Transducer housing with weights and spindle in test position inside insulated chamber.

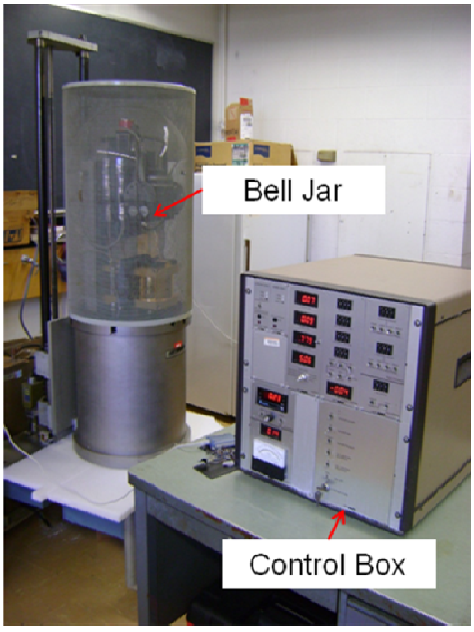


Figure 7: Bell jar lowered for testing with control box next to the tribometer.

Figure 8: Tubing system for nitrogen injection shown with connection to liquid nitrogen container.

Figure 5 shows the upper and lower slides of the tribometer extracted from the gold colored insulated test chamber. The pin holder extends out of the bottom of the black transducer housing and transmits forces from the pin to rods with strain gauges contacting the pin holder. The strain gauges are arranged to measure the normal and friction forces on the pin. The pin holder is held in the transducer housing by a screw incorporated into the transducer housing. For each test, a pin is secured in the pin holder. The transducer housing is suspended from the upper slide by springs, which are designed to counter the combined gravitational force of the transducer housing, pin holder and pin.

A constant normal force is applied by attaching weights to the suspended transducer housing via mounting holes on the outside of the transducer housing. The entire assembly is mounted to a slide controlled by an electric motor that lowers the slide into the test chamber, and a clutch attached to the motor holds the upper slide in place once at the designated position. The lower slide has an electric motor that rotates the spindle. The electric motor is controlled by a feedback system that uses tachometer signals as the input to a servo amplifier to maintain a constant user selected speed. A disk is secured to the spindle surface with a specially designed bolt. An electric motor moves the lower slide in and out of the test chamber, and a clutch attached to the motor secures the vertical position of the slide once at the user selected position.

#### 4.3.5.2. Data Collection and Analysis

Figure 9 shows a system diagram of the tribometer and data collection system. During each test, the friction force and normal force are measured by strain gauges in the transducer housing and are output to the tribometer control box. An internal computer in the control panel calculates the coefficient of friction and outputs voltage values corresponding to the friction force, normal force and coefficient of friction. A data acquisition system was used to record these output values on a computer using a LabVIEW program. The data was then analyzed using an Excel program to filter and display the information.

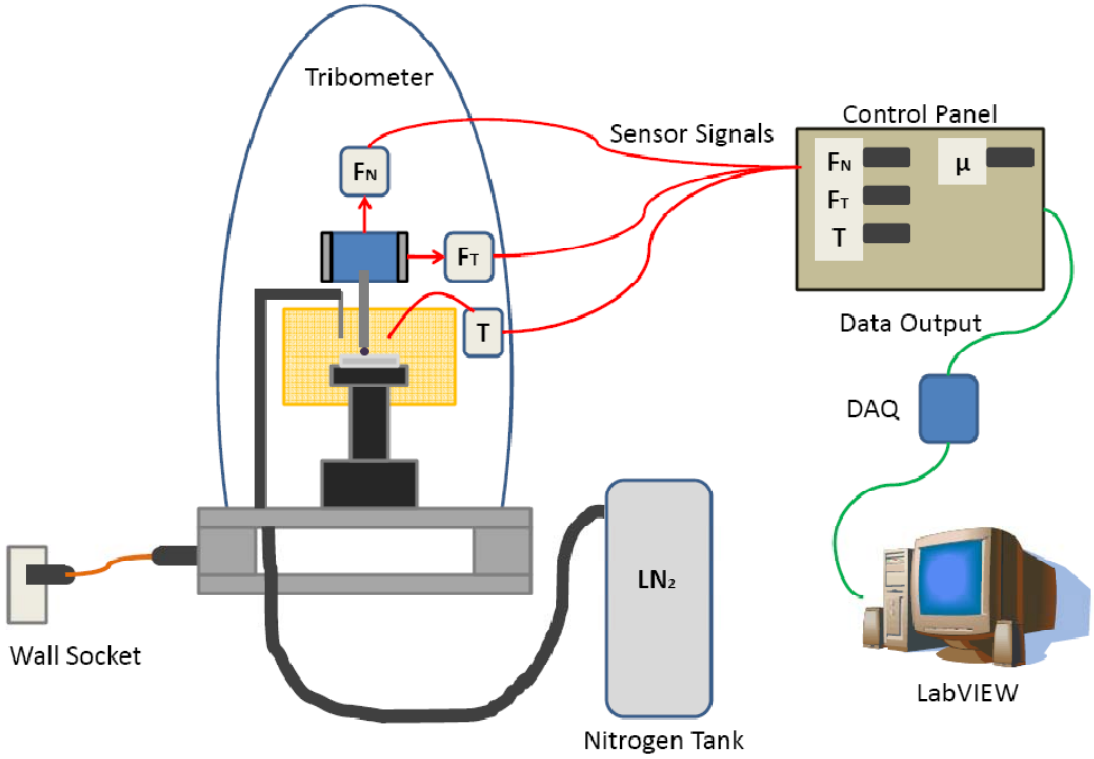


Figure 9: Tribometer and data collection system diagram.

For each test, the average coefficient of friction was calculated and the wear volume was determined from measurements of the wear track width on the disk. To increase accuracy, width measurements were taken using measurement software integrated into the high-resolution digital microscope used for surface analysis. Three width measurements were taken of each wear track and an average wear track width was computed. The wear volume was calculated using this average wear track width, the wear track radius and ball radius in accordance with ASTM standard G99.[38] The

normalized specific wear rate was then calculated based on the wear volume, normal load and linear speed of each test.

### 4.4. Testing Plan and Matrix

Four groups of tests were performed to evaluate the individual and combined influence of low temperature and hydrogen gas exposure on the tribological characteristics of polished Ti-6Al-4V disks. All disks were manufactured on the same lathe from the same commercially available raw material and each was polished using the same four-step process. All disks were then cleaned under identical conditions in an ultrasonic bath of acetone before sending six of the twelve disks to a private lab to be exposed to hydrogen gas. The six disks that were not exposed to hydrogen gas were split into Group 1 and 2 while the six hydrogen exposed disks were split into Group 3 and 4.

Each group consisted of three disks and two tests were performed on each disk for a total of 24 tests. The disks in Group 1 and Group 3 were tested under the same environmental conditions in which both were performed at the ambient room temperature, approximately 26°C, with nitrogen gas injected into the test chamber. The disks in Groups 2 and 4 were tested under the same environmental conditions in which liquid nitrogen was injected into the test chamber and the test chamber temperature was controlled to be approximately -105°C during each test.

Each disk was used for two tests, one test was performed under a 10 N normal load and a wear track radius of 1 cm and the second test was performed under a 20 N normal load at a wear track radius of 1.5 cm. The linear speed of the two types of tests was nearly identical at 0.056 m/s for the 1 cm radius tests and 0.055 m/s for the 1.5 cm

radius tests with respective rotational velocity of 53 and 35 revolutions per minute. All test sliding distances were the same at 10 m resulting in test durations of approximately 180 seconds. The test matrix is provided in Table 3 and the disk number and ball number for each test is listed in Table 4.

Table 3: Ball on disk test matrix.

| Sample Treatment | Group | Temp | Load (N) | Wear Radius (cm) | RPM | Linear Speed (m/s) | Distance (m) | Duration (s) |
|---|---|---|---|---|---|---|---|---|
| Non-exposed | 1 | RT | 10 | 1 | 53 | 0.056 | 10 | 180.2 |
| | | | 20 | 1.5 | 35 | 0.055 | 10 | 181.9 |
| | 2 | Cryo | 10 | 1 | 53 | 0.056 | 10 | 180.2 |
| | | | 20 | 1.5 | 35 | 0.055 | 10 | 181.9 |
| Hydrogen Exposed | 3 | RT | 10 | 1 | 53 | 0.056 | 10 | 180.2 |
| | | | 20 | 1.5 | 35 | 0.055 | 10 | 181.9 |
| | 4 | Cryo | 10 | 1 | 53 | 0.056 | 10 | 180.2 |
| | | | 20 | 1.5 | 35 | 0.055 | 10 | 181.9 |

Table 4: Disk and ball identification for each test.

| Group 1 | Inner Radius | | | Outer Radius | | |
|---|---|---|---|---|---|---|
| Disk | 1 | 2 | 3 | 1 | 2 | 3 |
| Pin | 1 | 2 | 3 | 4 | 5 | 6 |
| Group 2 | Inner Radius | | | Outer Radius | | |
| Disk | 4 | 5 | 6 | 4 | 5 | 6 |
| Pin | 7 | 8 | 9 | 10 | 11 | 12 |
| Group 3 | Inner Radius | | | Outer Radius | | |
| Disk | 7 | 8 | 9 | 7 | 8 | 9 |
| Pin | 13 | 14 | 15 | 16 | 17 | 18 |
| Group 4 | Inner Radius | | | Outer Radius | | |
| Disk | 10 | 11 | 12 | 10 | 11 | 12 |
| Pin | 19 | 20 | 21 | 22 | 23 | 24 |

# CHAPTER V

# RESULTS

This chapter displays the results obtained for the tests performed and presents graphs for comparison.

## 5.1. Pre-Test Optical Surface Analysis

Digital images were taken of the original surface of an exposed and unexposed disk for visual comparison. Figure 10 shows the original surface of the unexposed disk at 1000 times magnification. The figure displays morphology of the polished surface with grain boundaries showing a lighter color. Typically, grain boundaries were found on the order of 10 μm in diameter. There are several noticeable scratches from the polishing process but no obvious deep grooves or cracks were found.

Figure 11 shows the original surface of a hydrogen gas exposed disk. The image shows similar morphology and grain boundary structure and size as the unexposed surface in Figure 10. As with the unexposed disk, the surface has noticeable scratches from the polishing process and grain boundaries have a lighter color than the grains. No visible cracks or areas of hydrogen attack were found and no features were identified that visually distinguish between the exposed and unexposed disk surfaces.

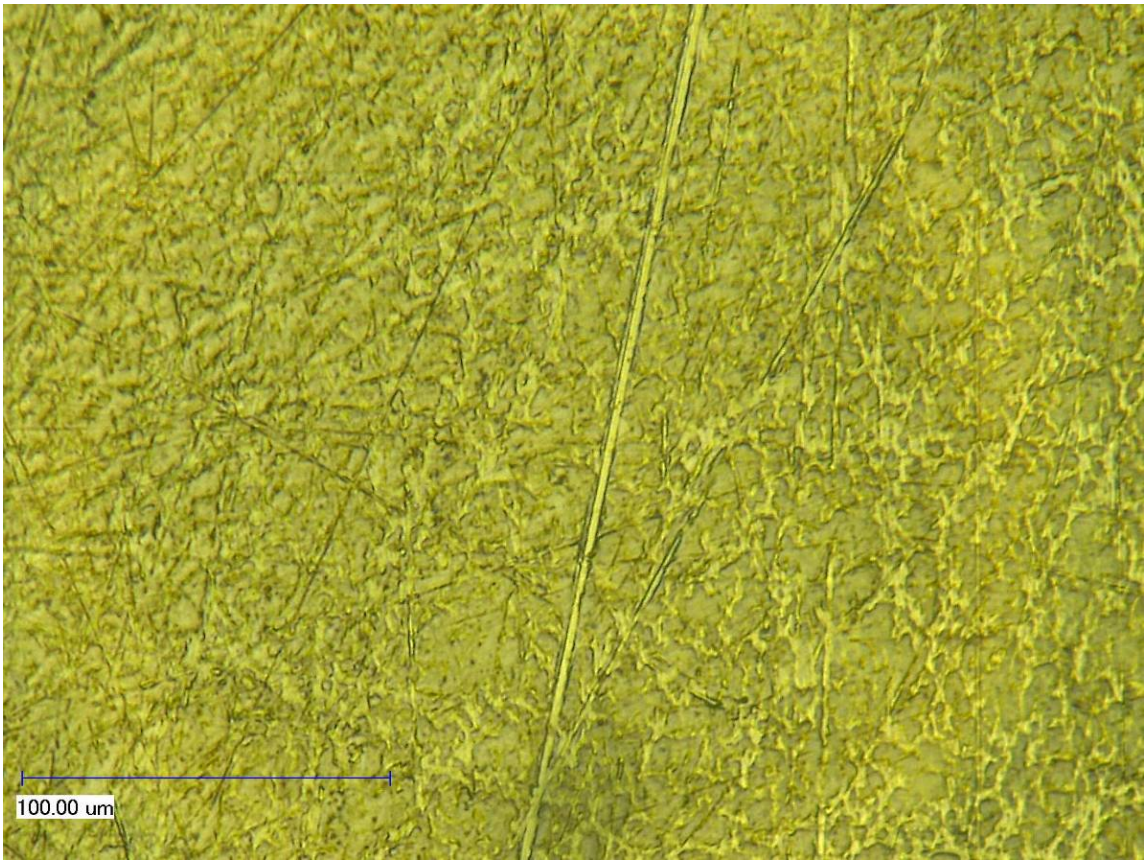


Figure 10: Original surface of an unexposed, polished disk at 1000 times magnification.

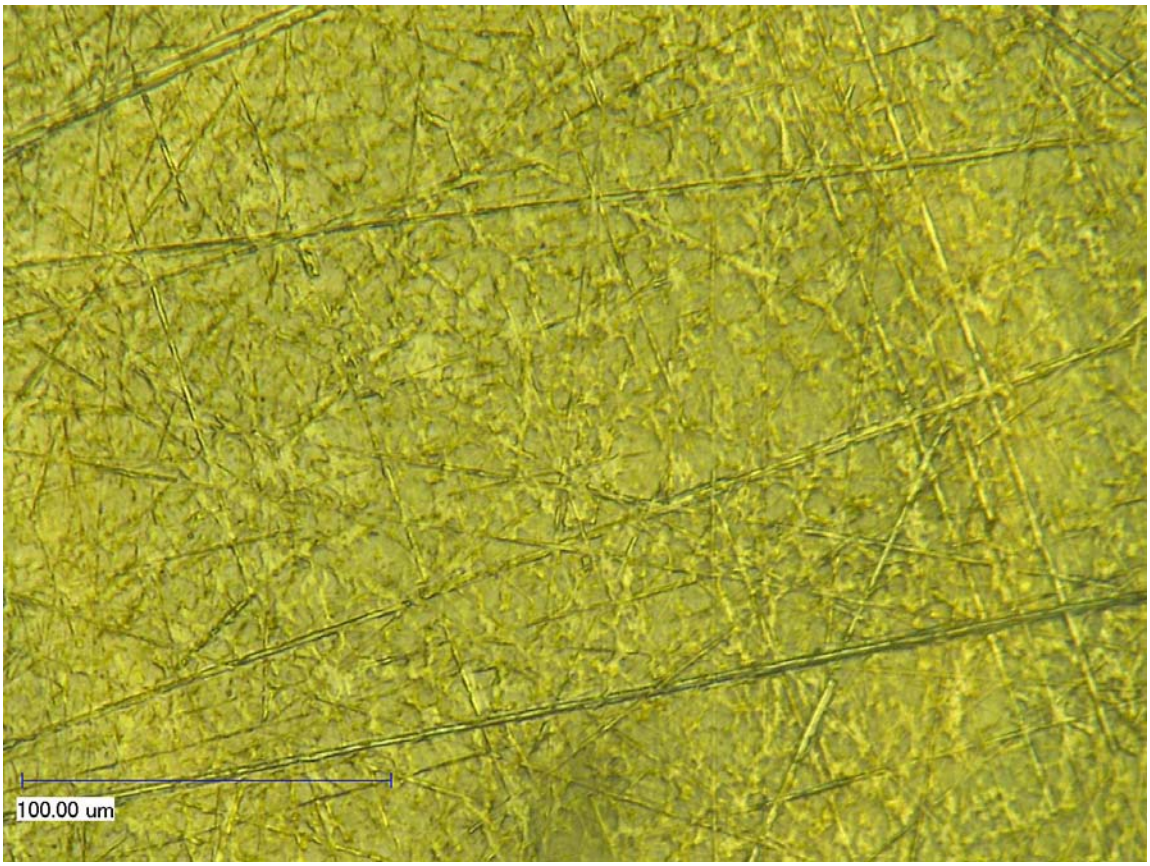


Figure 11: Original surface of a polished disk exposed to hydrogen gas at 1000 times magnification.

## 5.2. Average Surface Hardness

The hardness of each disk was tested using the Rockwell 15T Superficial scale on an Instron 2000 series automated hardness tester with a normal load of 15 kg. These tests were performed after tribological testing concluded to prevent damage to the surface prior to tribological testing. Exposure to hydrogen gas had a general effect of decreasing the surface hardness while low temperatures had the effect of increasing hardness as shown in Figure 12.

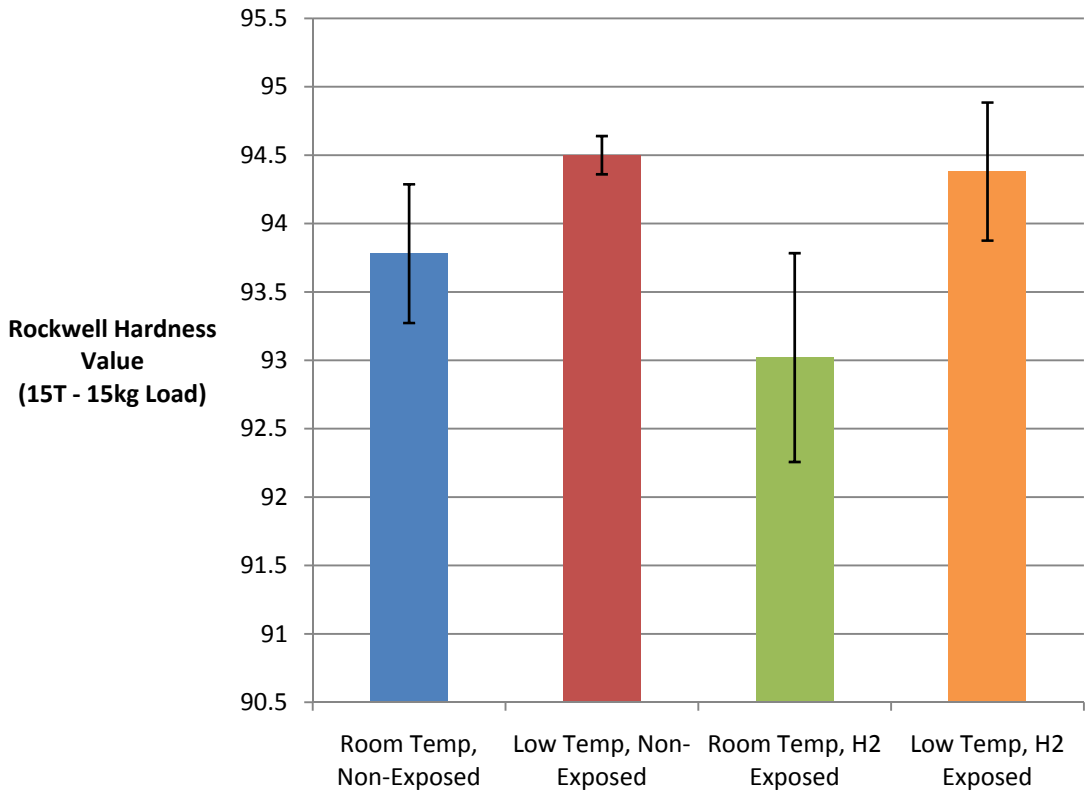


Figure 12: Average hardness test results for each group of testing.

## 5.3. Average Surface Roughness

Surface roughness measurements were taken using a Datatraq diamond stylus profilometer. The surfaces were very consistent with all disks having average surface roughness values in the 0.03 to 0.04 µm range as shown in Figure 13.

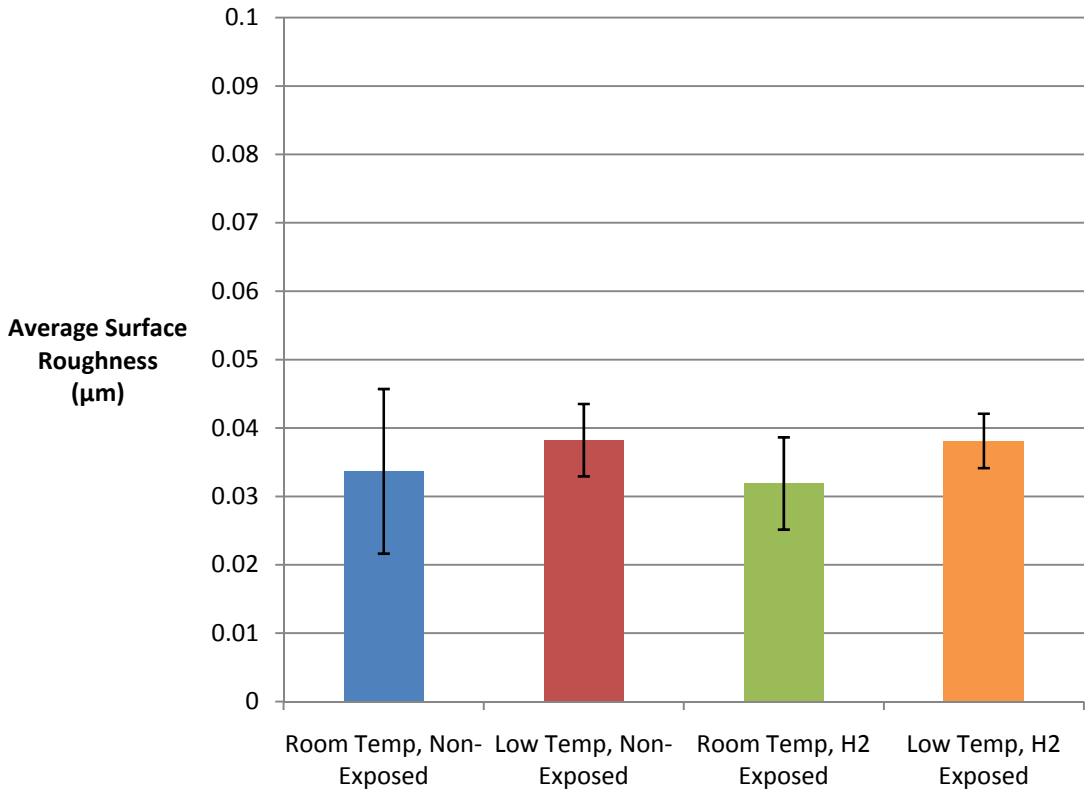


Figure 13: Average surface roughness values of each group of testing.

### 5.4. X-Ray Diffraction Analysis

X-ray diffraction analysis was performed to evaluate microstructural changes resulting from exposure to hydrogen gas. As shown in Figure 14, the hydrogen exposed surface shows several peaks not present in the unexposed surface and shows higher peaks for several of the Ti-6Al-4V characteristic peaks. The difference between the diffraction patterns gives evidence that exposure to hydrogen gas has produced a microstructural change on the surface of the disks. The diminished peak of the hydrogen exposed samples is consistent with XRD patterns from other research and compares well with results from a study of Ti-6Al-4V with varying hydrogen concentrations shown in Figure 15.[31] When Figure 14 is compared to the results of another study, where hydrides were formed as shown in Figure 16, the comparison illustrates that the disks tested did not form hydrides as a result of exposure to hydrogen gas.[33] This analysis shows that the goals of the hydrogen exposure were met; meaning that hydrogen was introduced into the lattice of the disk surface and hydrides were not formed. In addition, surface cracking did not occur and the average surface roughness values for all the disks were comparable.

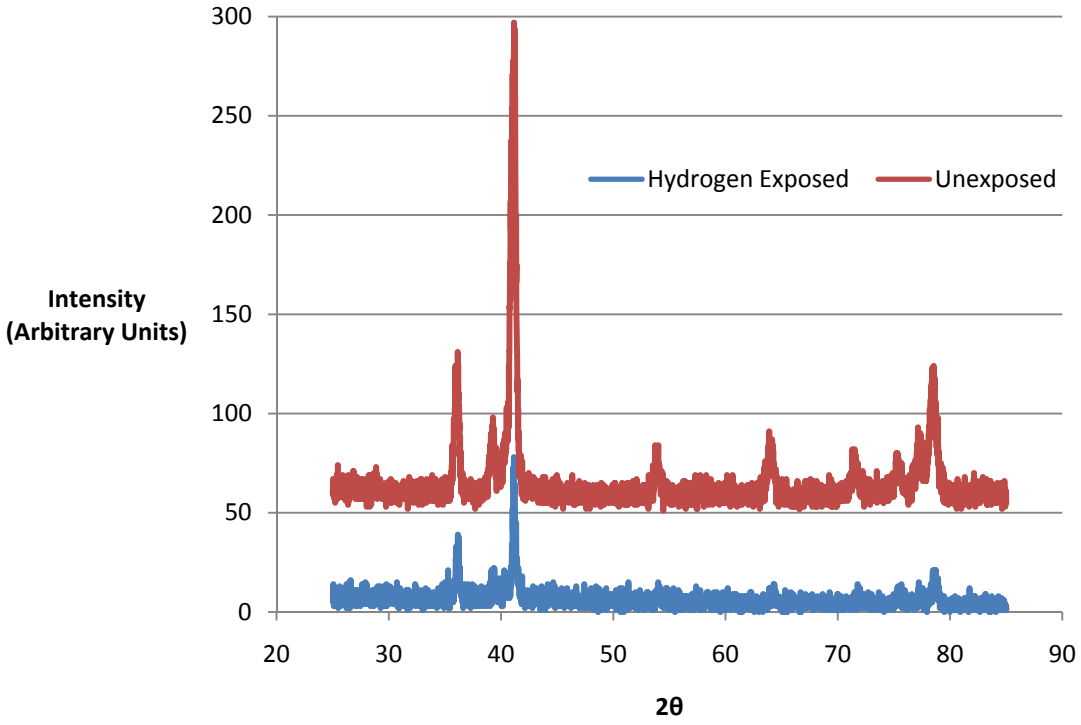


Figure 14: X-ray diffraction analysis of hydrogen gas exposed and unexposed samples.

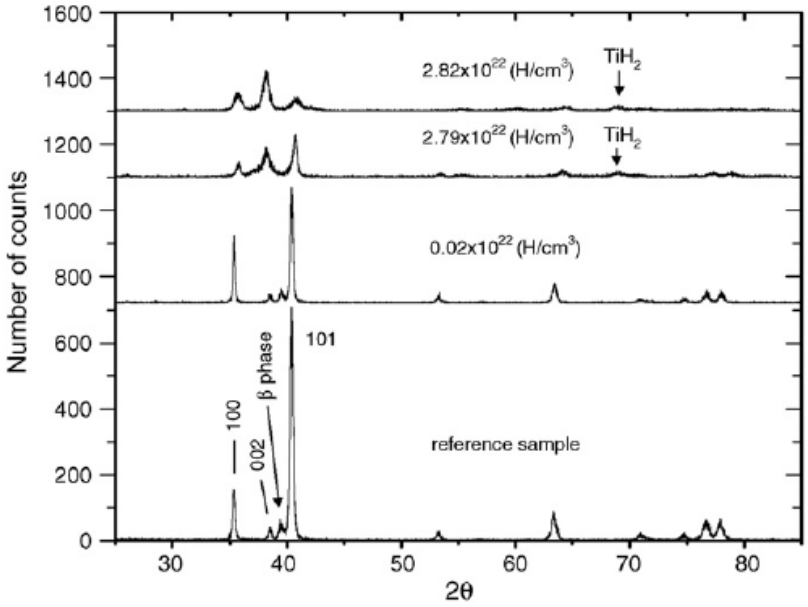


Figure 15: Reference XRD analysis showing typical diminishing peaks with increased hydrogen concentration.[31]

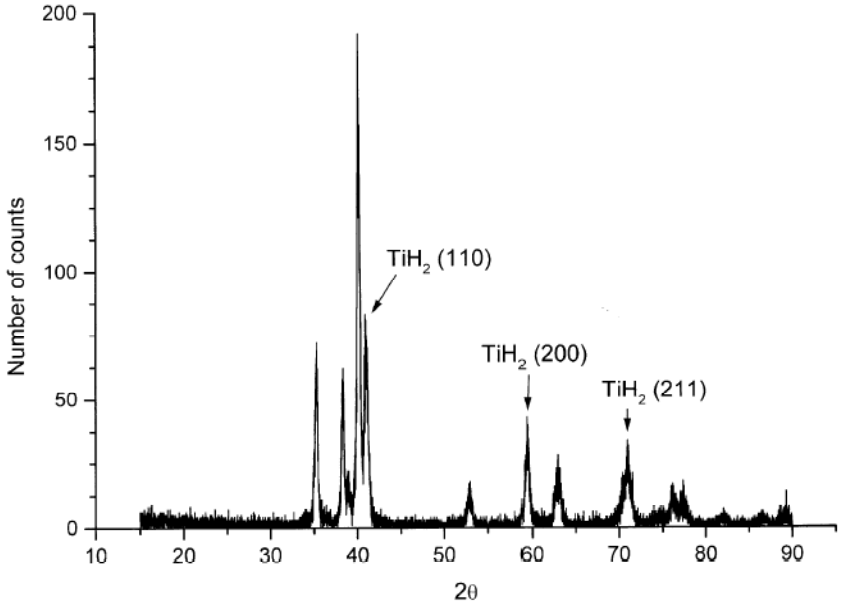


Figure 16: Reference XRD analysis showing the formation of hydrides.[33]

## 5.5. Tribological Testing

Table 5 lists the calculated specific wear rate, average coefficient of friction and the steady state coefficient of friction for each test. Table 6 displays the average and standard deviation of each of the values for each different type of test performed.

Table 5: Individual tribological test results.

| Group | Nominal Temperature | Load (N) | Specific Wear Rate (mm^3/Nm) | Average μ | Steady State μ |
|---|---|---|---|---|---|
| 1 | Room | 10 | 4.03E-03 | 0.31 | 0.28 |
| | | | 4.86E-03 | 0.34 | 0.33 |
| | | | 4.71E-03 | 0.34 | 0.32 |
| | Low | 20 | 5.35E-03 | 0.53 | 0.52 |
| | | | 8.66E-03 | 0.58 | 0.53 |
| | | | 6.10E-03 | 0.56 | 0.48 |
| 2 | Room | 10 | 4.18E-03 | 0.44 | 0.33 |
| | | | 3.04E-03 | 0.33 | 0.23 |
| | | | 5.62E-03 | 0.40 | 0.30 |
| | Low | 20 | 2.46E-03 | 0.43 | 0.38 |
| | | | 2.54E-03 | 0.41 | 0.37 |
| | | | 3.17E-03 | 0.38 | 0.36 |
| 3 | Room | 10 | 6.77E-03 | 0.40 | 0.31 |
| | | | 4.41E-03 | 0.47 | 0.38 |
| | | | 5.07E-03 | 0.49 | 0.43 |
| | Low | 20 | 7.35E-03 | 0.53 | 0.52 |
| | | | 5.24E-03 | 0.50 | 0.46 |
| | | | 5.60E-03 | 0.53 | 0.47 |
| 4 | Room | 10 | 3.30E-03 | 0.35 | 0.27 |
| | | | 3.50E-03 | 0.36 | 0.25 |
| | | | 3.15E-03 | 0.34 | 0.29 |
| | Low | 20 | 3.04E-03 | 0.41 | 0.38 |
| | | | 3.93E-03 | 0.44 | 0.40 |
| | | | 2.20E-03 | 0.40 | 0.37 |

Table 6: Test result average values and standard deviations.

| Group | Nominal Temperature | Load (N) | Specific Wear Rate (mm^3/Nm) | Standard Deviation (mm^3/Nm) | Average μ | Average μ Standard Deviation | Steady State μ | Steady State μ Standard Deviation |
|---|---|---|---|---|---|---|---|---|
| 1 | Room | 10 | 4.53E-03 | 4.42E-04 | 0.33 | 0.02 | 0.31 | 0.03 |
| | | 20 | 6.70E-03 | 1.74E-03 | 0.56 | 0.03 | 0.51 | 0.03 |
| 2 | Low | 10 | 4.28E-03 | 1.29E-03 | 0.39 | 0.06 | 0.29 | 0.05 |
| | | 20 | 2.73E-03 | 3.85E-04 | 0.41 | 0.03 | 0.37 | 0.01 |
| 3 | Room | 10 | 5.42E-03 | 1.22E-03 | 0.45 | 0.05 | 0.37 | 0.06 |
| | | 20 | 6.06E-03 | 1.13E-03 | 0.52 | 0.02 | 0.48 | 0.03 |
| 4 | Low | 10 | 3.32E-03 | 1.73E-04 | 0.35 | 0.01 | 0.27 | 0.02 |
| | | 20 | 3.06E-03 | 8.63E-04 | 0.42 | 0.02 | 0.38 | 0.02 |

Figure 17 and Figure 18 display data listed in Table 6. Figure 17 compares the average specific wear rate and standard deviation of the results and Figure 18 compares the average steady state average coefficient of friction and the standard deviation of the steady state averages of each group. Friction plots and a results table for each test as well as high-resolution digital images of each wear track are located in the Appendices. Only images displaying typical results or specific features of interest have been included, although the entire wear track for each test was analyzed to determine wear mechanisms and general trends.

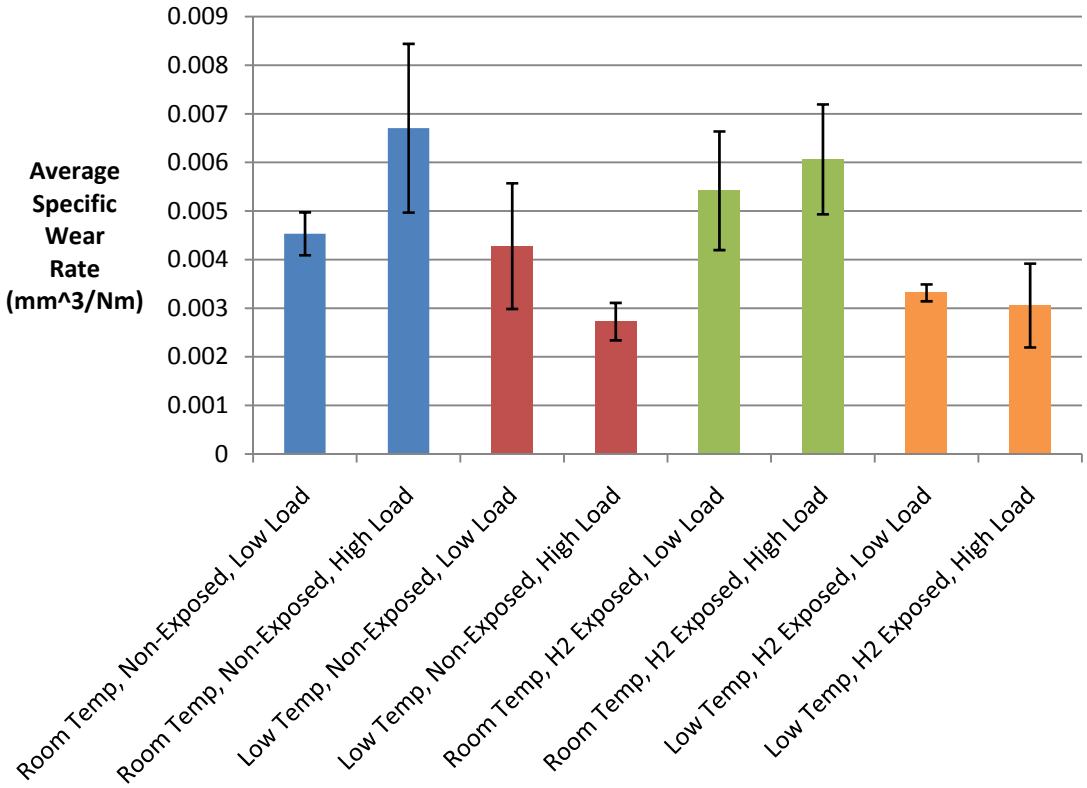


Figure 17: Average specific wear rate for each set of testing.

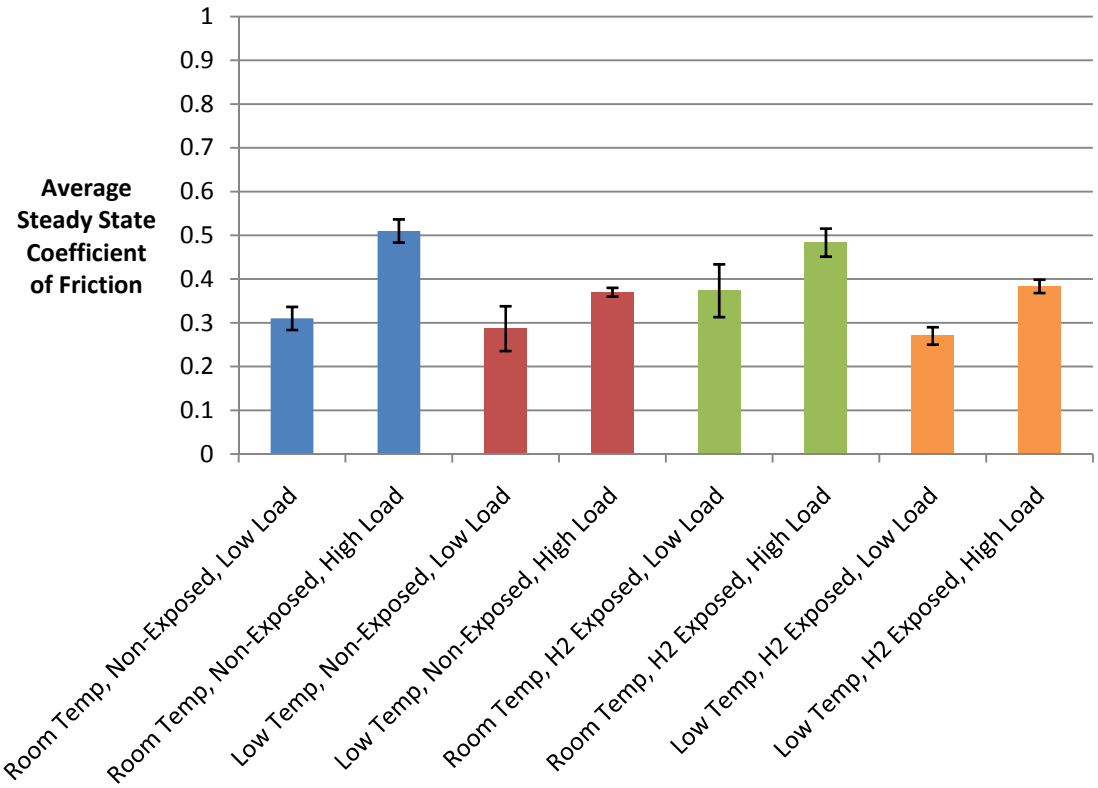


Figure 18: Average steady state coefficient of friction for each set of testing.

Table 7 and Figure 19 show the maximum Hertzian contact pressure calculated for both the room temperature and low temperature conditions. Table 8 and Figure 20 show the maximum temperature rises due to frictional contact. Table 9 and Figure 21 show the average temperature rises due to frictional contact. The contact pressure and frictional heating values were calculated based on properties listed for Ti-6Al-4V and $Si_3N_4$ at the respective testing temperatures. The property information was found in the ASM *Materials Properties Handbook: Titanium Alloys*[51] and ASM Alloy Digest: Silicon

Nitride.[52] The properties used for Ti-6Al-4V at room temperature (20°C) and low temperature (-110°C) are listed in Table 10 and Table 11 respectively and the used for silicon nitride for room and low temperatures are listed in Table 12.

Table 7: Maximum Hertzian contact pressure.

| Maximum Hertzian Contact Pressure (GPa) | | | | |
|---|---|---|---|---|
| | Unexposed | | Exposed | |
| Normal Load | RT | Low | RT | Low |
| 10 N | 1.13 | 1.16 | 1.13 | 1.16 |
| 20 N | 1.43 | 1.46 | 1.43 | 1.46 |

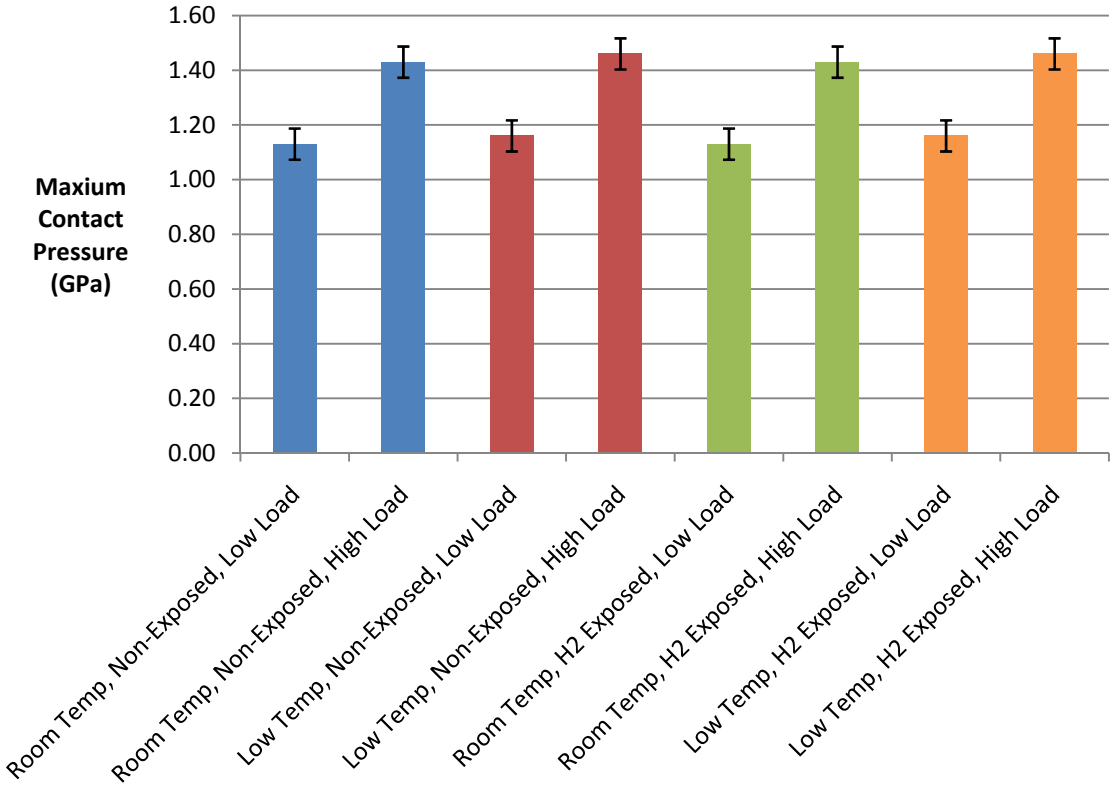


Figure 19: Maximum Hertzian contact pressure.

Table 8: Maximum flash temperature at contact.

| Maximum Frictional Heating Temperature Change (°C) | | | | |
|---|---|---|---|---|
| | Unexposed | | Exposed | |
| Normal Load | RT | Low | RT | Low |
| 10 N | 47.4 | 63.8 | 56.5 | 59.4 |
| 20 N | 110.2 | 115.2 | 103.7 | 118.3 |

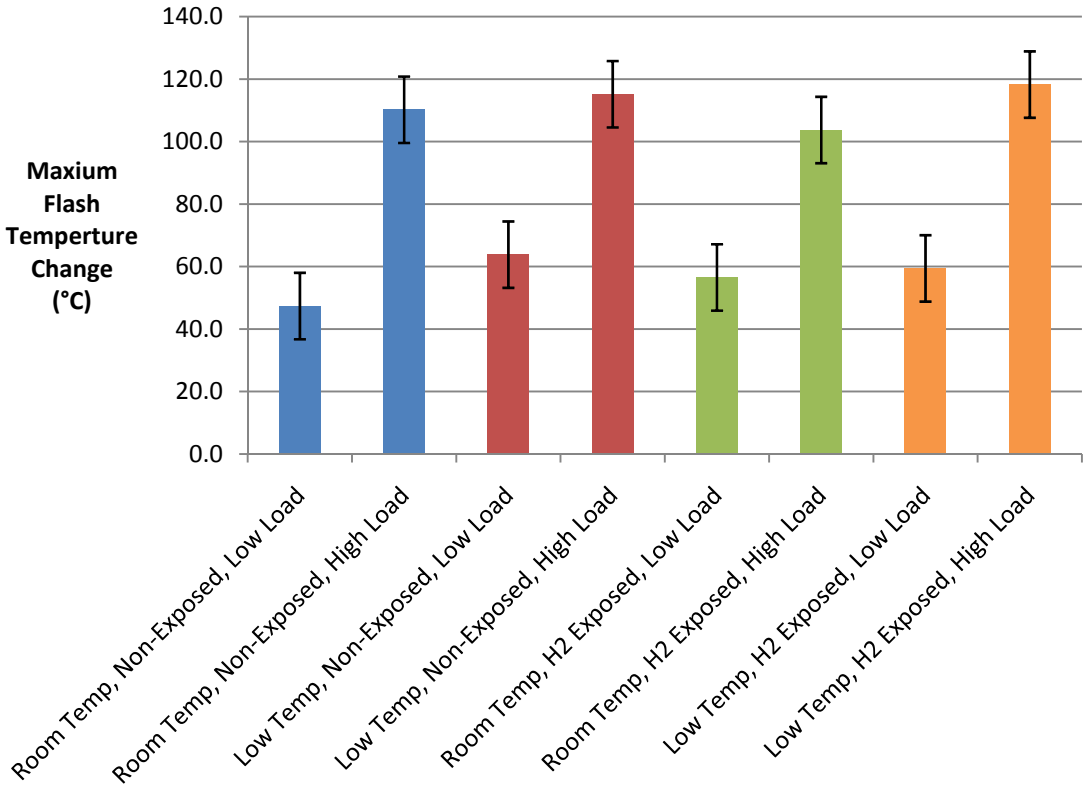


Figure 20: Maximum flash temperature at contact.

Table 9: Average flash temperature at contact.

| Average Frictional Heating Temperature Change (°C) | | | | |
|---|---|---|---|---|
| | Unexposed | | Exposed | |
| Normal Load | RT | Low | RT | Low |
| 10 N | 3.3 | 4.3 | 3.9 | 4.0 |
| 20 N | 10.8 | 10.9 | 10.1 | 11.2 |

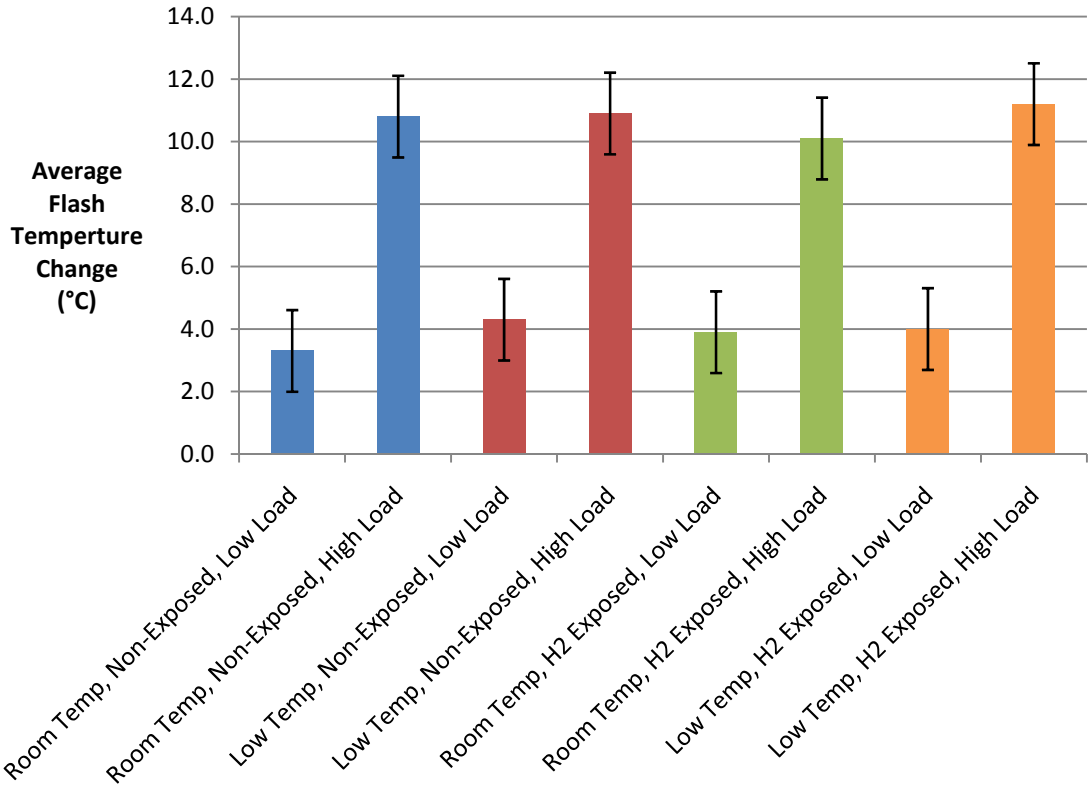


Figure 21: Average flash temperature at contact.

Table 10: Room temperature properties for Ti-6Al-4V.

| Room Temperature Properties | | |
|---|---|---|
| E | 112 | GPa |
| v | 0.23 | |
| k | 7 | W/mK |
| D | 0.027 | $cm^2/S$ |
| $\sigma_y$ | 850 | MPa |

Table 11: Low temperature properties for Ti-6Al-4V.

| Low Temperature Properties | | |
|---|---|---|
| E | 118 | GPa |
| v | 0.23 | |
| k | 5 | W/mK |
| D | 0.027 | $cm^2/S$ |
| $\sigma_y$ | 900 | MPa |

Table 12: Properties for silicon nitride.

| Silicon Nitride Properties | | |
|---|---|---|
| E | 294 | GPa |
| v | 0.28 | |
| k | 30.7 | W/mK |
| D | 1.35 | $cm^2/s$ |

# CHAPTER VI

# DISCUSSION OF RESULTS

This chapter discusses and compares the results presented in the previous chapter. Friction and wear values are discussed in relation to the observed wear mechanisms and trends are identified.

## 6.1. Group 1 – Non-Exposed, Room Temperature Tested

The basis for comparison of this research is the tribological characteristics of non-hydrogen exposed Ti-6Al-4V tested at room temperature. The Group 1 tests showed a consistent, direct correlation between the normal load and the tribological responses of friction coefficient and the specific wear rate. Testing at a higher normal load resulted in an increase in the friction coefficient and the specific wear rate, as displayed in Figure 17 and Figure 18.

The wear track on the disk displayed both plowing and adhesive wear mechanisms with plowing as the dominant mechanism at both low and high normal loads. Even though both mechanisms were present, the normal load did have an effect on the amount of each wear mechanism observed. At higher normal loads, there were well-defined parallel grooves along the entire wear track compared to non-continuous, non-parallel grooves at lower load as shown in Figure 22 and Figure 23. In general, higher loads produced a decrease in the amount of adhesive areas on the disk wear track and a corresponding decrease in the amount of disk material adhering to the ball compared to low loads. In addition, both loads produced one to two large local areas of adhesion per wear track as shown in Figure 24 and Figure 25.

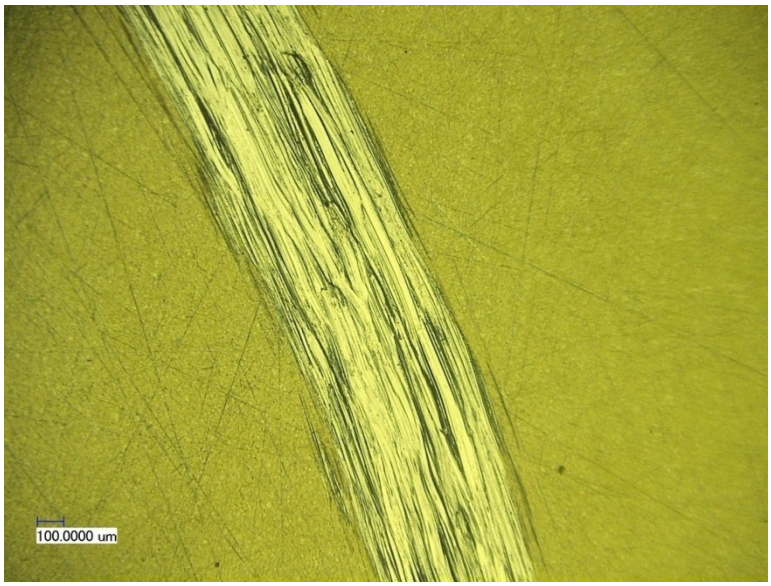


Figure 22: Group 1 low load typical wear track image from Disk 3 at 100 times magnification.

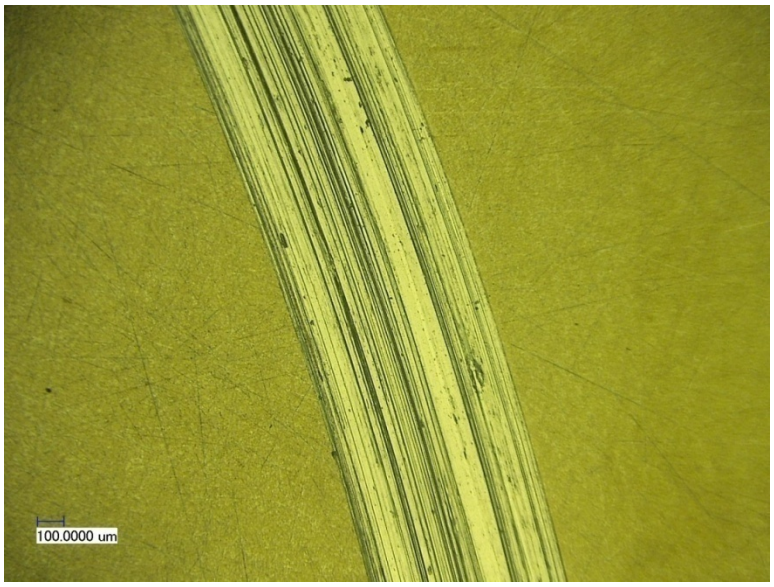


Figure 23: Group 1 high load typical wear track image from Disk 3 at 100 times magnification.

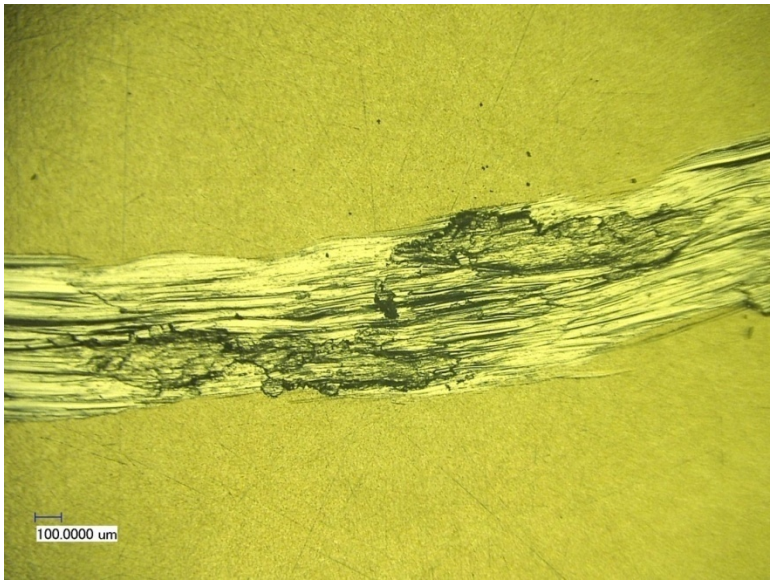


Figure 24: Group 1 low load adhesive area on Disk 2 at 100 times magnification.

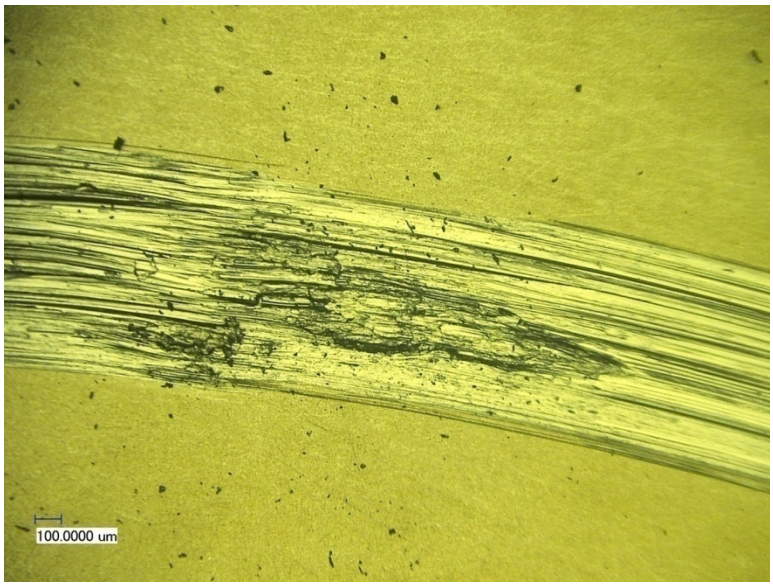


Figure 25: Group 1 high load adhesive area on Disk 2 at 100 times magnification.

### 6.2. Group 2 – Non-Exposed, Low Temperature Tested

The Group 2 tests were performed on disks that were non-hydrogen exposed but the test temperature was held at low temperature throughout each test. Under low temperature conditions, there is a direct correlation between the normal load and the friction coefficient in which the friction coefficient increased with an increased load. This behavior is consistent with the results from Group 1. However, the tribological characteristics of these conditions differed from the Group 1 testing in several areas. Contrary to what was observed at room temperature, the normal load had an inverse relationship with the specific wear rate, meaning there was a decrease in the specific wear rate at higher loads. Although plowing and adhesion are the observed wear mechanisms similar to Group 1, there was a fundamental change in the wear track appearance in relation to normal load for the Group 2 testing. At low loads, there are more parallel grooves and adhesion, as shown in Figure 26, compared to the room temperature low load tests. Figure 27 shows the high load wear track with a wavy nature to the surface and the grooves are relatively parallel to one another. This surface texture is interesting because the wavy nature of these wear tracks would usually indicate that the wear mechanism was stick-slip if it displayed the characteristic abrupt flat points at the crest of the wavy features; however, there is no evidence of this defining feature. In contrast to the room temperature tests, the grooves in the high load tests follow the wavy surface; they are not perfectly circular like the room temperature high load wear tracks. In both the low and high load tests, there were several localized areas of adhesion per wear track. Typically, these large adhesive areas are narrower and have sharper edges

than those observed at room temperature. The amount of material adhesion to the ball for the low load tests is less than the high load tests, which is also contrary to the trend at room temperature.

These changes in material behavior appear directly related to the test temperature. When the material is at a lower temperature, the material becomes harder and more resistant to plastic deformation, as shown in the hardness tests performed on the disks. This resistance to plastic deformation helps to explain the increase in uniformity and parallelism in the low load tests. However, the unique nature of the high load tests suggests another factor is influencing the wear pattern. Ostrovaskaya et al. found localized areas of high hardness in titanium alloys indicating that there is a possibility that a phase transformation at low temperature and higher pressures is causing the formation of localized harder or softer areas, leading to the formation of the wavy surface.[22]

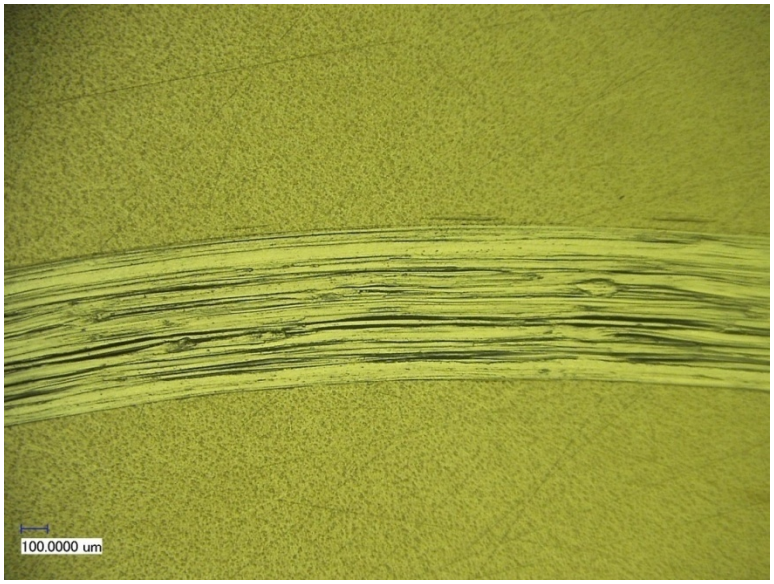


Figure 26: Group 2 low load typical wear track from Disk 4 at 100 times magnification.

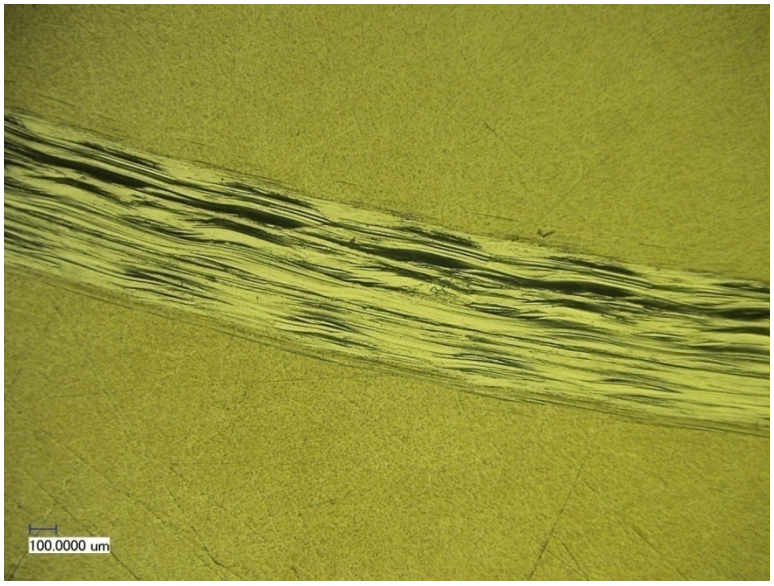


Figure 27: Group 2 high load typical wear track from Disk 4 at 100 times magnification.

### 6.3. Group 3 – Hydrogen Exposed, Room Temperature Tested

The disks in Group 3 were exposed to hydrogen gas and tested at room temperature. The tribological behavior exhibited the same trends as Group 1, meaning that there was a direct relationship between the normal load and both the friction coefficient and specific wear rate as shown in Figure 17 and Figure 18. When comparing the friction coefficient and specific wear rate values to the values obtained from testing the non-hydrogen exposed disks in Group 1, the hydrogen exposure appears to have differing effects based on the normal load applied. At low load, the exposure appears to increase the friction coefficient and specific wear rate as shown in Figure 17 and Figure 18. However, in the higher load tests the trend appears to be negated, or possibly reversed, where both the friction coefficient and specific wear rate decrease. After taking into account the uncertainty of the results obtained from the hydrogen exposed and non-exposed tests, the high load results cannot fully support the conclusion that there is a decrease in the values because of hydrogen exposure. However, the low load tests still demonstrate the increasing trend. This may be because friction and wear depend on several factors, such as surface roughness, hardness, the thickness of a surface layer, and the microstructure of the surface layer for the bulk. At a low load, the interactions between the contacted surfaces dominate the tribological performance. At a higher load, the bulk material properties are more pronounced.

In comparison with the non-exposed Group 1 disks, the Group 3 disk wear tracks showed more adhesion in terms of higher numbers of small adhesive areas and more severe adhesion in larger regions as shown in Figure 28 and Figure 29. Similar to the

Group 1 disk wear tracks, the lower load tests produced non-parallel groove and the higher load produced more uniform, parallel grooves along the entire wear track as shown in Figure 28 and Figure 29. Also like Group 1, both loads produced larger areas of adhesive wear.

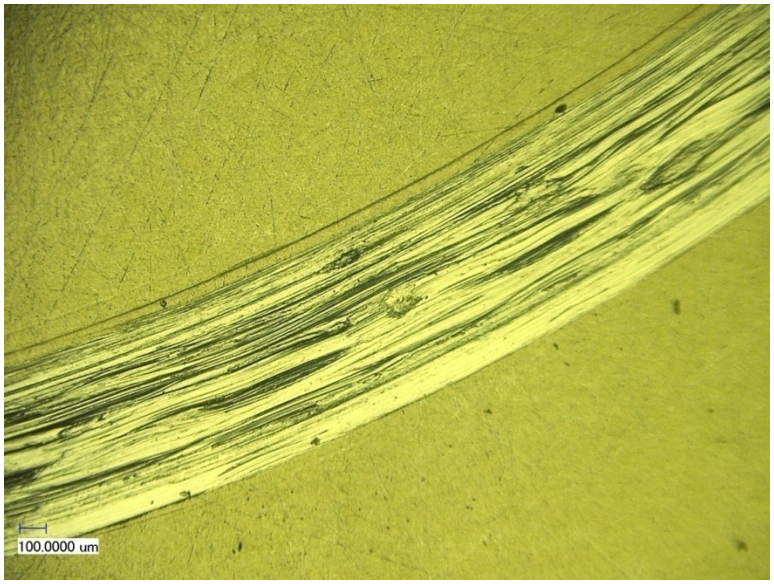


Figure 28: Group 3 low load wear track from Disk 7 at 100 times magnification.

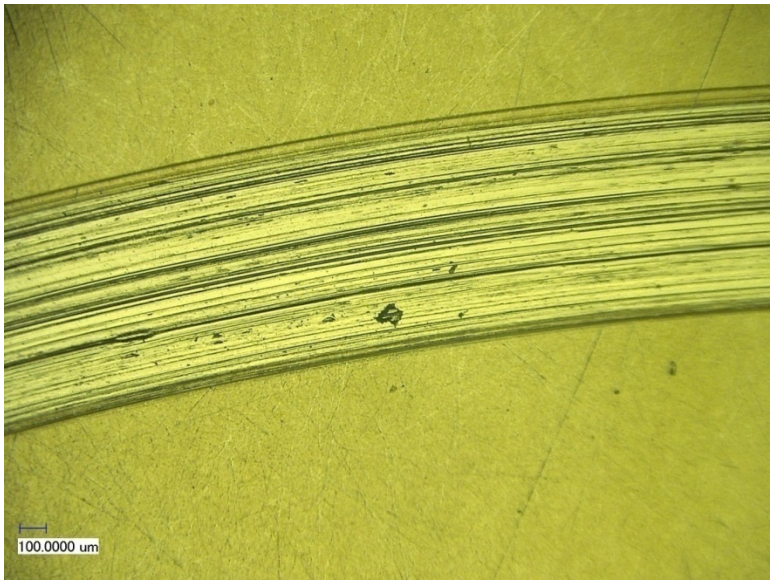


Figure 29: Group 3 high load wear track from Disk 7 at 100 times magnification.

### 6.4. Group 4 – Hydrogen Exposed, Low Temperature Tested

The disks in Group 4 were exposed to hydrogen gas and tested at low temperature. Following the same trends as the low temperature testing in Group 2, the friction coefficient has a direct correlation with normal load while the specific wear rate appears to have an inverse correlation. However, there is not a conclusive trend due to large uncertainty values for the high load testing. The friction coefficient values are very similar to the Group 2 results, showing little change as a result of hydrogen exposure. The Group 3 friction results are consistently higher than Group 4 for equivalent normal loads. This indicates that the friction response is more dependent on temperature than hydrogen gas exposure. The wear response shows a normal load dependence with a consistent decrease in wear at low load compared to Group 2 results, and a reverse trend at high load where the specific wear rate appears to increase with hydrogen exposure.

The high load testing does not demonstrate a strong wear trend because the values are statistically very similar due to large uncertainty values at low temperature and high load. In comparison with the Group 3 results, the wear response appears to have a strong temperature dependence, as there are markedly lower specific wear rates at low temperature compared to room temperature.

The wear tracks show wear patterns similar to that found in the Group 2 low temperature testing. In general the Group 4 wear tracks exhibited more small areas of adhesion and the larger areas of adhesion were typically in the center of the wear track and narrower than those found on disks tested at room temperature. The Group 4 low load tests showed some waviness on the wear track surface, similar to the previous low temperature testing in Group 2, but with more small areas of adhesion as shown in Figure 30. The Group 4 high load wear tracks exhibited the same wavy nature as observed on the Group 2 high load wear tracks and had patterns more consistent with traditional stick-slip as flat areas developed at the crest of the wavy features as shown in Figure 31. The wear mechanism is not traditional stick-slip and is still classified as plowing with adhesion, but the unusual nature of Group 2 and Group 4 testing indicates that there is a fundamental change in the wear characteristics at low temperature.

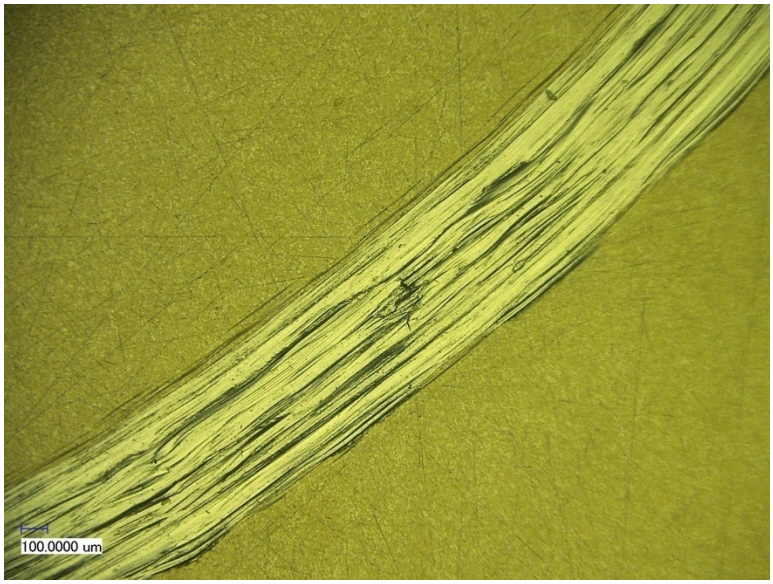


Figure 30: Group 4 low load wear track from Disk 10 at 100 times magnification.

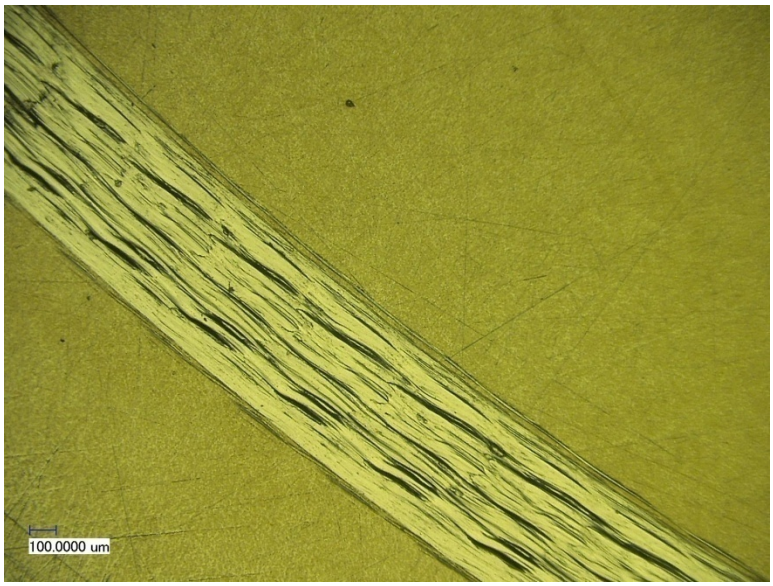


Figure 31: Group 4 high load wear track from Disk 10 at 100 times magnification.

## 6.5. The Influence of Temperature and Hydrogen Gas Exposure on Wear Response

The topography of the wavy surface observed on the low temperature wear tracks and more prominently on the high load, low temperature wear tracks, may be explained by the interaction of wear debris in the wear track causing uneven pressure distribution along the wear track. Stachowiak and Batchelor discuss the role of entrapped debris and thermal expansion on the formation of wear surface topography in Chapter 10 of *Engineering Tribology*.[2] In sliding contact between solid surfaces in which the bodies have different harnesses values, wear debris can become trapped on the wear track and the interaction between the debris and the harder sliding body can dominate the wear response. As the harder sliding body, the ball, contacts the softer flat surface, the disk, indents the surface. When sliding begins, there is a build up of surface material that forms in front of the harder sliding body and causes lift off of the sliding body. As the body slides along the flat surface it deforms the surface by forming grooves with a ploughing wear mechanism, and it also produces wear debris as material breaks loose from the surface. As the wear track forms and more debris is trapped in the groove, the debris falls into lower areas and provides support for the sliding body as it passes over with each rotation. In this situation, the sliding body does not contact the softer surface uniformly and large grooves and lumps can form as a result of the non-uniform contact. The topography grows as sliding progresses and the lumps become the primary locations of contact early in the wear process. Bettge and Starcevic showed that wear surface topography can increase with higher frictional power and the lumps can increase in

size.[53] The lumps will deform plastically with further wear moving their locations slowly and may work harden under repeated deformation and stress cycling. Also with increased sliding, many wear particles that formed from the initial sliding contact will tend to move from the areas of highest local pressure in the center of the wear track to lower pressure zones toward the sides of the wear track and a percentage will be ejected from the contact zone entirely. As the debris distribution changes with increased sliding, the nature of the surface contact will change as well. Subsurface stresses due to Hertzian contact will promote adhesive wear in local areas of high stress due to the weakening of bonding to the bulk material. This will primarily occur in the center of the wear track at the points of maximum Hertzian pressure. Stachowiak and Batchelor also comment that at higher sliding velocities that frictional heating of the topographic features will lead to softening and eventually reduce the amplitude of the lumps.[2] Chandrasekaran et al. found that high sliding velocities caused a reduction in the size of the topographic features due to frictional heating, and that frictional heating did not have much influence on the topography at lower velocities.[54] In this research the sliding velocity was low, 0.055 m/s, and there was not high maximum or average frictional heating as shown in Figure 20 and Figure 21 in Section 5.5; therefore, the lumps were not softened substantially and work hardening continued with increased sliding.

Stachowiak and Batchelor's description of this wearing process is consistent with the observed morphology of the low temperature disks and helps explain why this behavior is more pronounced at higher loads. Low temperature induced reductions in ductility may cause more surface layer wear debris to form during sliding initiating this

type of wearing process. Hydrogen exposure may also reduce the ductility of the surface producing wear debris that allows this behavior to be more pronounced at the lower load. The trend of centered, narrower adhesive areas at low temperature is also consistent with the description of this wear pattern.

The increase in adhesion on the hydrogen exposed samples may also be due to wear particle interaction. Adhesion is greatly affected by the formation of a transfer layer where a collection of small particles adhere to the sliding surface and can grow.[2] With continued sliding, the layer grows and the particles agglomerate. The build up will either break free or continue to grow, potentially causing seizure due to the strong adhesive force between the disk particles adhering to the sliding body and the disk.[2] If the mechanical properties of a thin surface layer on the disks are deteriorated due to hydrogen diffusion, then particles of the surface layer will break away more quickly than on untreated disks. The small particles can be pressed and adhere to the silicon nitride ball more, forming the transfer layer more quickly than during untreated tests. With a larger transfer layer on the ball forming more quickly during testing of hydrogen exposed disks, there is more time during the test in which the surface of the wear track is subjected to higher adhesive forces producing more adhesive wear compared to tests of untreated disks. As the disk wears, some parts of the build up on the ball break off from the ball and are ejected from the contact area.

# CHAPTER VII

# CONCLUSIONS

This chapter summarizes the results and states the significance of the research and major conclusions.

After analyzing the effects that the variables of test temperature, normal load and previous hydrogen gas exposure had on the friction coefficient, specific wear rate and wear mechanisms general trends were found. Low test temperatures caused a general decrease in the friction coefficient and the specific wear rate observed for both hydrogen gas exposed and unexposed disks. Exposure to hydrogen gas did not show a strong or consistent influence on the coefficient of friction observed. There was an observed trend in the wear response that appears to be the combined effect of hydrogen gas exposure, test temperature and normal load. Hydrogen gas exposure in combination with ambient test temperatures and low load show a general increase in the specific wear rate while a high load affect is minimized or possibly reversed, resulting in a decrease in the specific wear rate. Hydrogen gas exposure appears to have the opposite correlation to normal load at low temperatures in which a decrease in the specific wear rate is observed at low loads and a minimized effect or possible increase in specific wear rate is observed at high normal loads.

Among all tests, the wear mechanisms were plowing and adhesion, plowing as the dominant mechanism. Hydrogen gas exposure appeared to induce a slight increase in the amount of general adhesion at both loads and under both test temperatures. An increased normal load caused deeper, more parallel grooves in ambient temperature

tests. An unexpected finding is that the combination of high load and low temperature induced a wear pattern similar to a traditional stick-slip mechanism that has crests and troughs along the wear track. This wear pattern was found to a much lesser degree at low load tests and amplified in high load tests. The trend of increase adhesion with hydrogen gas exposure created the most severe example of this wear pattern. This behavior may be due to a change in the material deformation mechanism from dislocation motion to deformation twinning or due to wear particle interaction that occurs at low temperatures.

# CHAPTER VIII

# FUTURE RECOMMENDATIONS

This research has provided evidence that there is distinct change in the way that Ti-6Al-4V wears at lower temperature and that hydrogen gas exposure appears to increase adhesive wear. In addition, this research has introduced a new and successful method to perform tribological testing at low temperature by cooling an environment with the use of liquid nitrogen injection. Both of these areas have ample room for future studies in order to understand the role of temperature and hydrogen exposure on the wear of materials. More materials can be tested using similar low temperature methods to gain a better understanding of how wear typically changes in response to low temperature, especially how the role of the ductile to brittle transition in some metals will change the wear mechanisms and the friction response. Understanding the effect of the ductile to brittle transition due to thermal changes will also help gain insight into the similarities and differences in the role that hydrogen plays in the wear response of materials. Developing a testing method to perform tribological investigations in a hydrogen gas environment would help to better simulate the actual working conditions of future material in a hydrogen contacting application.

To expand the information known about materials that may be used with future hydrogen controlling or containing components there are many opportunities to expand on the methods used in this research. An investigation into the hardening mechanisms of Ti-6Al-4V under load and at low temperature is necessary to help explain the wear response observed in Group 2 and 4 testing at low temperature. Phase analysis,

microhardness testing and an analysis of the deformation mechanisms is recommended for future work. Tribological testing of materials over a range of known concentrations of hydrogen and at known surface penetration depths will provide a much better understanding of the role of hydrogen in the tribological response.

## REFERENCES


[1] R. L. Tobler, *Proceedings of the 1979 Cryogenic Engineering Conference*, 1979, p. 66-76.

[2] G. W. Stachowiak and A. W. Batchelor, *Engineering Tribology*, 3rd ed. (Elsevier Butterworth-Heinemann, Amsterdam; Boston, 2005).

[3] *Wear: Materials, Mechanisms and Practice*, edited by G. W. Stachowiak (Wiley, Chichester, England; Hoboken, NJ, 2005).

[4] R. G. Bayer, *Mechanical Wear Fundamentals and Testing*, 2nd ed. (M. Dekker, New York, 2004).

[5] R. G. Bayer, *Engineering Design for Wear,* 2nd ed. (M. Dekker, New York, 2004).

[6] T. M. Flynn, *Cryogenic Engineering*, 2nd, Revised and Expanded ed. (Marcel Dekker, New York, 2005), p. 257-299.

[7] A. Iwabuchi, Y. Tatsuyanagi, K. Yoshida, and M. Sugimoto, Wear **159,** 107-114 (1992).

[8] W. Hübner, Tribology International **34,** 231-236 (2001).

[9] W. Hübner, T. Gradt, T. Schneider, and H. Börner, Wear **216,** 150-159 (1998).

[10] J. L. Bozet, Wear **162-164,** 1025-1028 (1993).

[11] G. Theiler, W. Hübner, T. Gradt, P. Klein, and K. Friedrich, Tribology International **35,** 449-458 (2002).

[12] J.-L. Lizon, Advances in Cryogenic Engineering (Materials) **36,** 7 (1990).

[13] T. P. Yukhno, Y. V. Vvedensky, and L. N. Sentyurikhina, Tribology International **34,** 293-298 (2001).

[14] Y. L. Ostrovskaya, V. E. Strel'nitskij, V. I. Kuleba, and G. D. Gamulya, Tribology International **34,** 255-263 (2001).

[15] T. Gradt, H. Börner, and T. Schneider, Tribology International **34,** 225-230 (2001).

[16] S. Paul, N. R. Dhar, and A. B. Chattopadhyay, Journal of Materials Processing Technology **116,** 44-48 (2001).

[17] S. Hong, Y. Ding, and W. Jeong, International Journal of Machine Tools and Manufacture **41,** 2271-2285 (2001).

[18] S. Hong, Y. Ding, and J. Jeong, Machining Science & Technology **6,** 235-250 (2002).

[19] E. E. Bisson and W. J. Anderson, Advanced Bearing Technology, NASA-SP-38. (NASA, Washington, D.C., 1964).

[20] T. Gradt, T. Schneider, W. Hübner, and H. Börner, International Journal of Hydrogen Energy **23,** 397-403 (1998).

[21] F. P. Bowden and T. H. C. Childs, Nature **219,** 1333-1335 (1968).

[22] Y. L. Ostrovskaya, T. P. Yukhno, G. D. Gamulya, Y. V. Vvedenskij, and V. I. Kuleba, Tribology International **34,** 265-276 (2001).

[23] I. M. Hutchings, Journal of Physics D: Applied Physics**,** A212 (1992).

[24] A. Molinari, G. Straffelini, B. Tesi, and T. Bacci, Wear **208,** 105-112 (1997).

[25] C. G. Interrante and L. Raymond, in *Corrosion Tests and Standards: Application and Interpretation*, 2nd ed., edited by R. Baboian (ASTM International, West Conshohocken, PA, 2005), p. 322-340.

[26] L. Raymond, *Hydrogen Embrittlement: Prevention and Control* (ASTM, Philadelphia, PA, 1988).

[27] *Hydrogen Embrittlement Testing*, edited by L. Raymond (American Society for Testing and Materials, Philadelphia, 1972).

[28] H. Yashiro, B. Pound, N. Kumagai, and K. Tanno, Corrosion Science **40,** 781-791 (1998).

[29] X. X. Jiang, S. H. Li, C. T. Duan, and M. Li, Lubrication Engineering **46,** 529-532 (1990).

[30] D. Eliezer, E. Tal-Gutelmacher, C. E. Cross, and T. Boellinghaus, Materials Science and Engineering: A **433,** 298-304 (2006).

[31] J. Qazi, J. Rahim, F. Fores, O. Senkov, and A. Genc, Metallurgical and Materials Transactions A **32,** 2453-2463 (2001).

[32] E. Tal-Gutelmacher and D. Eliezer, JOM Journal of the Minerals, Metals and Materials Society **57,** 46-49 (2005).

[33] A. López-Suárez, J. Rickards, and R. Trejo-Luna, International Journal of Hydrogen Energy **28,** 1107-1113 (2003).

[34] L. Ma, G. Liang, J. Tan, L. Rong, and Y. Li, Journal of Materials Science and Technology **15,** 67-70 (1999).

[35] T. Ogata, in *Advances in Cryogenic Engineering: Transactions of the International Cryogenic Materials Conference*; *Vol. 54*, edited by U. Balachandran (American Institute of Physics, Japan, 2008), p. 124-131.

[36] H. Pinto, A. Pyzalla, R. Büscher, A. Fischer, K. Aßmus, and W. Hübner, Wear **259,** 424-431 (2005).

[37] R. H. Jones and G. J. Thomas, *Materials for the Hydrogen Economy* (CRC Press, Boca Raton, 2008).

[38] ASTM, *Standard Number G 99, Test Method for Wear Testing with a Pin-on-disk Apparatus* (ASTM, West Conshohocken, PA, 2006).

[39] J. E. Shigley, C. R. Mischke, and T. H. Brown, *Standard Handbook of Machine Design*, 3 ed. (McGraw-Hill, New York, 2004).

[40] R. S. Cowan and W. O. Winer, in *Friction, Lubrication, and Wear Testing*; *Vol. 18* (ASM International, 2002).

[41] ASTM, *Standard Number B 348, Specification for Titanium and Titanium Alloy Bars and Billets* (ASTM, West Conshohocken, PA, 2006).

[42] ASTM, *Standard Number G 148, Evaluation of Hydrogen Uptake, Permeation, and Transport in Metals by an Electrochemical Technique* (ASTM, West Conshohocken, PA, 2006).

[43] *Surface Engineering for Corrosion and Wear Resistance*; *Vol.*, edited by J. R. Davis (ASM International; IOM Communications, Materials Park, OH 2001).

[44] R. Baboian, *Corrosion Tests and Standards: Application and Interpretation*, 2nd ed. (ASTM International, West Conshohocken, PA, 2005).

[45] C. Azevedo, P. S. A. Bezerra, F. Esteves, C. J. B. M. Joia, and O. R. Mattos, Electrochimica Acta **44,** 4431-4442 (1999).

[46] M. J. Danielson, Corrosion Science **44,** 829-840 (2002).

[47] S. K. Yen, Corrosion Science **41,** 2031-2051 (1999).

[48] T. Ogawa, K. Yokoyama, K. Asaoka, and J. Sakai, Biomaterials **25,** 2419-2425 (2004).

[49] T. Ogawa, K. Yokoyama, K. Asaoka, and J. Sakai, Journal of Alloys and Compounds **396,** 269-274 (2005).

[50] C. L. Briant, Z. F. Wang, and N. Chollocoop, Corrosion Science **44,** 1875-1888 (2002).

[51] G. Welsch, R. Boyer, and E. W. Collings, *Materials Properties Handbook: Titanium Alloys* (ASM International, Materials Park, OH, 1994).

[52] *Alloy Digest, Filing Code CER4* (ASM International, 2002).

[53] D. Bettge and J. Starcevic, Wear **254,** 195-202 (2003).

[54] M. Chandrasekaran, A. W. Batchelor, and N. L. Loh, Journal of Materials Science **35,** 1597-1602 (2000).

# APPENDIX A

Group 1 – Room Temperature, Non-Exposed, Disks 1-3

| | |
|---|---|
| Nominal Temperature | Room Temp |
| Material | Ti-6Al-4V |
| Load (N) | 10 |
| H2 Exposed | No |
| Disk | 1 |
| Ball | 1 |
| Duration (min) | 3 |
| Distance (m) | 10 |
| Wear Track Radius (mm) | 10 |
| Wear Track Width (mm) | 0.625 |
| Ball Radius (mm) | 3.175 |
| Average μ | 0.31 |
| Steady State μ | 0.28 |
| Wear Volume (mm^3) | 0.4029 |
| Specific Wear Rate (mm^3/Nm) | 4.0288E-03 |

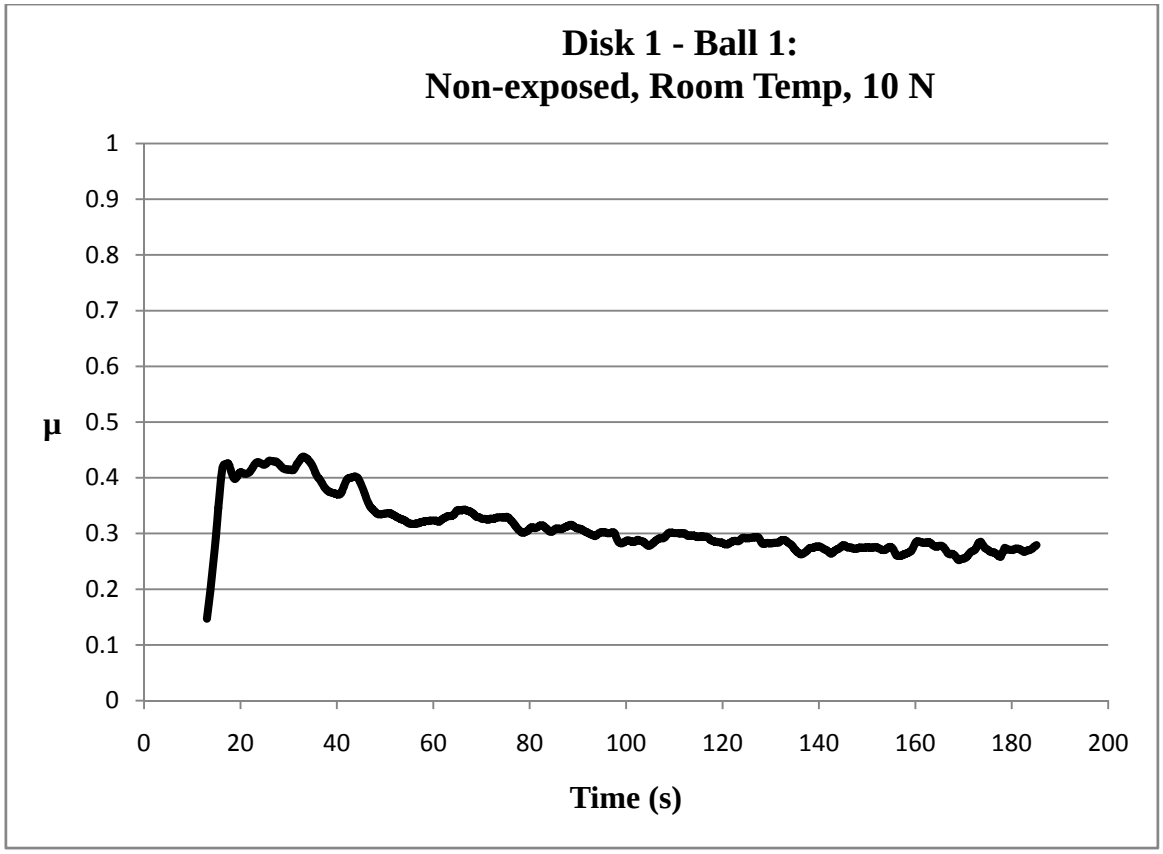
Disk 1 - Ball 1:
Non-exposed, Room Temp, 10 N
μ
1
0.9
0.8
0.7
0.6
0.5
0.4
0.3
0.2
0.1
0
0
20
40
60
80
100
120
140
160
180
200
Time (s)

| | |
|---|---|
| Nominal Temperature | Room Temp |
| Material | Ti-6Al-4V |
| Load (N) | 10 |
| H2 Exposed | No |
| Disk | 2 |
| Ball | 2 |
| Duration (min) | 3 |
| Distance (m) | 10 |
| Wear Track Radius (mm) | 10 |
| Wear Track Width (mm) | 0.665 |
| Ball Radius (mm) | 3.175 |
| Average μ | 0.34 |
| Steady State μ | 0.33 |
| Wear Volume (mm^3) | 0.4860 |
| Specific Wear Rate (mm^3/Nm) | 4.8599E-03 |

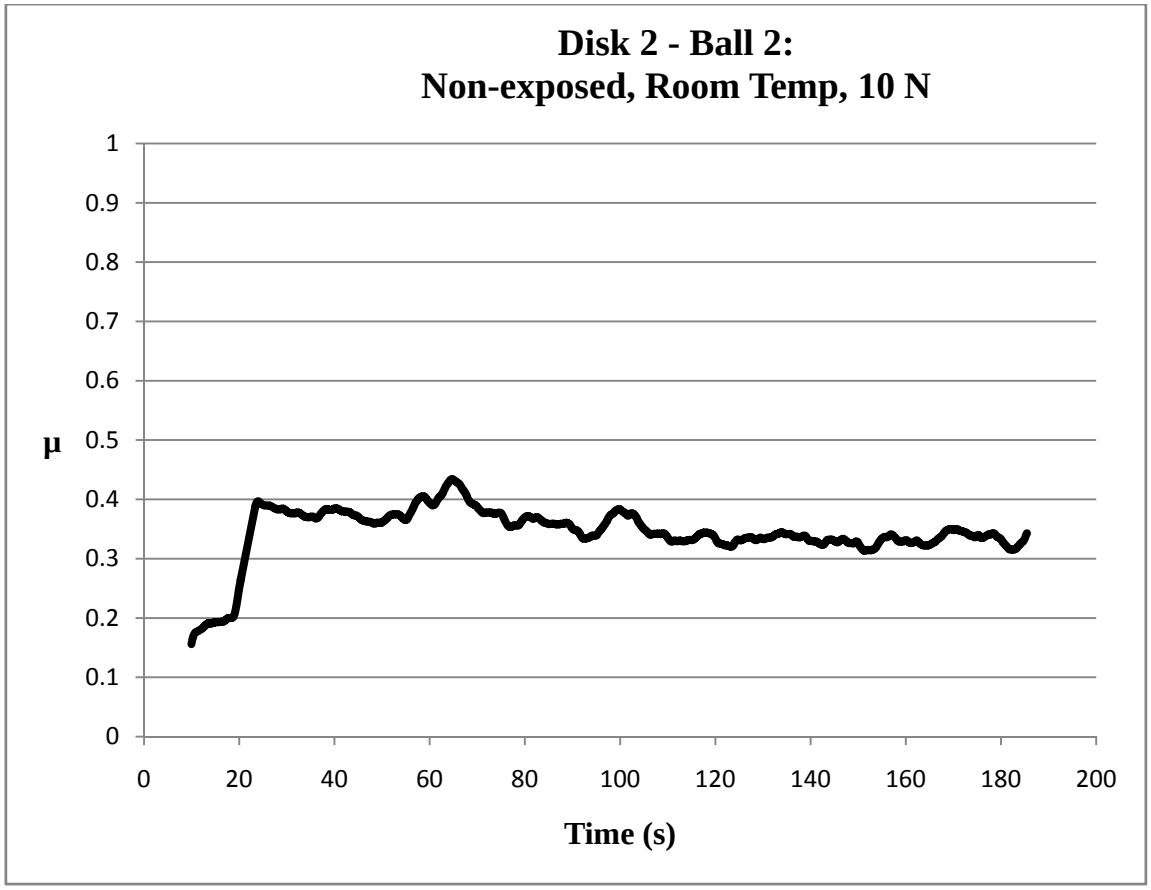
Disk 2 - Ball 2:
Non-exposed, Room Temp, 10 N
μ
1
0.9
0.8
0.7
0.6
0.5
0.4
0.3
0.2
0.1
0
0
20
40
60
80
100
120
140
160
180
200
Time (s)

| | |
|---|---|
| Nominal Temperature | Room Temp |
| Material | Ti-6Al-4V |
| Load (N) | 10 |
| H2 Exposed | No |
| Disk | 3 |
| Ball | 3 |
| Duration (min) | 3 |
| Distance (m) | 10 |
| Wear Track Radius (mm) | 10 |
| Wear Track Width (mm) | 0.658 |
| Ball Radius (mm) | 3.175 |
| Average μ | 0.34 |
| Steady State μ | 0.32 |
| Wear Volume (mm^3) | 0.4706 |
| Specific Wear Rate (mm^3/Nm) | 4.7055E-03 |

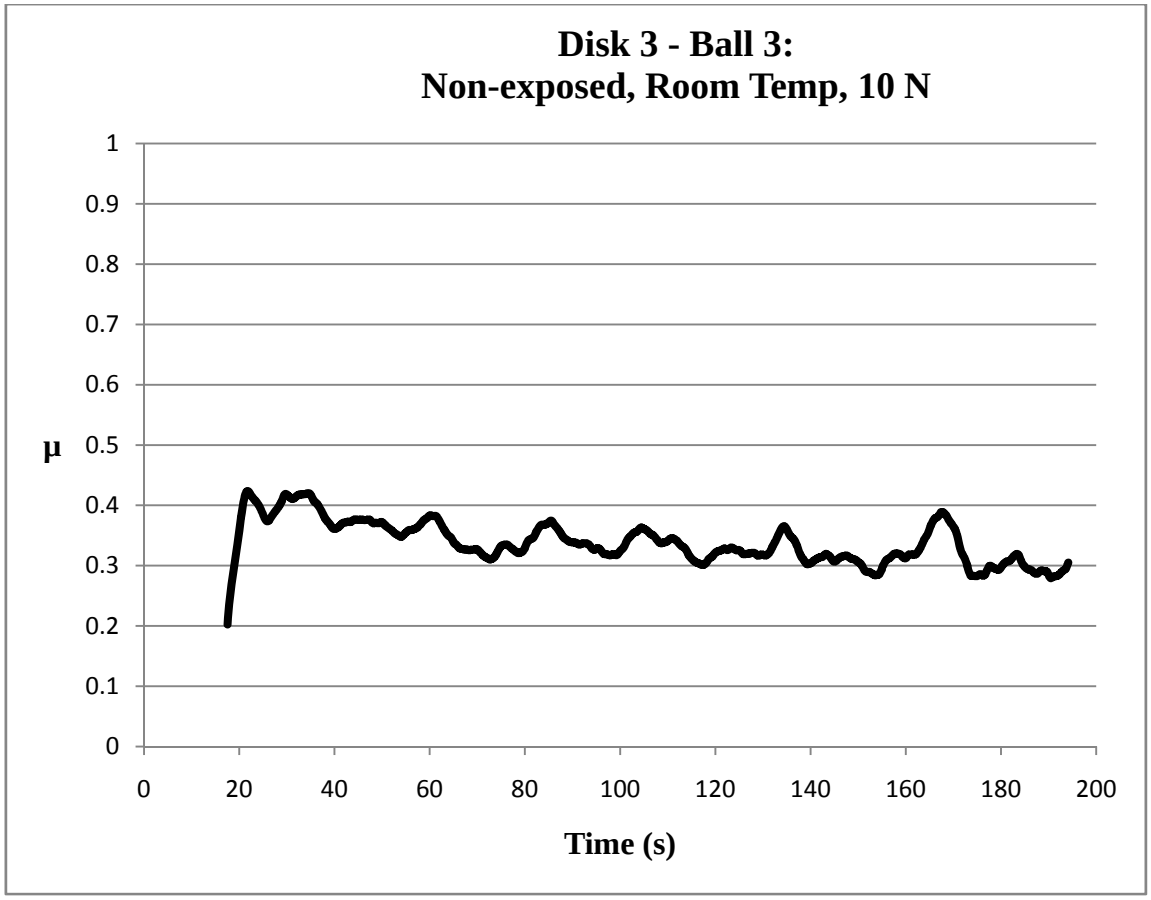
Disk 3 - Ball 3:
Non-exposed, Room Temp, 10 N
μ
1
0.9
0.8
0.7
0.6
0.5
0.4
0.3
0.2
0.1
0
0
20
40
60
80
100
120
140
160
180
200
Time (s)

| | |
|---|---|
| Nominal Temperature | Room Temp |
| Material | Ti-6Al-4V |
| Load (N) | 20 |
| H2 Exposed | No |
| Disk | 1 |
| Ball | 4 |
| Duration (min) | 3 |
| Distance (m) | 10 |
| Wear Track Radius (mm) | 15 |
| Wear Track Width (mm) | 0.755 |
| Ball Radius (mm) | 3.175 |
| Average μ | 0.53 |
| Steady State μ | 0.52 |
| Wear Volume (mm^3) | 1.0704 |
| Specific Wear Rate (mm^3/Nm) | 5.3521E-03 |

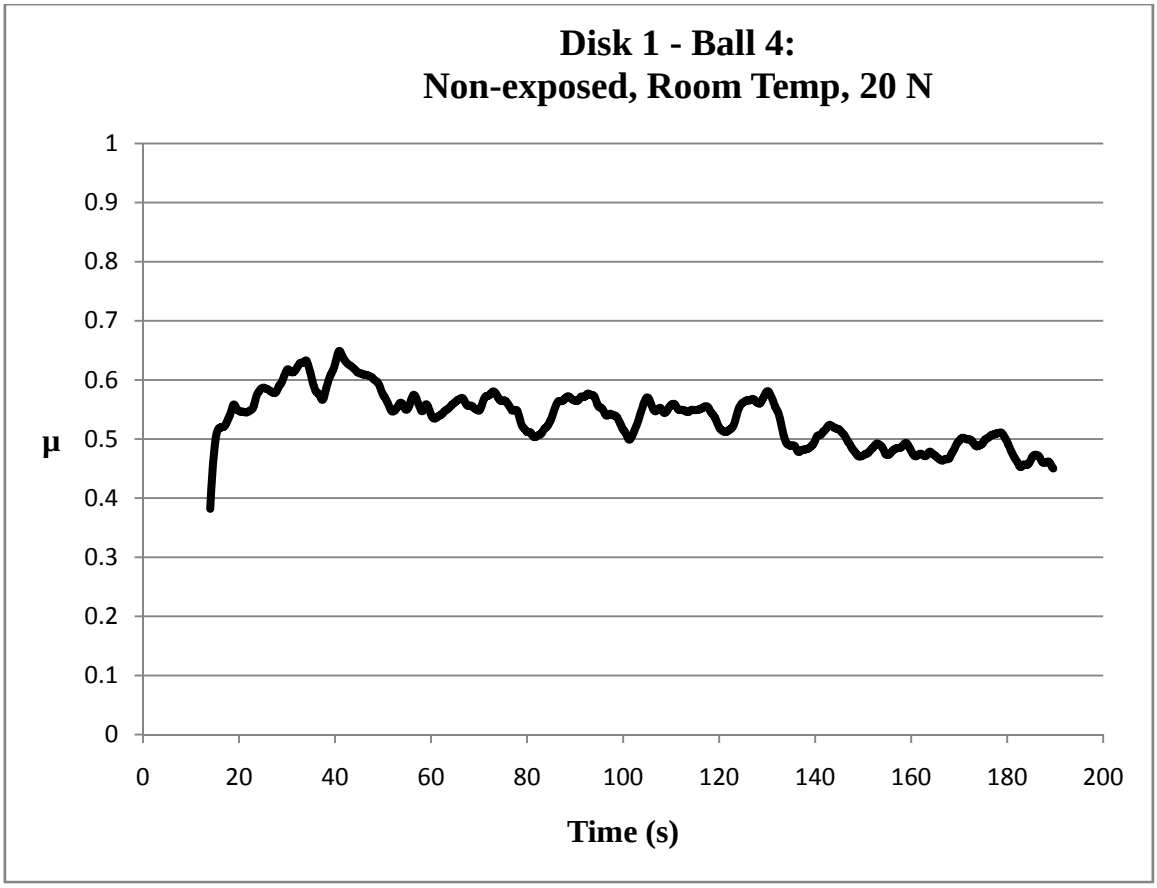
Disk 1 - Ball 4:
Non-exposed, Room Temp, 20 N
μ
1
0.9
0.8
0.7
0.6
0.5
0.4
0.3
0.2
0.1
0
0
20
40
60
80
100
120
140
160
180
200
Time (s)

| | |
|---|---|
| Nominal Temperature | Room Temp |
| Material | Ti-6Al-4V |
| Load (N) | 20 |
| H2 Exposed | No |
| Disk | 2 |
| Ball | 5 |
| Duration (min) | 3 |
| Distance (m) | 10 |
| Wear Track Radius (mm) | 15 |
| Wear Track Width (mm) | 0.886 |
| Ball Radius (mm) | 3.175 |
| Average μ | 0.58 |
| Steady State μ | 0.53 |
| Wear Volume (mm^3) | 1.7324 |
| Specific Wear Rate (mm^3/Nm) | 8.6621E-03 |

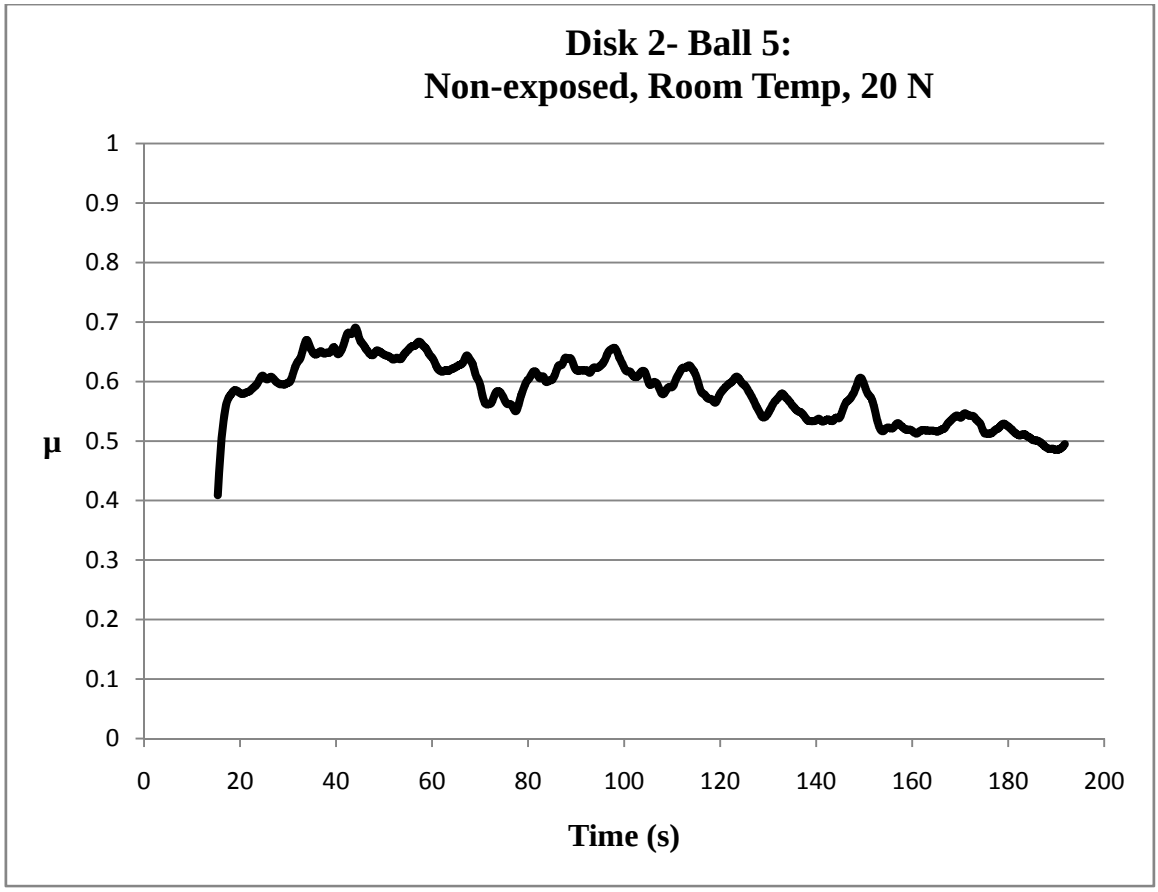
Disk 2- Ball 5:
Non-exposed, Room Temp, 20 N
μ
1
0.9
0.8
0.7
0.6
0.5
0.4
0.3
0.2
0.1
0
0
20
40
60
80
100
120
140
160
180
200
Time (s)

| | |
|---|---|
| Nominal Temperature | Room Temp |
| Material | Ti-6Al-4V |
| Load (N) | 20 |
| H2 Exposed | No |
| Disk | 3 |
| Ball | 6 |
| Duration (min) | 3 |
| Distance (m) | 10 |
| Wear Track Radius (mm) | 15 |
| Wear Track Width (mm) | 0.789 |
| Ball Radius (mm) | 3.175 |
| Average μ | 0.56 |
| Steady State μ | 0.48 |
| Wear Volume (mm^3) | 1.2198 |
| Specific Wear Rate (mm^3/Nm) | 6.0990E-03 |

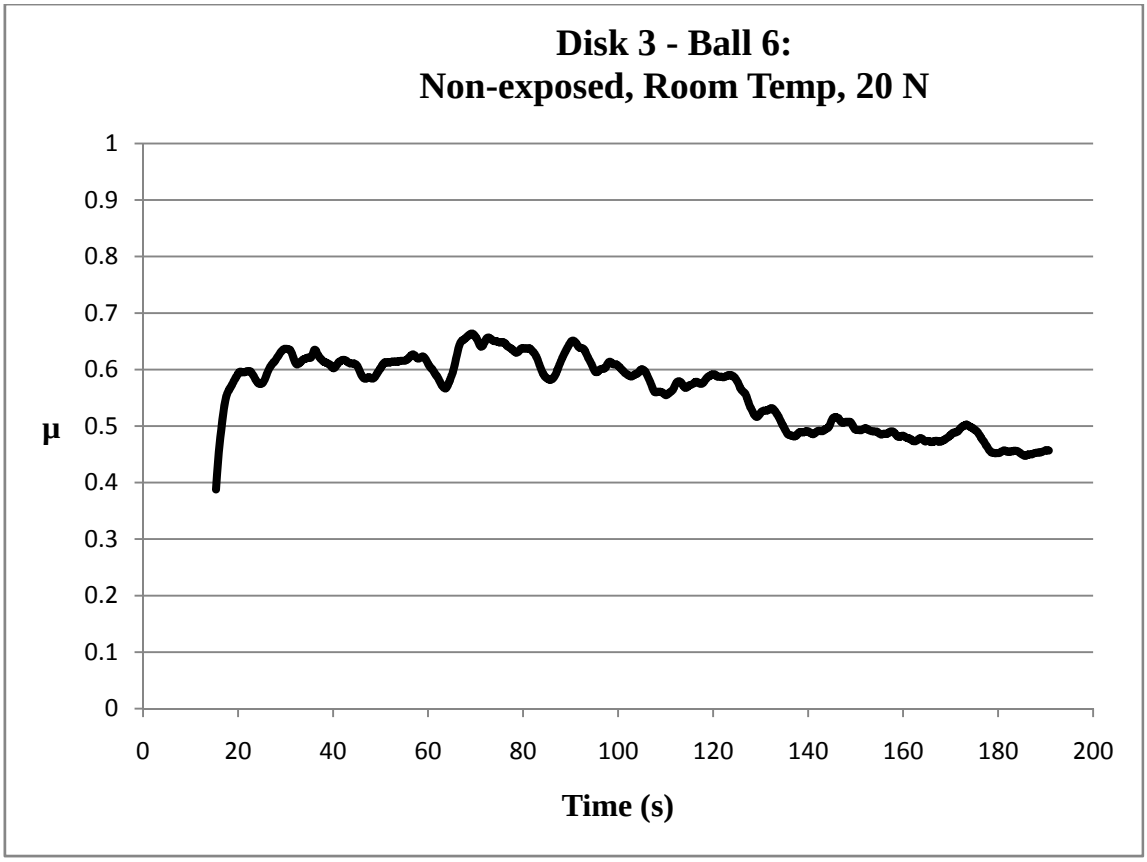
Disk 3 - Ball 6:
Non-exposed, Room Temp, 20 N
μ
1
0.9
0.8
0.7
0.6
0.5
0.4
0.3
0.2
0.1
0
0
20
40
60
80
100
120
140
160
180
200
Time (s)

Group 2 – Low Temperature, Non-Exposed, Disks 4-6

| | |
|---|---|
| Nominal Temperature | Low Temp |
| Material | Ti-6Al-4V |
| Load (N) | 10 |
| H2 Exposed | No |
| Disk | 4 |
| Ball | 7 |
| Duration (min) | 3 |
| Distance (m) | 10 |
| Wear Track Radius (mm) | 10 |
| Wear Track Width (mm) | 0.632 |
| Ball Radius (mm) | 3.175 |
| Average μ | 0.44 |
| Steady State μ | 0.33 |
| Wear Volume (mm^3) | 0.4180 |
| Specific Wear Rate (mm^3/Nm) | 4.1797E-03 |

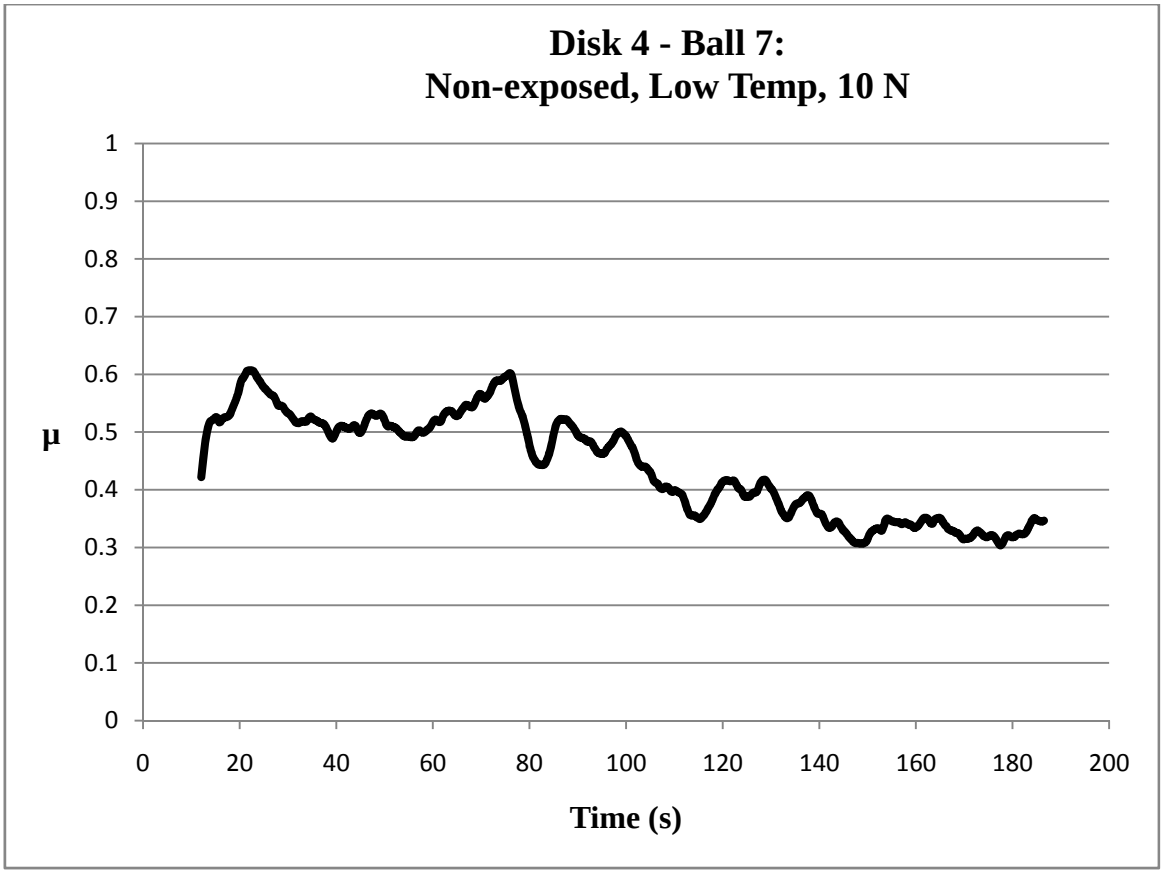
Disk 4 - Ball 7:
Non-exposed, Low Temp, 10 N
μ
1
0.9
0.8
0.7
0.6
0.5
0.4
0.3
0.2
0.1
0
0
20
40
60
80
100
120
140
160
180
200
Time (s)

| | |
|---|---|
| Nominal Temperature | Low Temp |
| Material | Ti-6Al-4V |
| Load (N) | 10 |
| H2 Exposed | No |
| Disk | 5 |
| Ball | 8 |
| Duration (min) | 3 |
| Distance (m) | 10 |
| Wear Track Radius (mm) | 10 |
| Wear Track Width (mm) | 0.568 |
| Ball Radius (mm) | 3.175 |
| Average μ | 0.33 |
| Steady State μ | 0.23 |
| Wear Volume (mm^3) | 0.3037 |
| Specific Wear Rate (mm^3/Nm) | 3.0366E-03 |

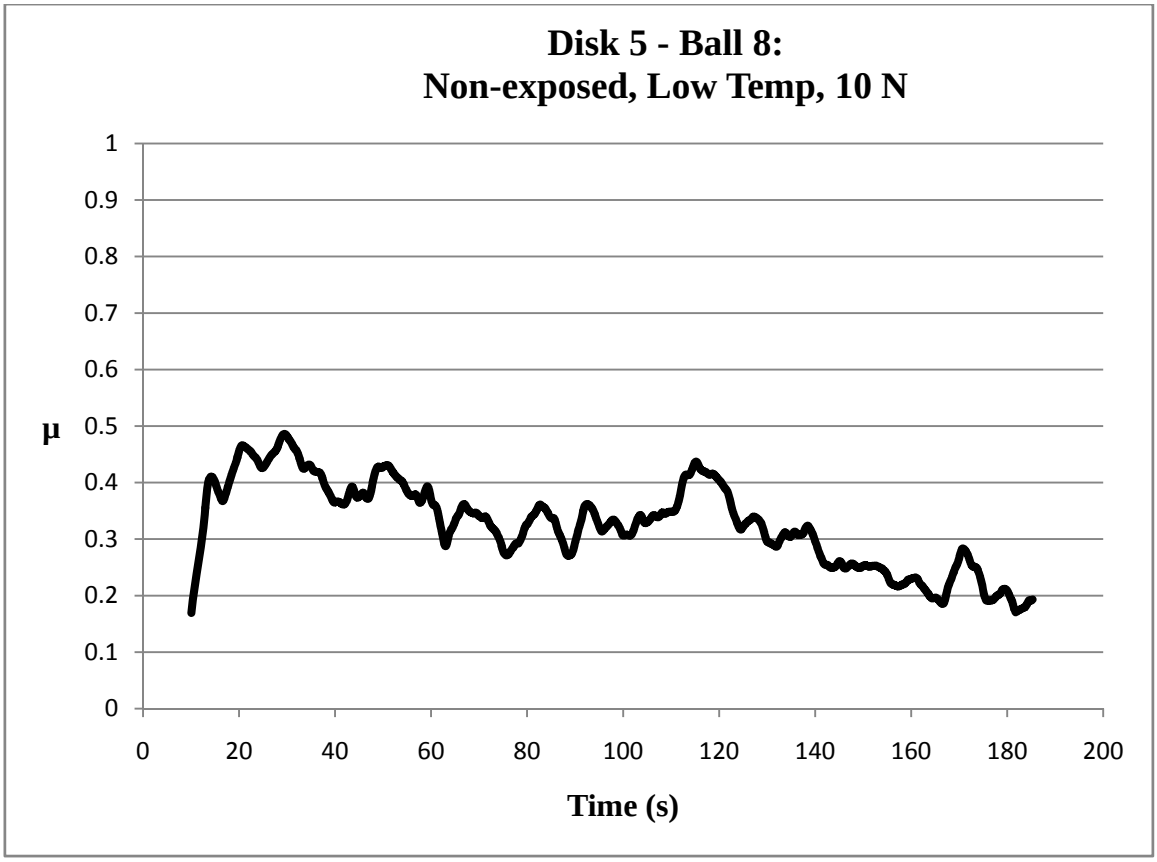
Disk 5 - Ball 8:
Non-exposed, Low Temp, 10 N
μ
1
0.9
0.8
0.7
0.6
0.5
0.4
0.3
0.2
0.1
0
0
20
40
60
80
100
120
140
160
180
200
Time (s)

| | |
|---|---|
| Nominal Temperature | Low Temp |
| Material | Ti-6Al-4V |
| Load (N) | 10 |
| H2 Exposed | No |
| Disk | 6 |
| Ball | 9 |
| Duration (min) | 3 |
| Distance (m) | 10 |
| Wear Track Radius (mm) | 10 |
| Wear Track Width (mm) | 0.698 |
| Ball Radius (mm) | 3.175 |
| Average μ | 0.40 |
| Steady State μ | 0.30 |
| Wear Volume (mm^3) | 0.5618 |
| Specific Wear Rate (mm^3/Nm) | 5.6179E-03 |

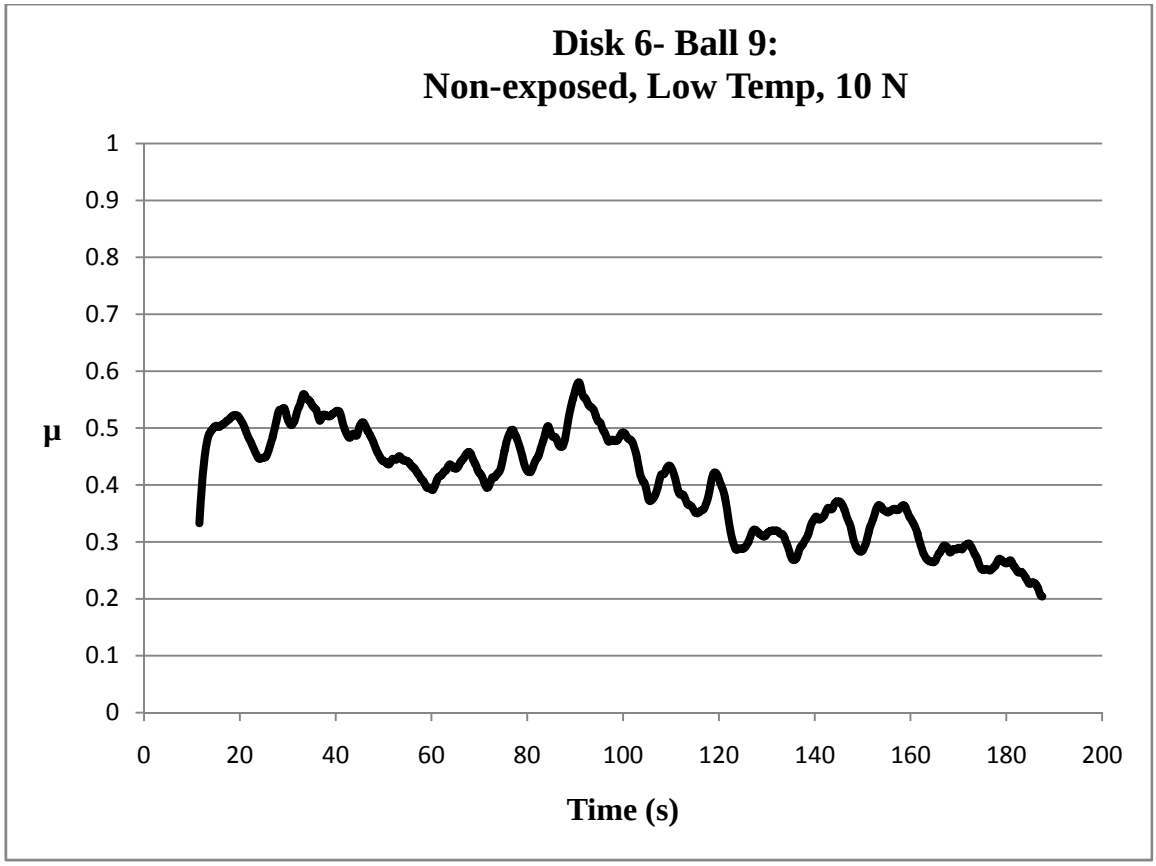
Disk 6- Ball 9:
Non-exposed, Low Temp, 10 N
μ
1
0.9
0.8
0.7
0.6
0.5
0.4
0.3
0.2
0.1
0
0
20
40
60
80
100
120
140
160
180
200
Time (s)

| | |
|---|---|
| Nominal Temperature | Low Temp |
| Material | Ti-6Al-4V |
| Load (N) | 20 |
| H2 Exposed | No |
| Disk | 4 |
| Ball | 10 |
| Duration (min) | 3 |
| Distance (m) | 10 |
| Wear Track Radius (mm) | 15 |
| Wear Track Width (mm) | 0.584 |
| Ball Radius (mm) | 3.175 |
| Average μ | 0.43 |
| Steady State μ | 0.38 |
| Wear Volume (mm^3) | 0.4928 |
| Specific Wear Rate (mm^3/Nm) | 2.4642E-03 |

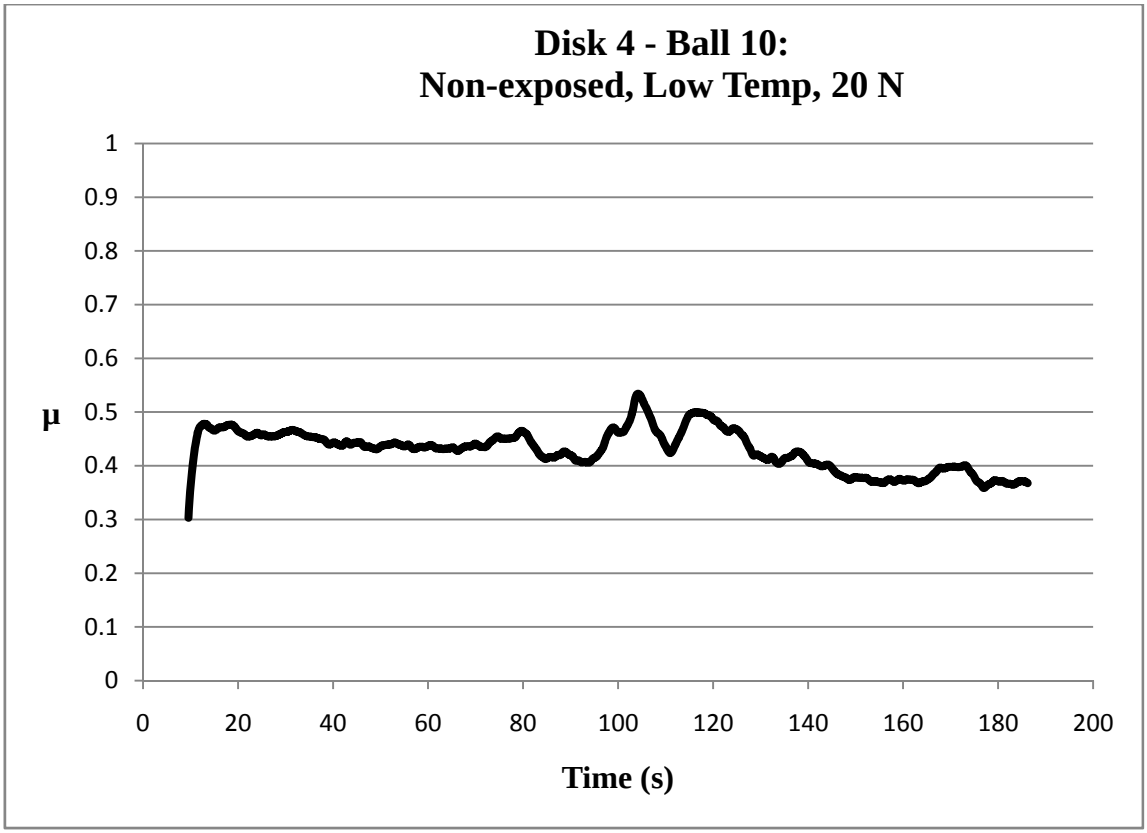
Disk 4 - Ball 10:
Non-exposed, Low Temp, 20 N
μ
1
0.9
0.8
0.7
0.6
0.5
0.4
0.3
0.2
0.1
0
0
20
40
60
80
100
120
140
160
180
200
Time (s)

| | |
|---|---|
| Nominal Temperature | Low Temp |
| Material | Ti-6Al-4V |
| Load (N) | 20 |
| H2 Exposed | No |
| Disk | 5 |
| Ball | 11 |
| Duration (min) | 3 |
| Distance (m) | 10 |
| Wear Track Radius (mm) | 15 |
| Wear Track Width (mm) | 0.590 |
| Ball Radius (mm) | 3.175 |
| Average μ | 0.41 |
| Steady State μ | 0.37 |
| Wear Volume (mm^3) | 0.5086 |
| Specific Wear Rate (mm^3/Nm) | 2.5432E-03 |

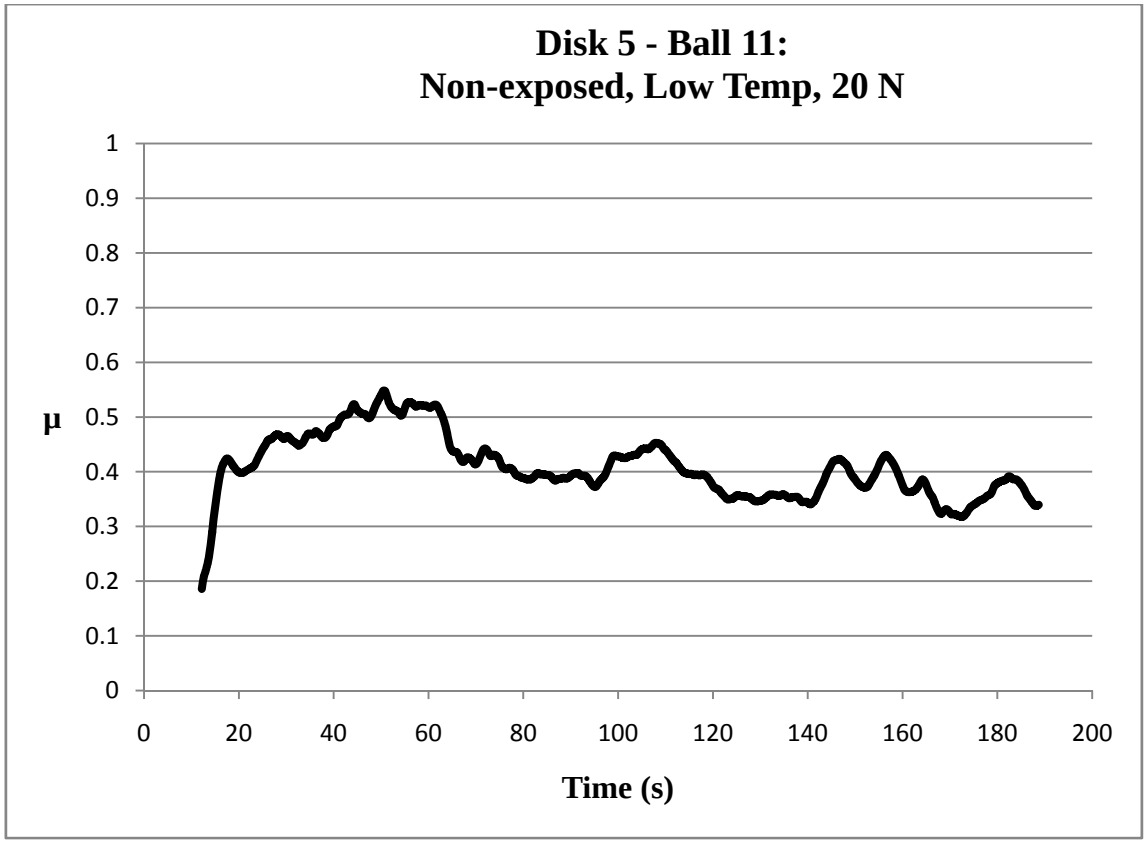
Disk 5 - Ball 11:
Non-exposed, Low Temp, 20 N
μ
1
0.9
0.8
0.7
0.6
0.5
0.4
0.3
0.2
0.1
0
0
20
40
60
80
100
120
140
160
180
200
Time (s)

| | |
|---|---|
| Nominal Temperature | Low Temp |
| Material | Ti-6Al-4V |
| Load (N) | 20 |
| H2 Exposed | No |
| Disk | 6 |
| Ball | 12 |
| Duration (min) | 3 |
| Distance (m) | 10 |
| Wear Track Radius (mm) | 15 |
| Wear Track Width (mm) | 0.634 |
| Ball Radius (mm) | 3.175 |
| Average μ | 0.38 |
| Steady State μ | 0.36 |
| Wear Volume (mm^3) | 0.6335 |
| Specific Wear Rate (mm^3/Nm) | 3.1676E-03 |

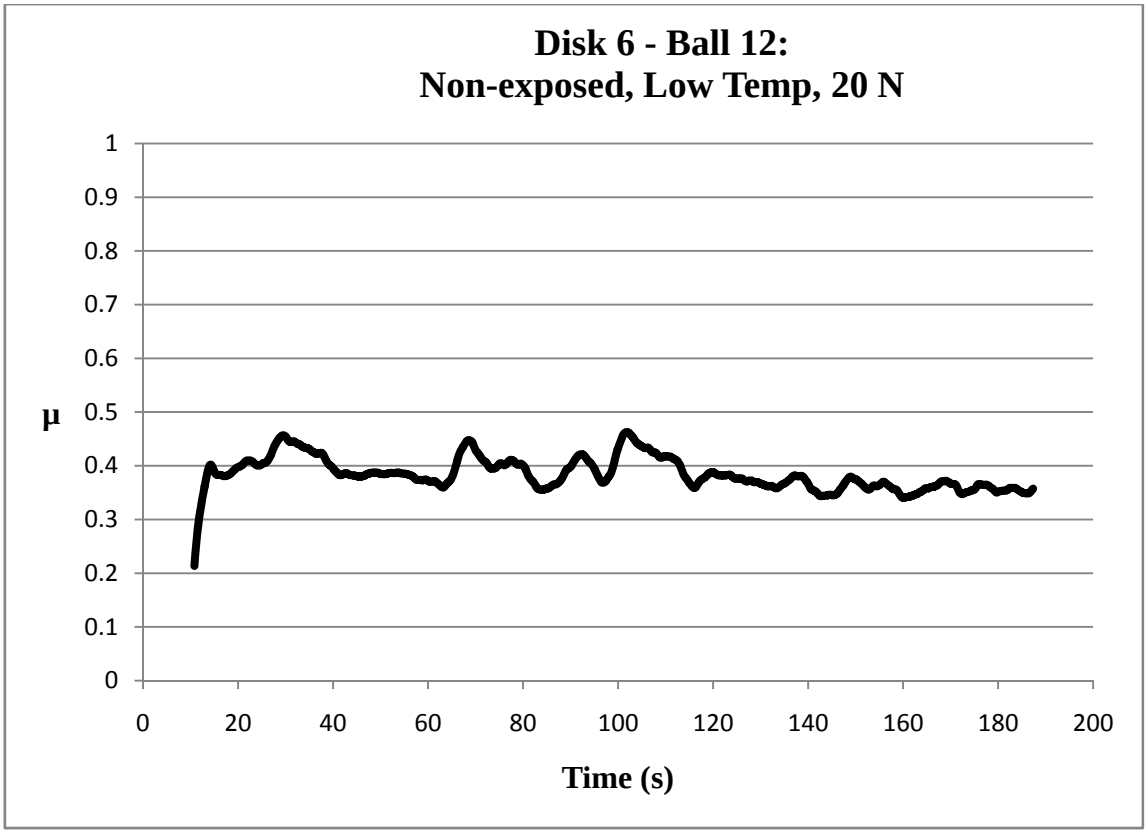
Disk 6 - Ball 12:
Non-exposed, Low Temp, 20 N
μ
1
0.9
0.8
0.7
0.6
0.5
0.4
0.3
0.2
0.1
0
0
20
40
60
80
100
120
140
160
180
200
Time (s)

Group 3 – Room Temperature, Exposed, Disks 7-9

| | |
|---|---|
| Nominal Temperature | Room Temp |
| Material | Ti-6Al-4V |
| Load (N) | 10 |
| H2 Exposed | Yes |
| Disk | 7 |
| Ball | 13 |
| Duration (min) | 3 |
| Distance (m) | 10 |
| Wear Track Radius (mm) | 10 |
| Wear Track Width (mm) | 0.742 |
| Ball Radius (mm) | 3.175 |
| Average μ | 0.40 |
| Steady State μ | 0.31 |
| Wear Volume (mm^3) | 0.6775 |
| Specific Wear Rate (mm^3/Nm) | 6.7746E-03 |

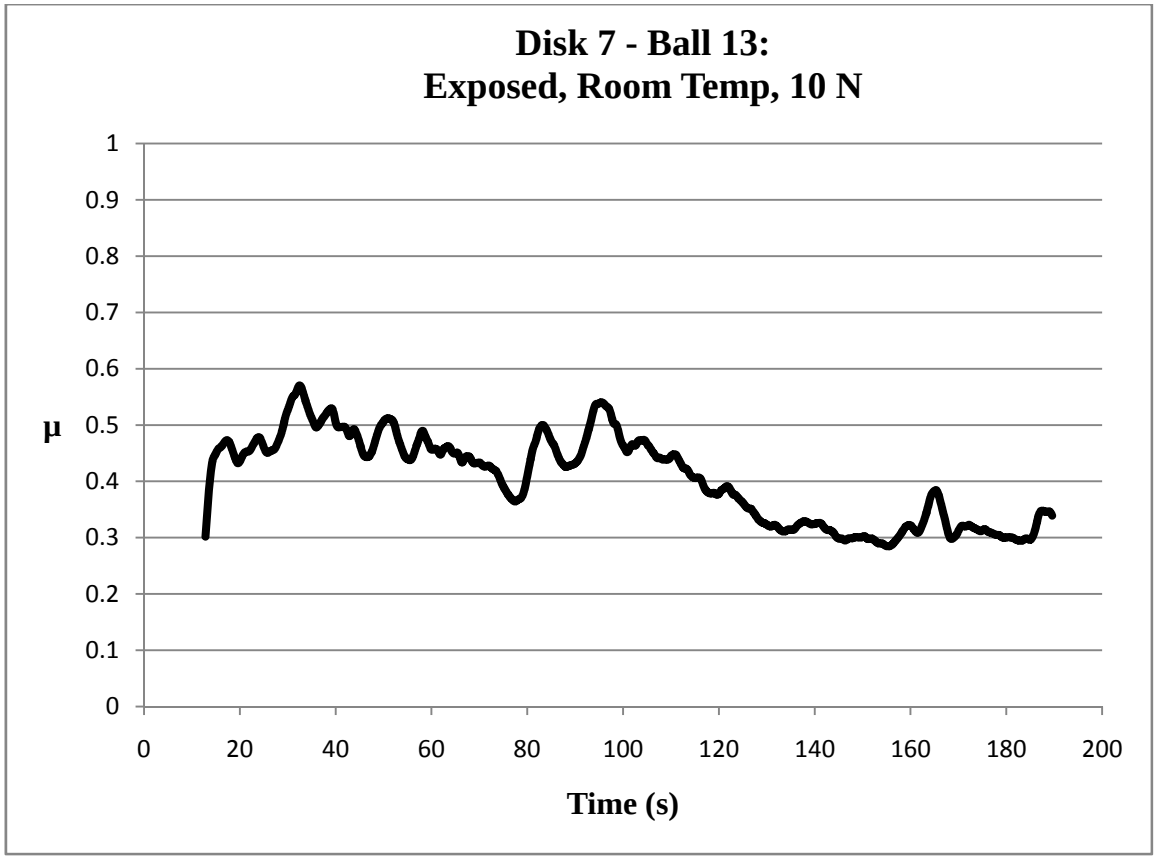
Disk 7 - Ball 13:
Exposed, Room Temp, 10 N
μ
1
0.9
0.8
0.7
0.6
0.5
0.4
0.3
0.2
0.1
0
0
20
40
60
80
100
120
140
160
180
200
Time (s)

| | |
|---|---|
| Nominal Temperature | Room Temp |
| Material | Ti-6Al-4V |
| Load (N) | 10 |
| H2 Exposed | Yes |
| Disk | 8 |
| Ball | 14 |
| Duration (min) | 3 |
| Distance (m) | 10 |
| Wear Track Radius (mm) | 10 |
| Wear Track Width (mm) | 0.644 |
| Ball Radius (mm) | 3.175 |
| Average μ | 0.47 |
| Steady State μ | 0.38 |
| Wear Volume (mm^3) | 0.4409 |
| Specific Wear Rate (mm^3/Nm) | 4.4093E-03 |

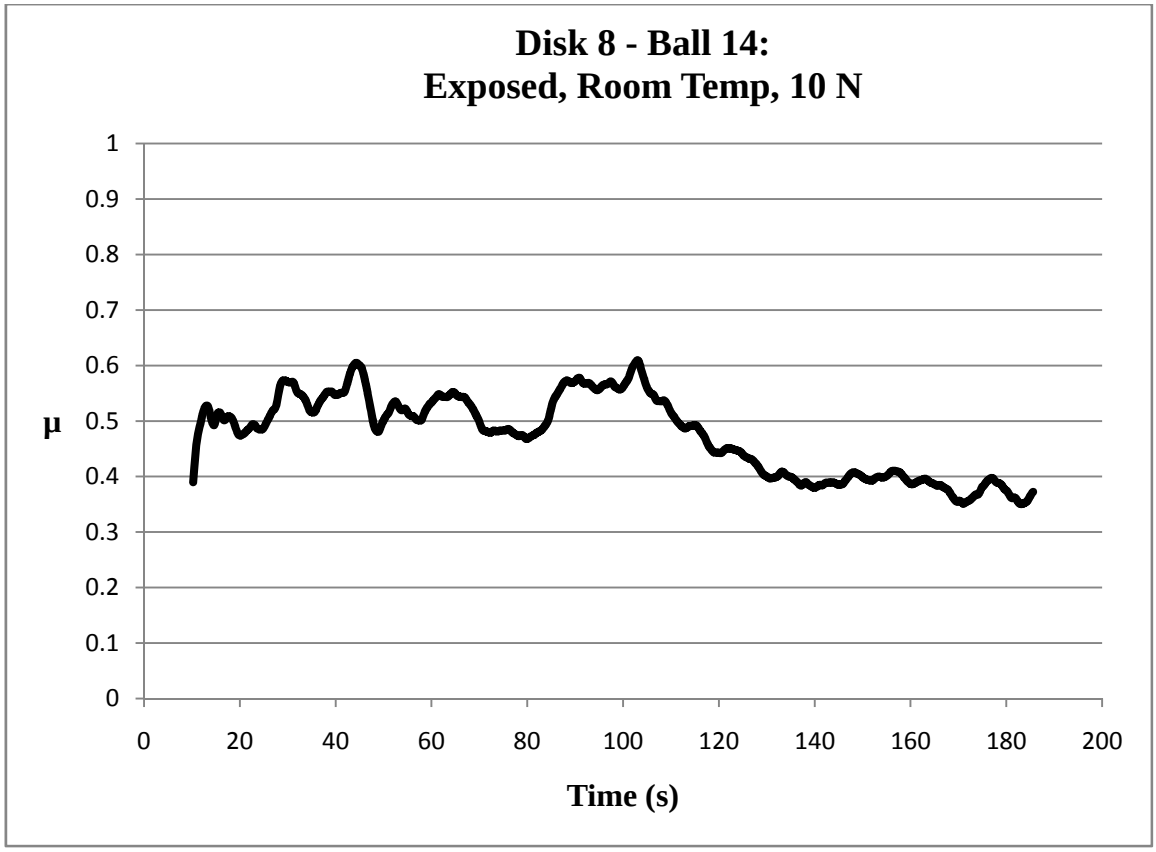
Disk 8 - Ball 14:
Exposed, Room Temp, 10 N
μ
1
0.9
0.8
0.7
0.6
0.5
0.4
0.3
0.2
0.1
0
0
20
40
60
80
100
120
140
160
180
200
Time (s)

| | |
|---|---|
| Nominal Temperature | Room Temp |
| Material | Ti-6Al-4V |
| Load (N) | 10 |
| H2 Exposed | Yes |
| Disk | 9 |
| Ball | 15 |
| Duration (min) | 3 |
| Distance (m) | 10 |
| Wear Track Radius (mm) | 10 |
| Wear Track Width (mm) | 0.674 |
| Ball Radius (mm) | 3.175 |
| Average μ | 0.49 |
| Steady State μ | 0.43 |
| Wear Volume (mm^3) | 0.5068 |
| Specific Wear Rate (mm^3/Nm) | 5.0676E-03 |

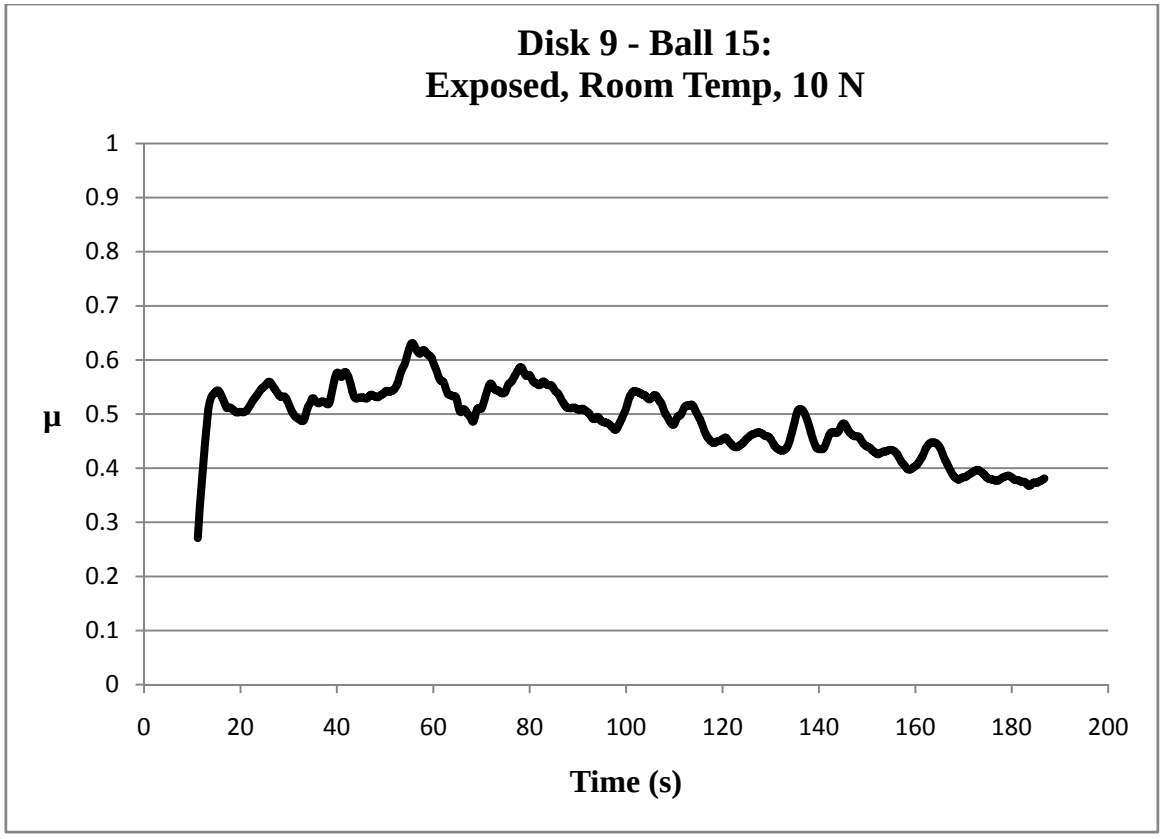
Disk 9 - Ball 15:
Exposed, Room Temp, 10 N
μ
1
0.9
0.8
0.7
0.6
0.5
0.4
0.3
0.2
0.1
0
0
20
40
60
80
100
120
140
160
180
200
Time (s)

| | |
|---|---|
| Nominal Temperature | Room Temp |
| Material | Ti-6Al-4V |
| Load (N) | 20 |
| H2 Exposed | Yes |
| Disk | 7 |
| Ball | 16 |
| Duration (min) | 3 |
| Distance (m) | 10 |
| Wear Track Radius (mm) | 15 |
| Wear Track Width (mm) | 0.839 |
| Ball Radius (mm) | 3.175 |
| Average μ | 0.53 |
| Steady State μ | 0.52 |
| Wear Volume (mm^3) | 1.4704 |
| Specific Wear Rate (mm^3/Nm) | 7.3520E-03 |

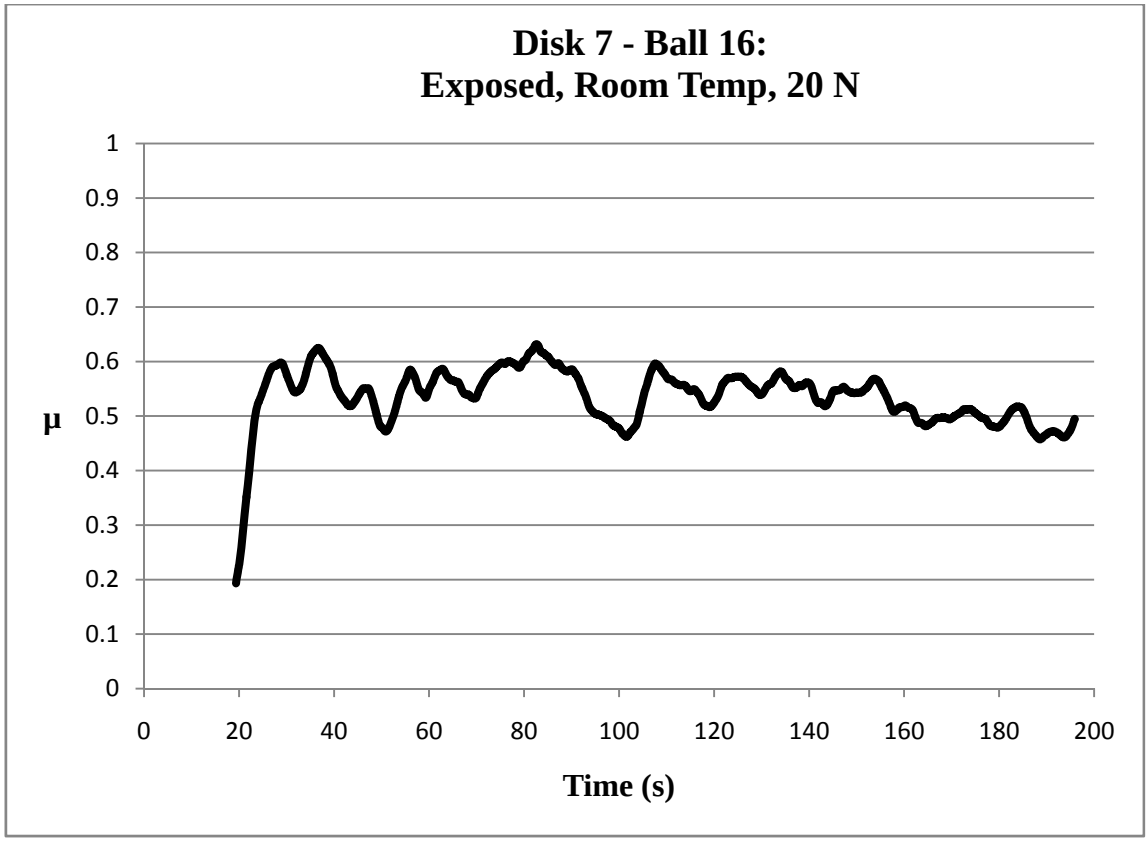
Disk 7 - Ball 16:
Exposed, Room Temp, 20 N
μ
1
0.9
0.8
0.7
0.6
0.5
0.4
0.3
0.2
0.1
0
0
20
40
60
80
100
120
140
160
180
200
Time (s)

| | |
|---|---|
| Nominal Temperature | Room Temp |
| Material | Ti-6Al-4V |
| Load (N) | 20 |
| H2 Exposed | Yes |
| Disk | 8 |
| Ball | 17 |
| Duration (min) | 3 |
| Distance (m) | 10 |
| Wear Track Radius (mm) | 15 |
| Wear Track Width (mm) | 0.750 |
| Ball Radius (mm) | 3.175 |
| Average μ | 0.50 |
| Steady State μ | 0.46 |
| Wear Volume (mm^3) | 1.0475 |
| Specific Wear Rate (mm^3/Nm) | 5.2376E-03 |

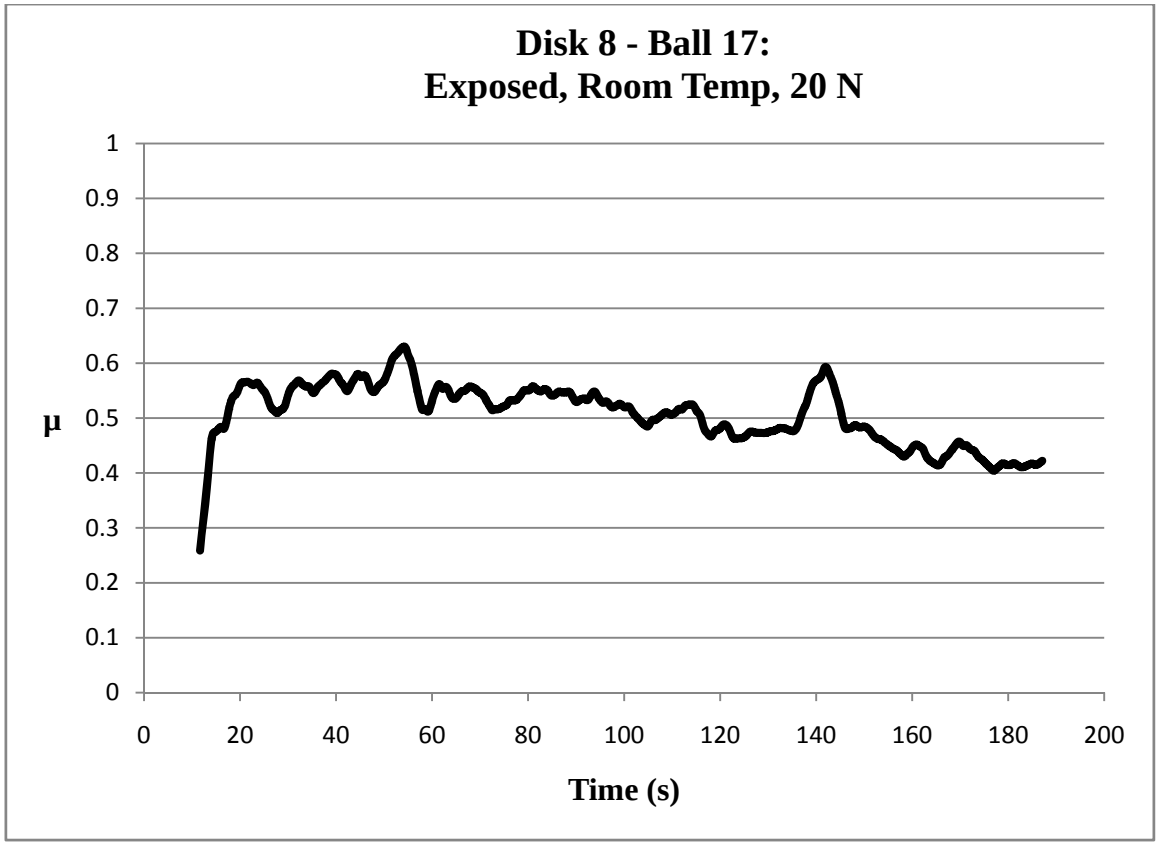
Disk 8 - Ball 17:
Exposed, Room Temp, 20 N
μ
1
0.9
0.8
0.7
0.6
0.5
0.4
0.3
0.2
0.1
0
0
20
40
60
80
100
120
140
160
180
200
Time (s)

| | |
|---|---|
| Nominal Temperature | Room Temp |
| Material | Ti-6Al-4V |
| Load (N) | 20 |
| H2 Exposed | Yes |
| Disk | 9 |
| Ball | 18 |
| Duration (min) | 3 |
| Distance (m) | 10 |
| Wear Track Radius (mm) | 15 |
| Wear Track Width (mm) | 0.767 |
| Ball Radius (mm) | 3.175 |
| Average μ | 0.53 |
| Steady State μ | 0.47 |
| Wear Volume (mm^3) | 1.1201 |
| Specific Wear Rate (mm^3/Nm) | 5.6004E-03 |

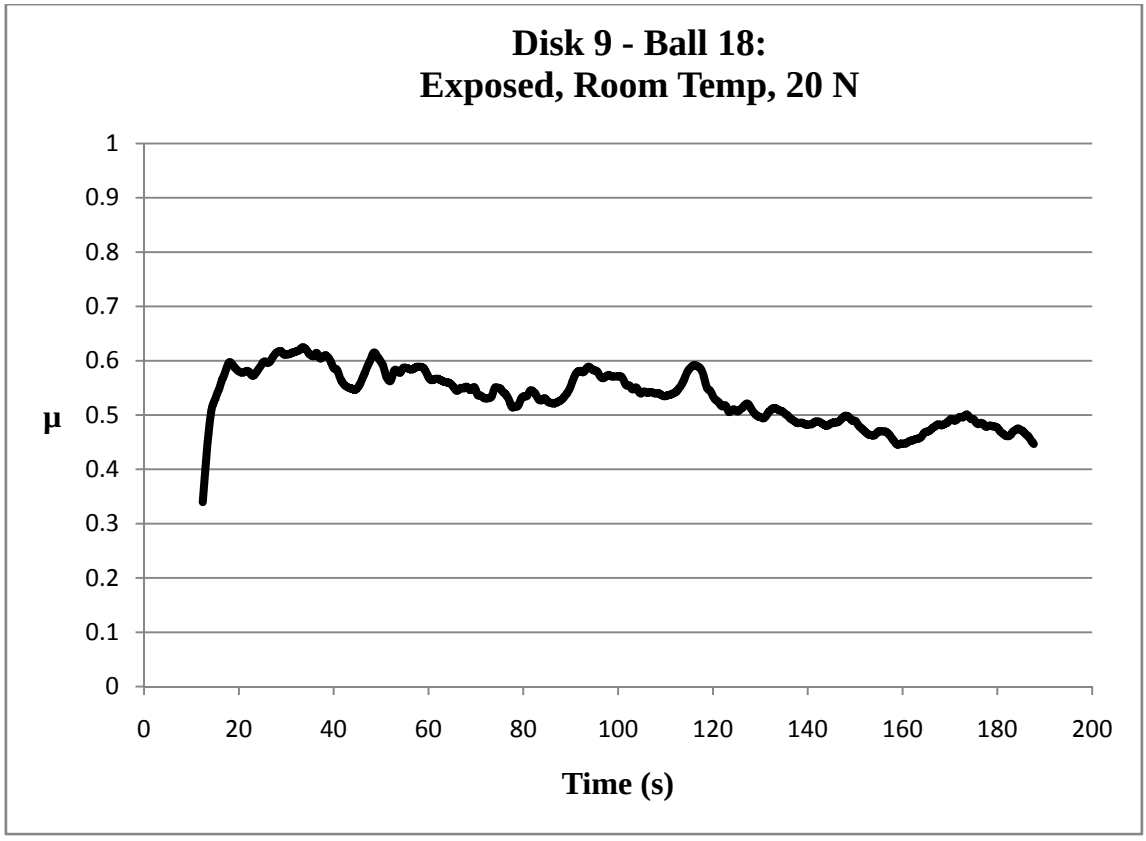
Disk 9 - Ball 18:
Exposed, Room Temp, 20 N
μ
1
0.9
0.8
0.7
0.6
0.5
0.4
0.3
0.2
0.1
0
0
20
40
60
80
100
120
140
160
180
200
Time (s)

Group 4 – Low Temperature, Exposed, Disk 10-12

| | |
|---|---|
| Nominal Temperature | Low Temp |
| Material | Ti-6Al-4V |
| Load (N) | 10 |
| H2 Exposed | Yes |
| Disk | 10 |
| Ball | 19 |
| Duration (min) | 3 |
| Distance (m) | 10 |
| Wear Track Radius (mm) | 10 |
| Wear Track Width (mm) | 0.585 |
| Ball Radius (mm) | 3.175 |
| Average μ | 0.35 |
| Steady State μ | 0.27 |
| Wear Volume (mm^3) | 0.3304 |
| Specific Wear Rate (mm^3/Nm) | 3.3043E-03 |

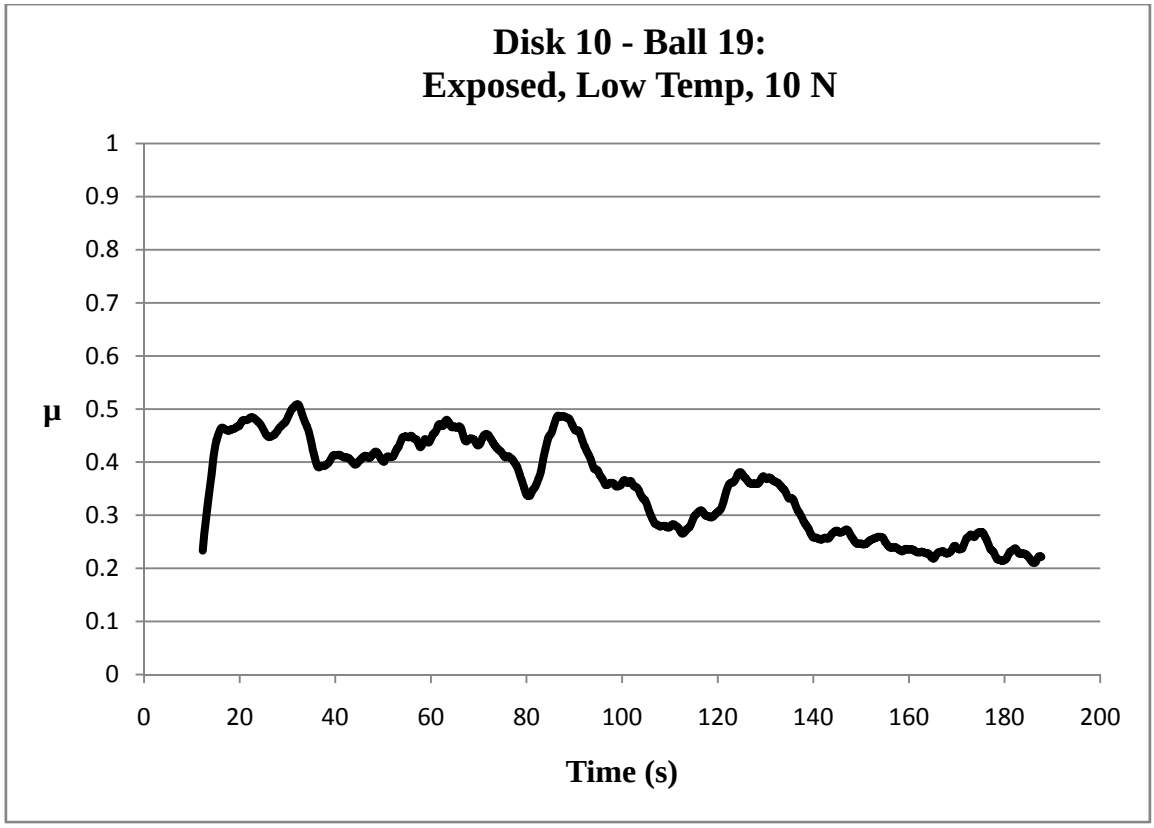
Disk 10 - Ball 19:
Exposed, Low Temp, 10 N
μ
1
0.9
0.8
0.7
0.6
0.5
0.4
0.3
0.2
0.1
0
0
20
40
60
80
100
120
140
160
180
200
Time (s)

| | |
|---|---|
| Nominal Temperature | Low Temp |
| Material | Ti-6Al-4V |
| Load (N) | 10 |
| H2 Exposed | Yes |
| Disk | 11 |
| Ball | 20 |
| Duration (min) | 3 |
| Distance (m) | 10 |
| Wear Track Radius (mm) | 10 |
| Wear Track Width (mm) | 0.596 |
| Ball Radius (mm) | 3.175 |
| Average μ | 0.36 |
| Steady State μ | 0.25 |
| Wear Volume (mm^3) | 0.3496 |
| Specific Wear Rate (mm^3/Nm) | 3.4962E-03 |

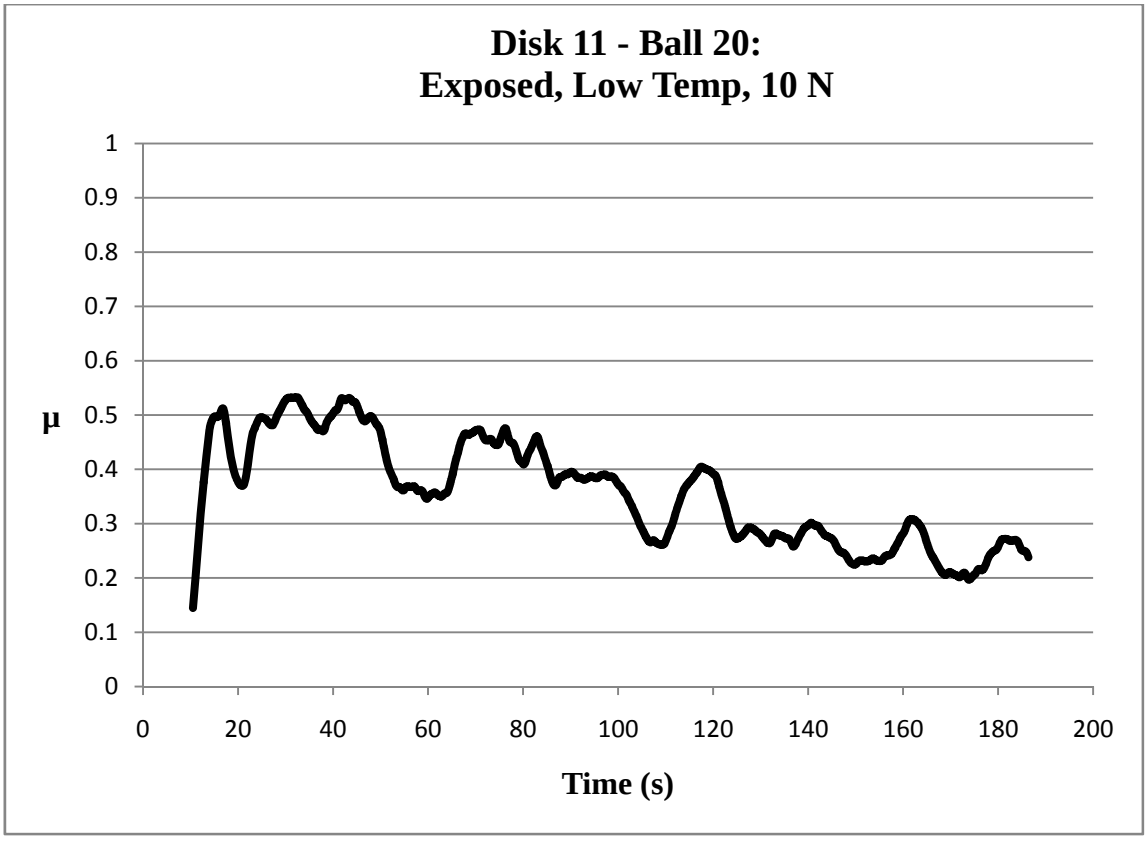
Disk 11 - Ball 20:
Exposed, Low Temp, 10 N
μ
1
0.9
0.8
0.7
0.6
0.5
0.4
0.3
0.2
0.1
0
0
20
40
60
80
100
120
140
160
180
200
Time (s)

| | |
|---|---|
| Nominal Temperature | Low Temp |
| Material | Ti-6Al-4V |
| Load (N) | 10 |
| H2 Exposed | Yes |
| Disk | 12 |
| Ball | 21 |
| Duration (min) | 3 |
| Distance (m) | 10 |
| Wear Track Radius (mm) | 10 |
| Wear Track Width (mm) | 0.575 |
| Ball Radius (mm) | 3.175 |
| Average μ | 0.34 |
| Steady State μ | 0.29 |
| Wear Volume (mm^3) | 0.3151 |
| Specific Wear Rate (mm^3/Nm) | 3.1507E-03 |

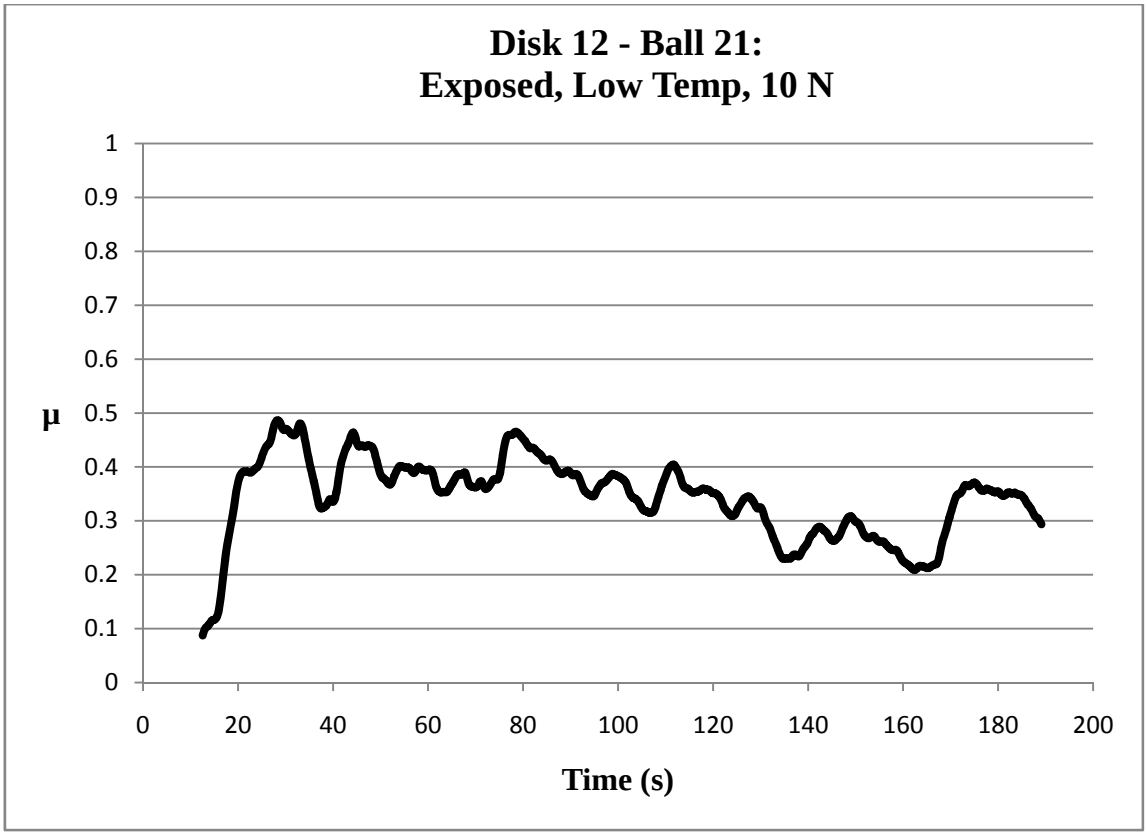
Disk 12 - Ball 21:
Exposed, Low Temp, 10 N
μ
1
0.9
0.8
0.7
0.6
0.5
0.4
0.3
0.2
0.1
0
0
20
40
60
80
100
120
140
160
180
200
Time (s)

| | |
|---|---|
| Nominal Temperature | Low Temp |
| Material | Ti-6Al-4V |
| Load (N) | 20 |
| H2 Exposed | Yes |
| Disk | 10 |
| Ball | 22 |
| Duration (min) | 3 |
| Distance (m) | 10 |
| Wear Track Radius (mm) | 15 |
| Wear Track Width (mm) | 0.626 |
| Ball Radius (mm) | 3.175 |
| Average μ | 0.41 |
| Steady State μ | 0.38 |
| Wear Volume (mm^3) | 0.6083 |
| Specific Wear Rate (mm^3/Nm) | 3.0413E-03 |

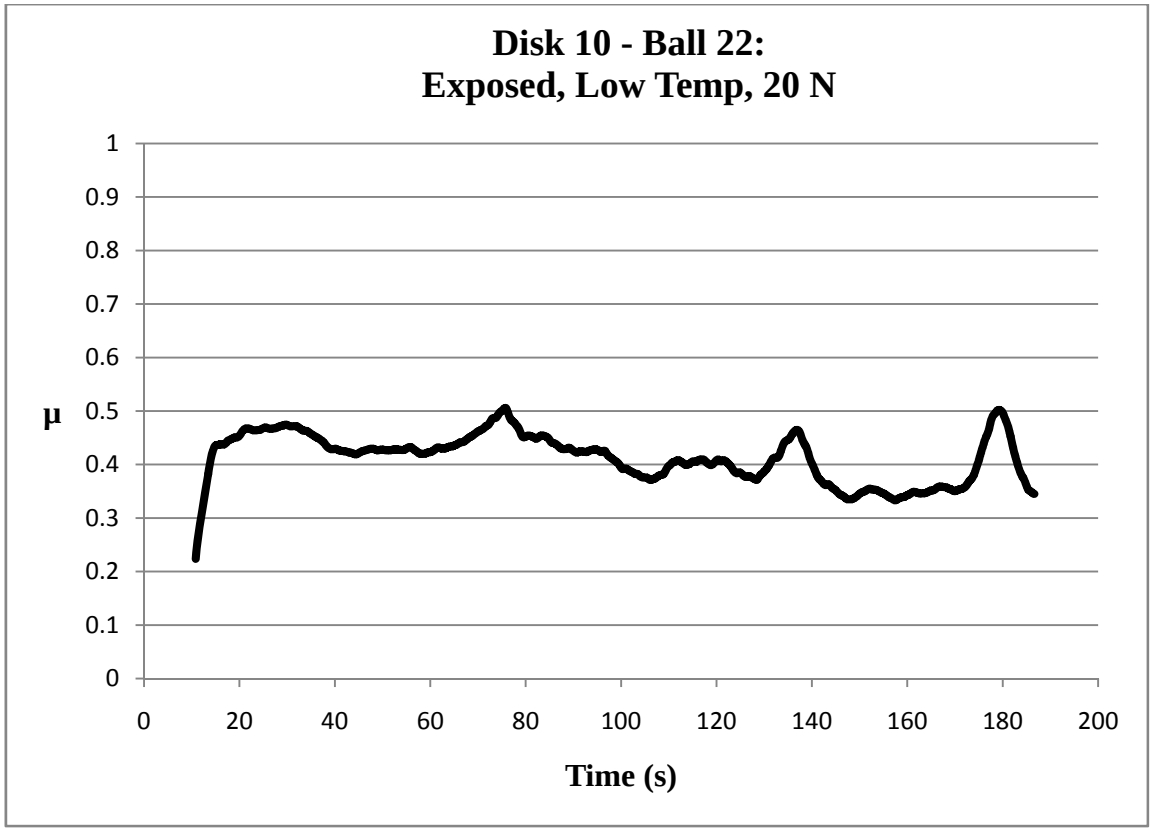
Disk 10 - Ball 22:
Exposed, Low Temp, 20 N
μ
1
0.9
0.8
0.7
0.6
0.5
0.4
0.3
0.2
0.1
0
0
20
40
60
80
100
120
140
160
180
200
Time (s)

| | |
|---|---|
| Nominal Temperature | Low Temp |
| Material | Ti-6Al-4V |
| Load (N) | 20 |
| H2 Exposed | Yes |
| Disk | 11 |
| Ball | 23 |
| Duration (min) | 3 |
| Distance (m) | 10 |
| Wear Track Radius (mm) | 15 |
| Wear Track Width (mm) | 0.681 |
| Ball Radius (mm) | 3.175 |
| Average μ | 0.44 |
| Steady State μ | 0.40 |
| Wear Volume (mm^3) | 0.7852 |
| Specific Wear Rate (mm^3/Nm) | 3.9258E-03 |

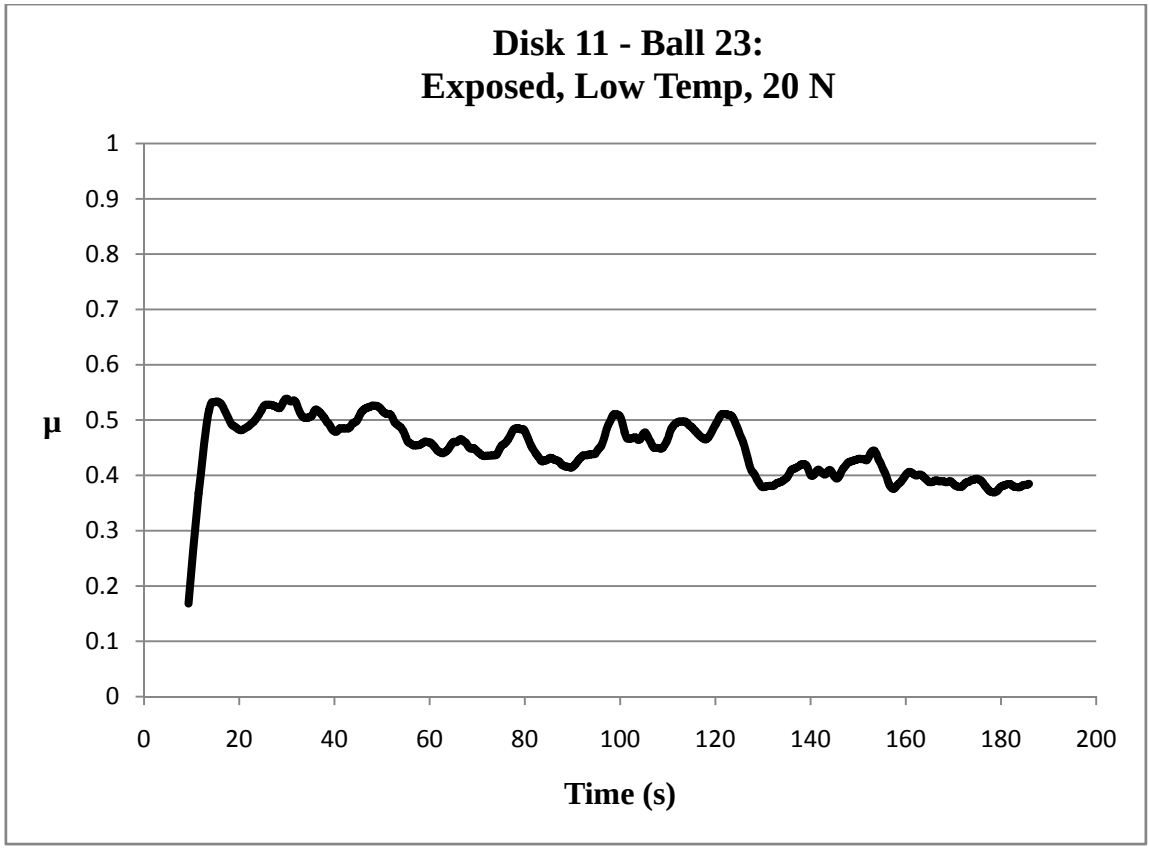
Disk 11 - Ball 23:
Exposed, Low Temp, 20 N
μ
1
0.9
0.8
0.7
0.6
0.5
0.4
0.3
0.2
0.1
0
0
20
40
60
80
100
120
140
160
180
200
Time (s)

| | |
|---|---|
| Nominal Temperature | Low Temp |
| Material | Ti-6Al-4V |
| Load (N) | 20 |
| H2 Exposed | Yes |
| Disk | 12 |
| Ball | 24 |
| Duration (min) | 3 |
| Distance (m) | 10 |
| Wear Track Radius (mm) | 15 |
| Wear Track Width (mm) | 0.562 |
| Ball Radius (mm) | 3.175 |
| Average μ | 0.40 |
| Steady State μ | 0.37 |
| Wear Volume (mm^3) | 0.4400 |
| Specific Wear Rate (mm^3/Nm) | 2.2002E-03 |

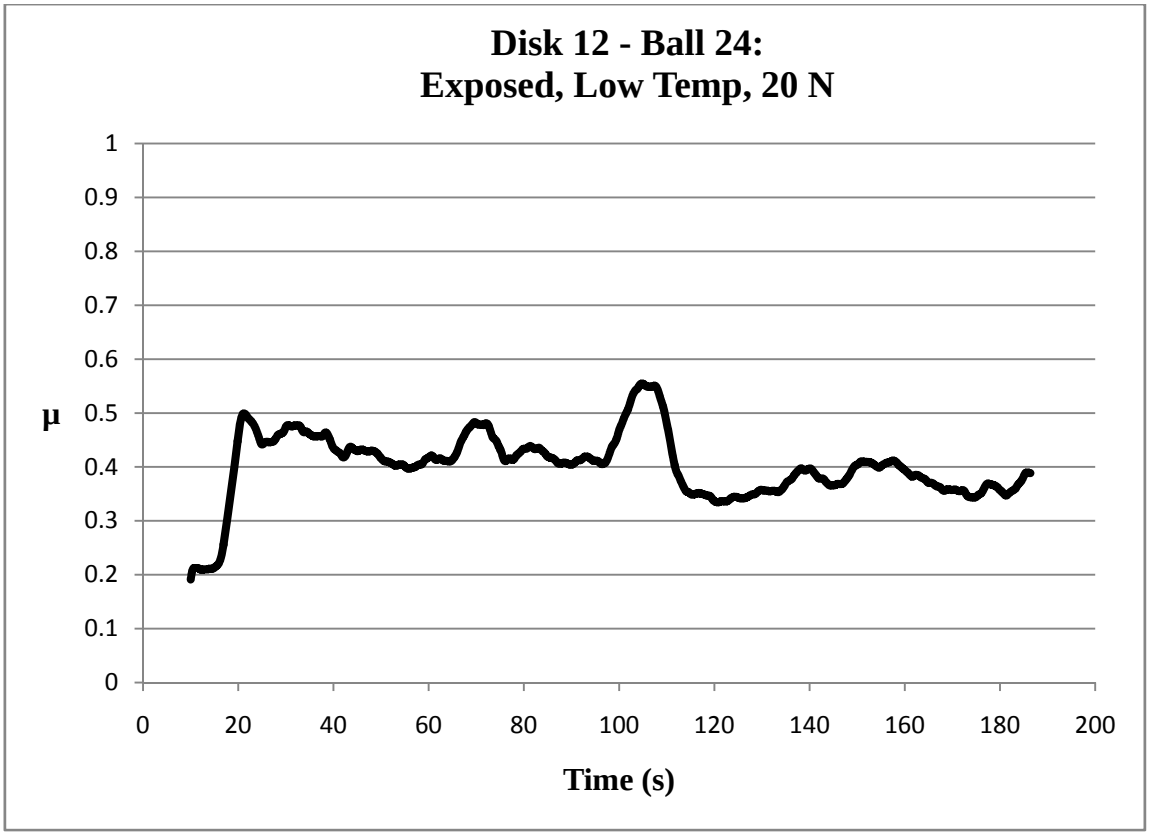
Disk 12 - Ball 24:
Exposed, Low Temp, 20 N
μ
1
0.9
0.8
0.7
0.6
0.5
0.4
0.3
0.2
0.1
0
0
20
40
60
80
100
120
140
160
180
200
Time (s)

# APPENDIX B

Group 1 – Room Temperature, Non-Exposed, Disks 1-3

Disk 1 Inner

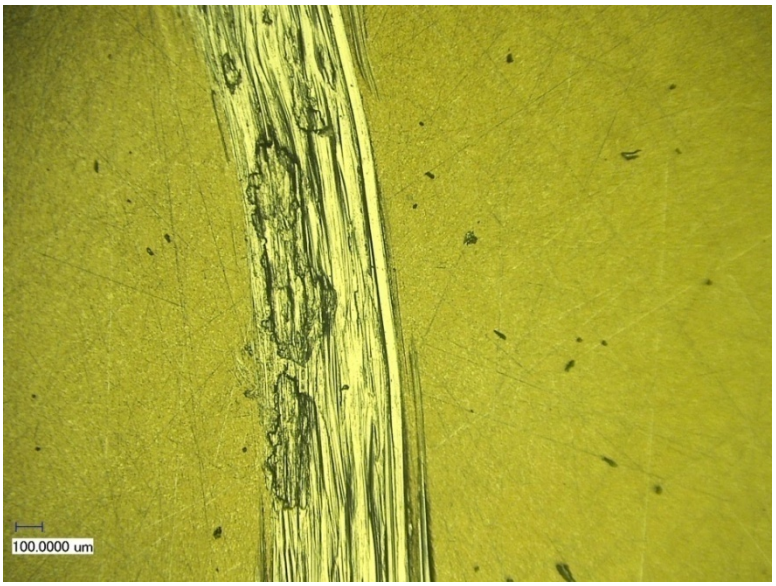


Figure 32: Disk 1 inner track, 10 N load at 100 times magnification.

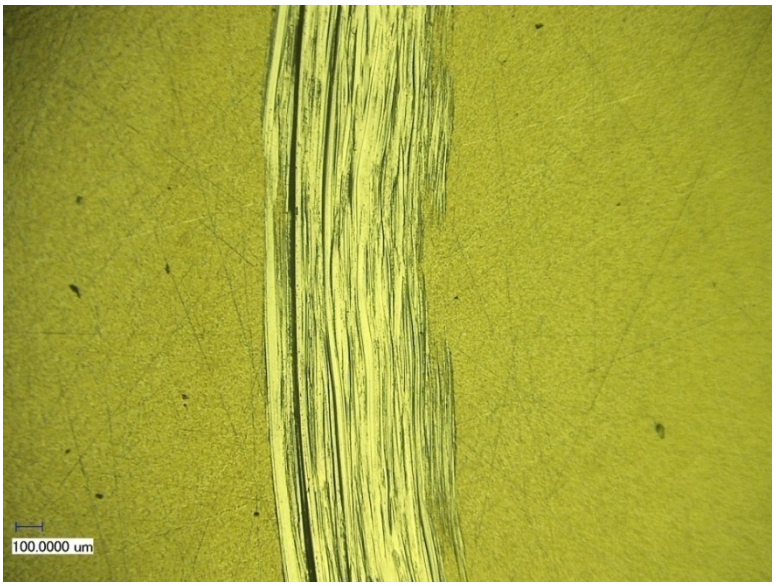


Figure 33: Disk 1 inner at 100 times magnification typical surface.

Pin 1

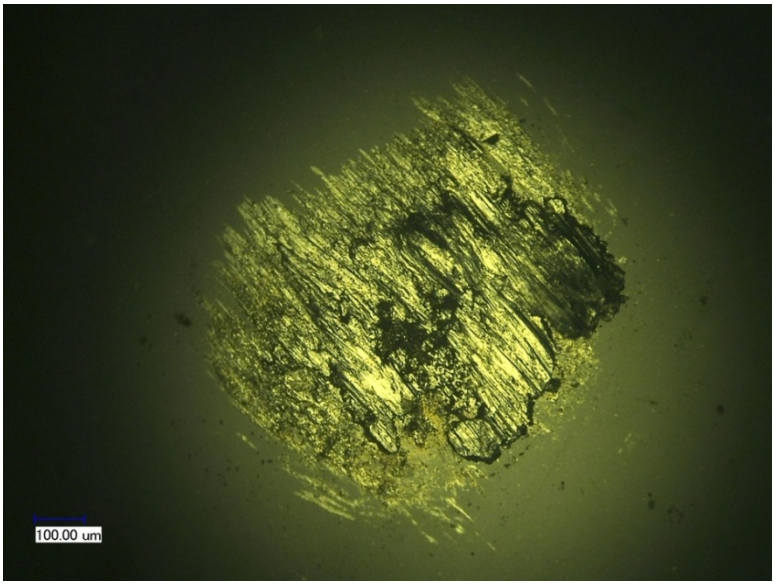


Figure 34: Pin 1 at 200 times magnification.

Disk 1 Outer

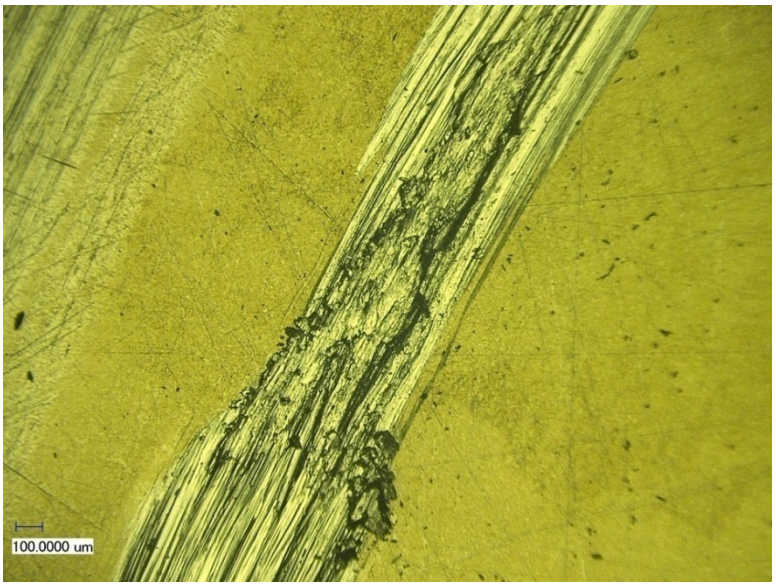


Figure 35: Disk 1 outer track, 20 N load at 100 times magnification.

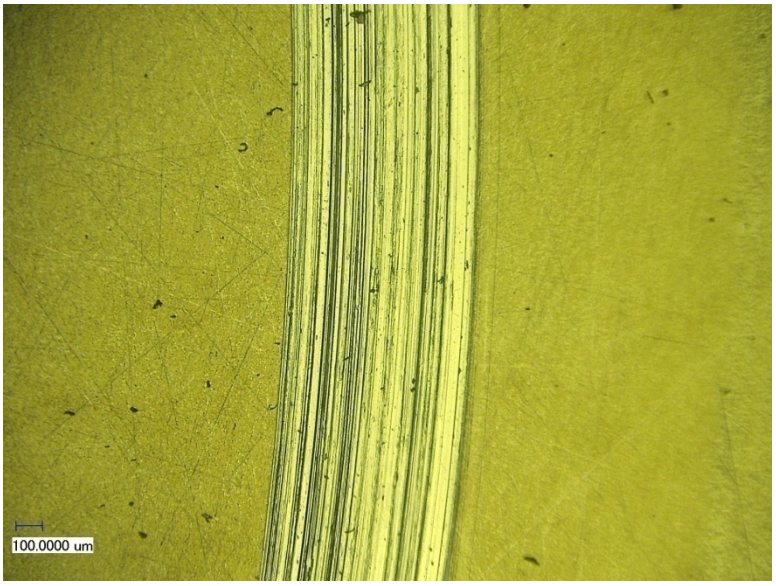


Figure 36: Disk 1 outer track, 20 N load at 100 times magnification typical surface.

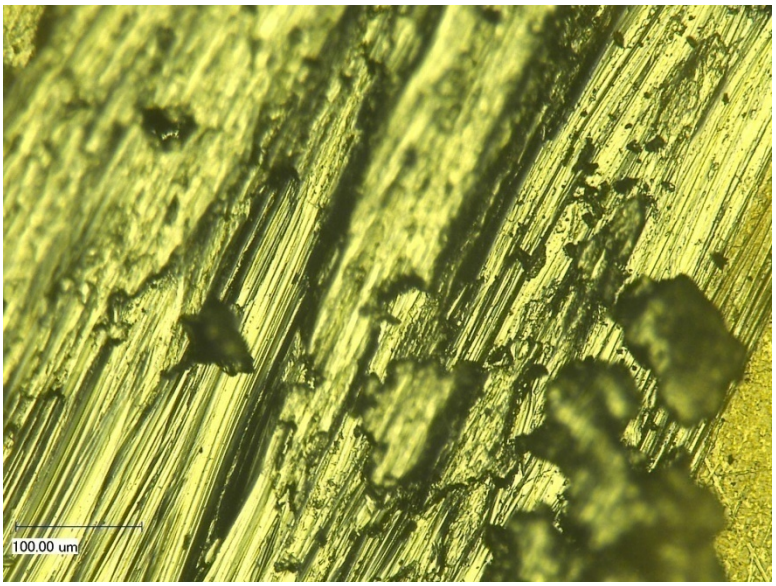


Figure 37: Disk 1 outer track, 20 N load at 500 times magnification showing adhesion.

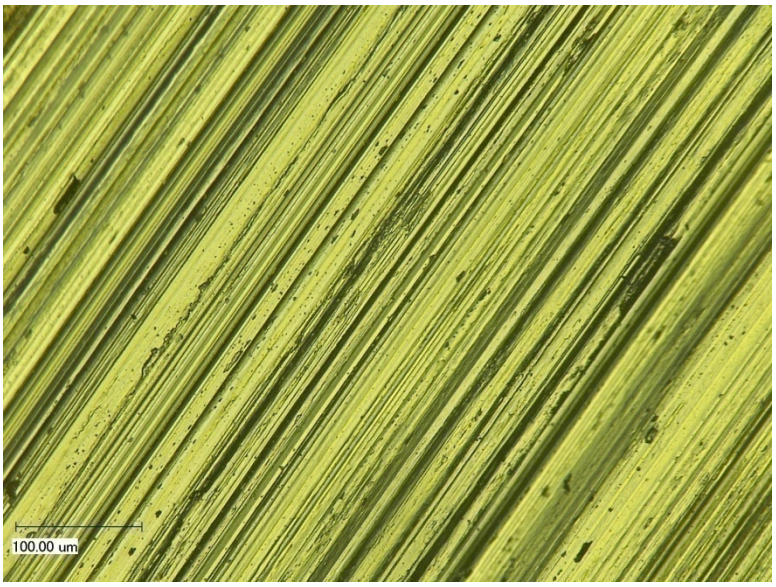


Figure 38: Disk 1 outer track, 20 N load at 500 times magnification typical surface.

Pin 5

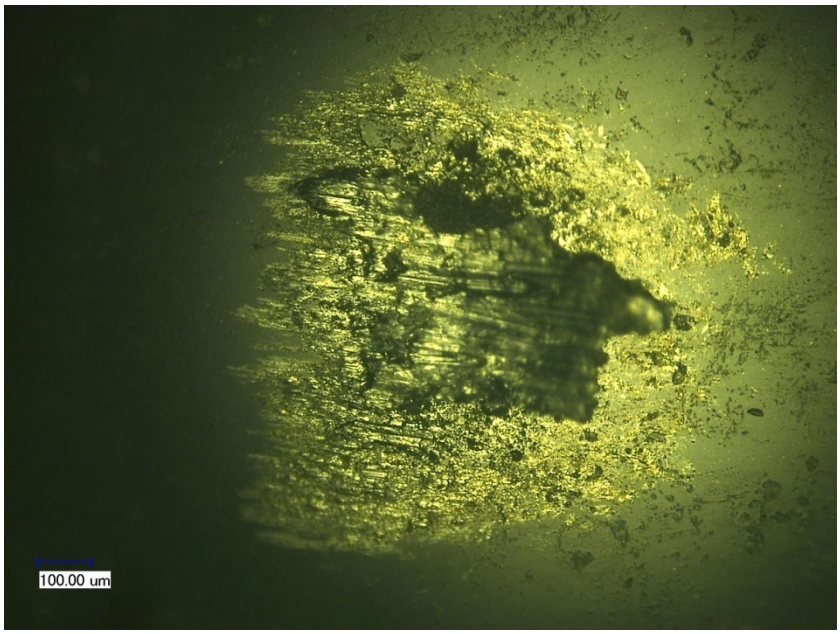


Figure 39: Pin 5 at 200 times magnification.

Disk 2 Inner

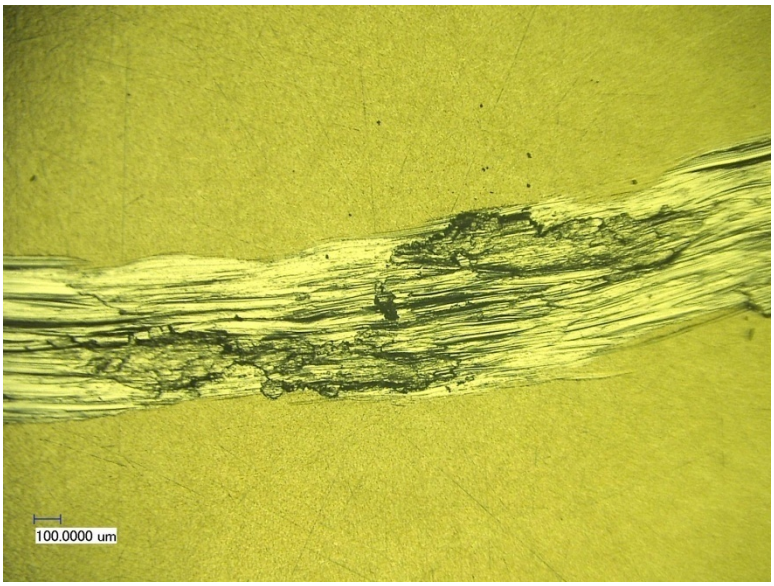


Figure 40: Disk 2 inner track, 10 N load 100 times magnification.

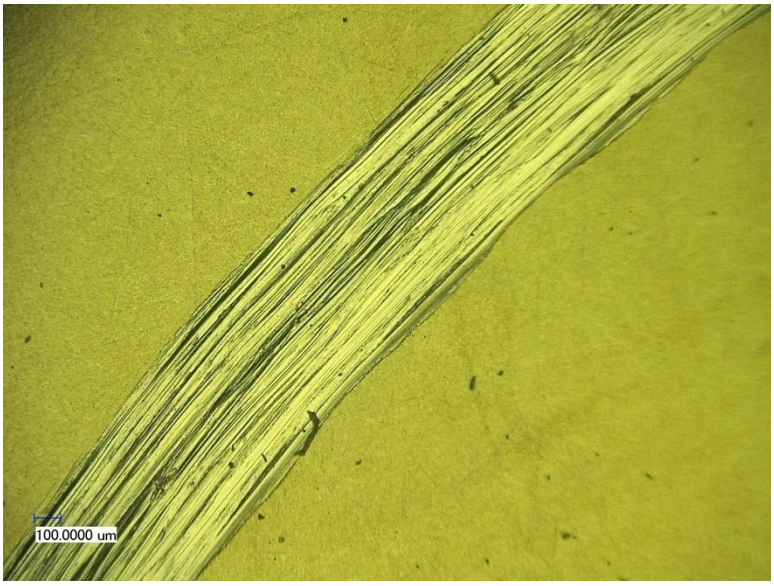


Figure 41: Disk 2 inner track, 10 N load 100 times magnification typical surface.

Pin 2

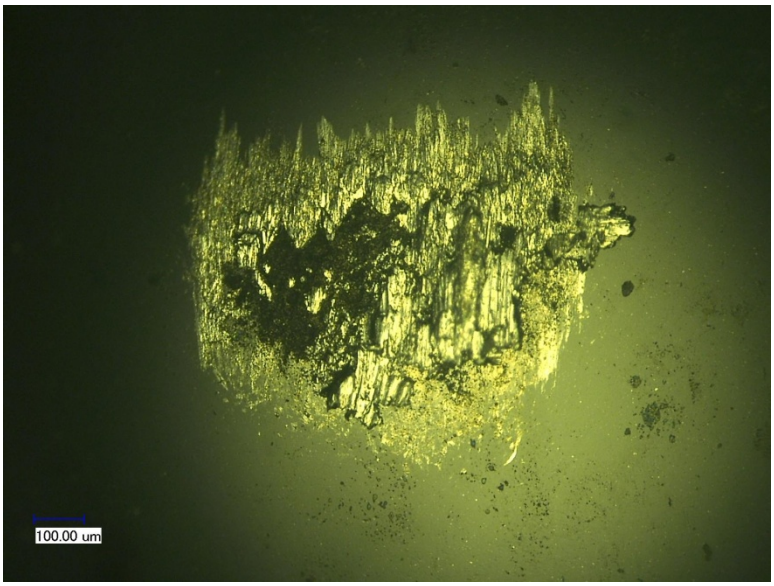


Figure 42: Pin 2 at 200 times magnification.

Disk 2 Outer

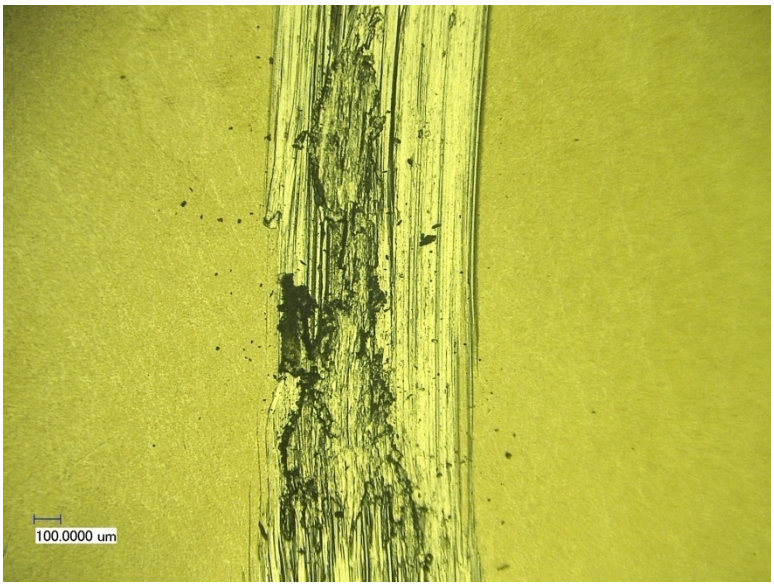


Figure 43: Disk 2 outer track, 20 N load at 100 times magnification with adhesion.

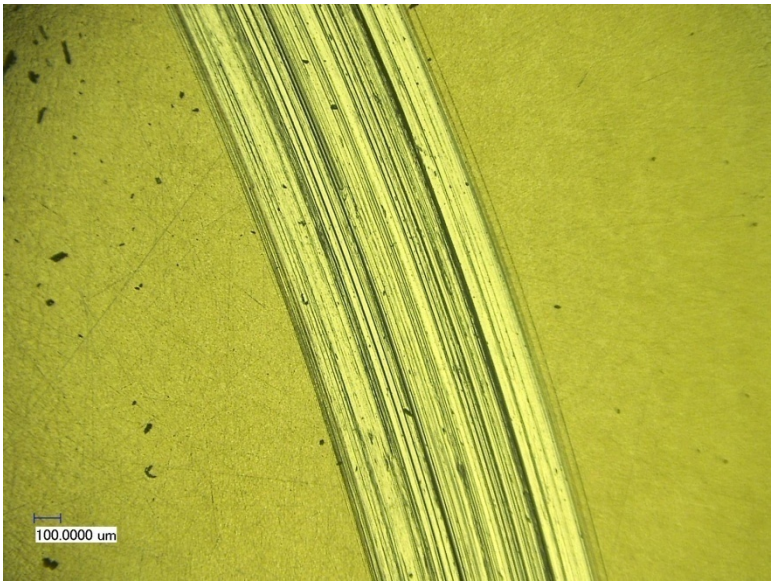


Figure 44: Disk 2 outer track, 20 N load at 100 times magnification typical surface.

Pin 5

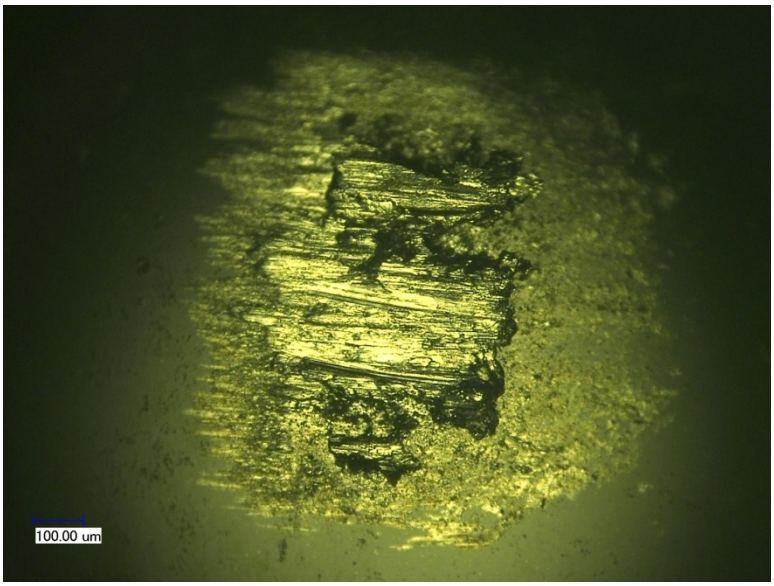


Figure 45: Pin 5 at 200 times magnification.

Disk 3 Inner

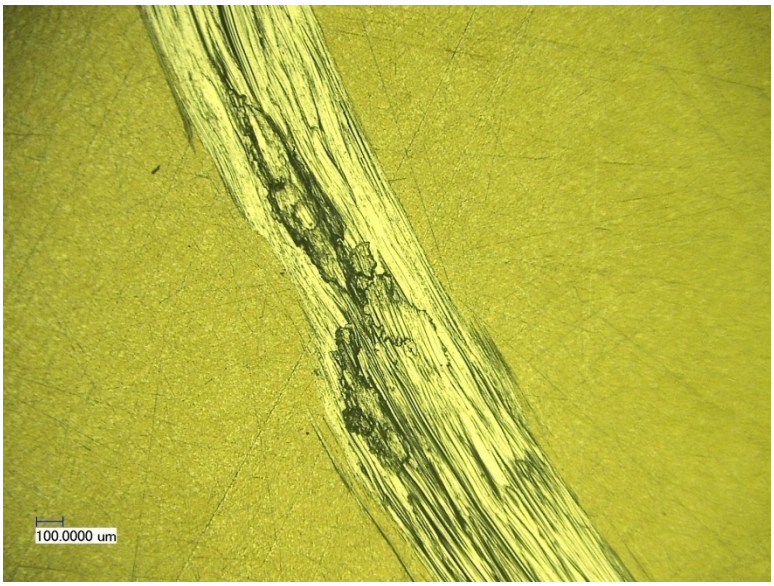


Figure 46: Disk 3 inner track, 10 N load at 100 times magnification with adhesion.

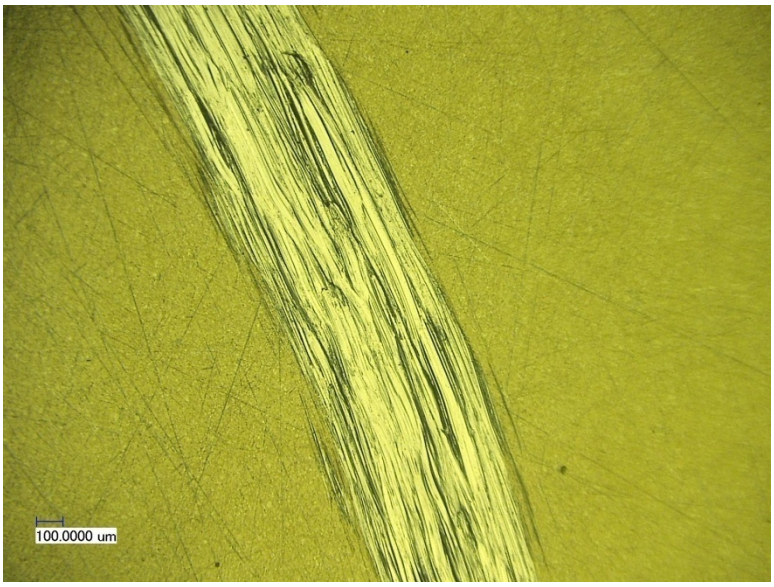


Figure 47: Disk 3 inner track, 10 N load at 100 times magnification typical surface.

Pin 3

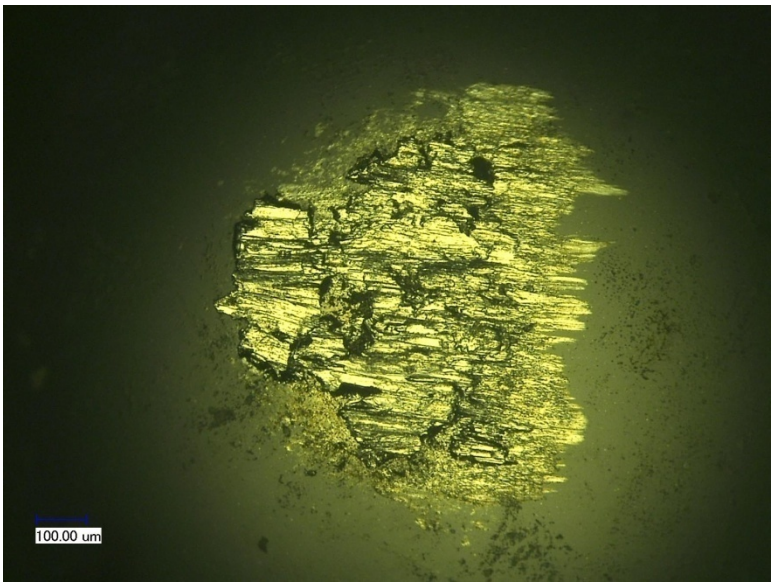


Figure 48: Pin 3 at 200 times magnification.

Disk 3 Outer

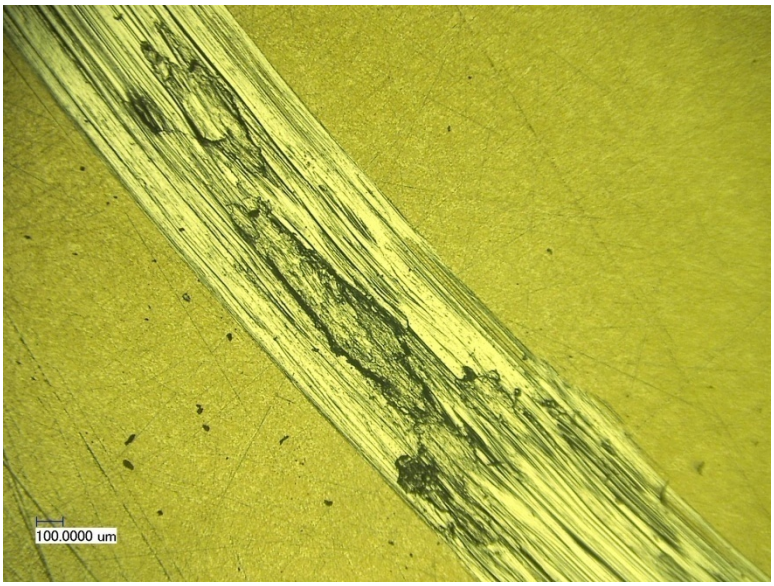


Figure 49: Disk 3 outer track, 20 N load at 100 times magnification with adhesion.

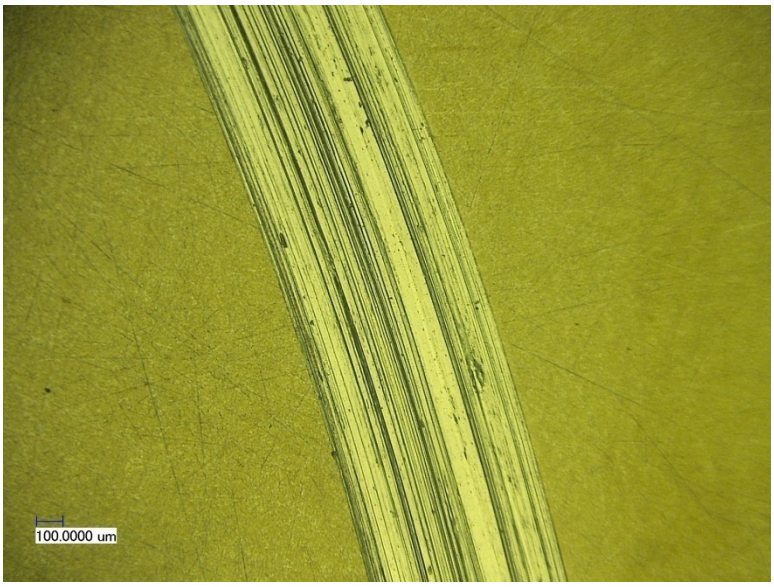


Figure 50: Disk 2 outer track, 20 N load at 100 times magnification typical surface.

Pin 6

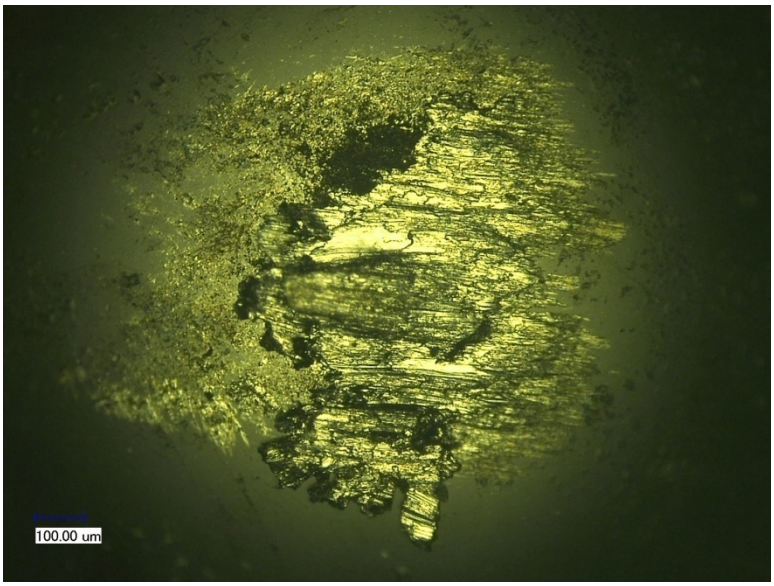


Figure 51: Pin 6 at 200 times magnification.

## Group 2 – Low Temperature, Non-Exposed, Disks 4-6

### Disk 4 Inner

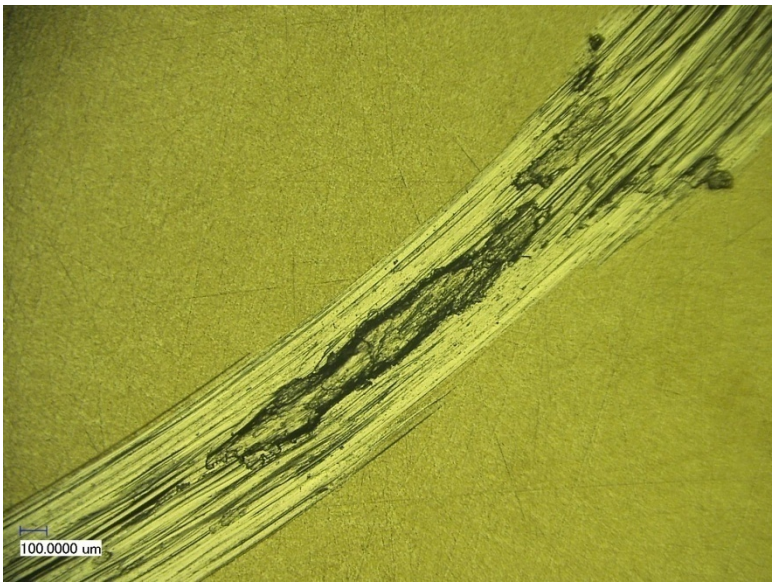


Figure 52: Disk 4 inner track, 10 N load at 100 times magnification with adhesion.

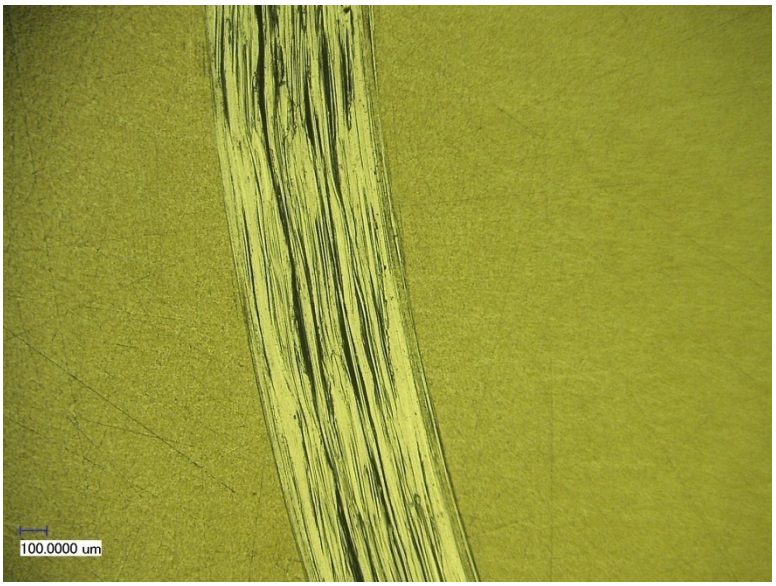


Figure 53: Disk 4 inner track, 10 N load at 100 times magnification with wavy surface.

Pin 7

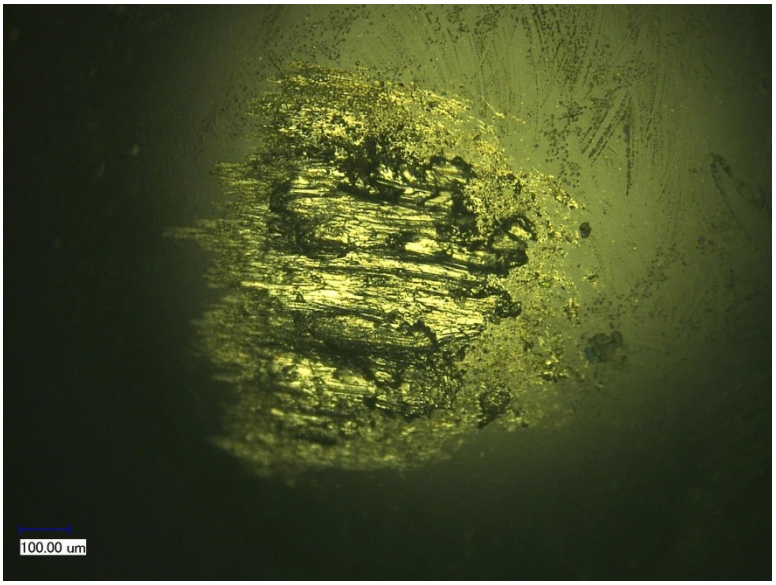


Figure 54: Pin 7 at 200 times magnification.

Disk 4 Outer

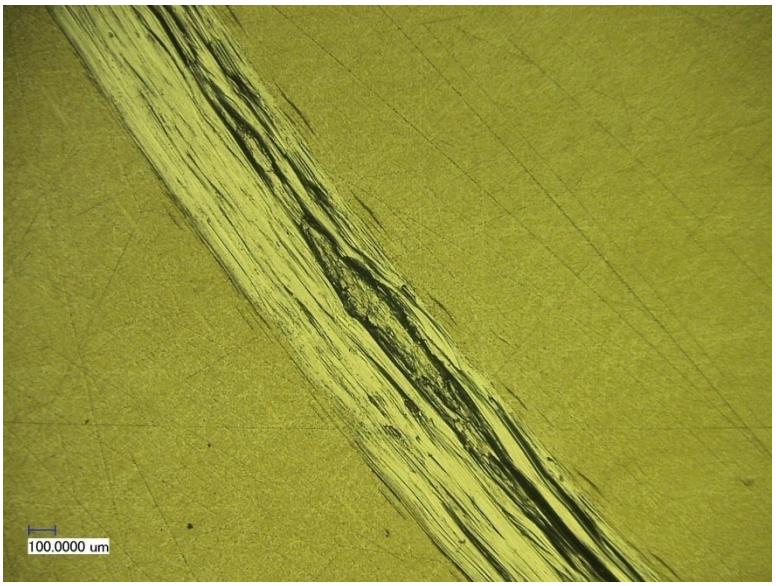


Figure 55: Disk 4 outer track, 20 N load at 100 times magnification with adhesion, deep groves and wavy surface.

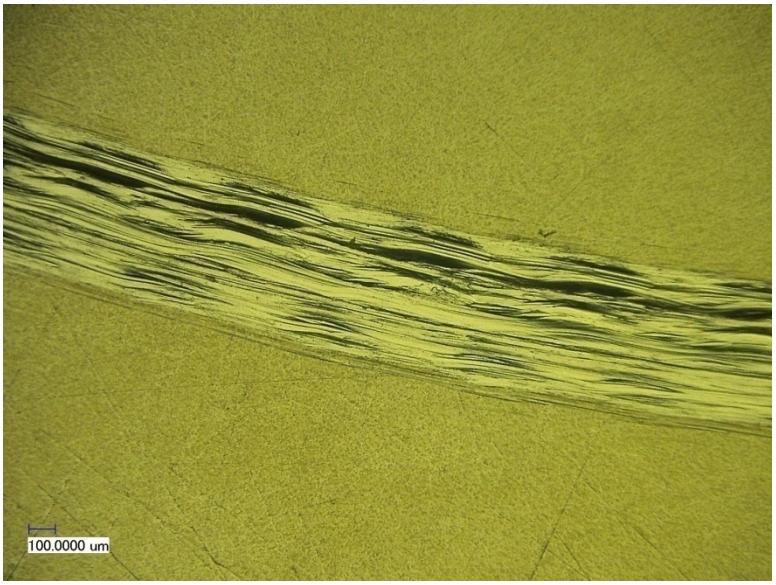


Figure 56: Disk 4 outer track, 20 N load at 100 times magnification with wavy pattern.

Pin 10

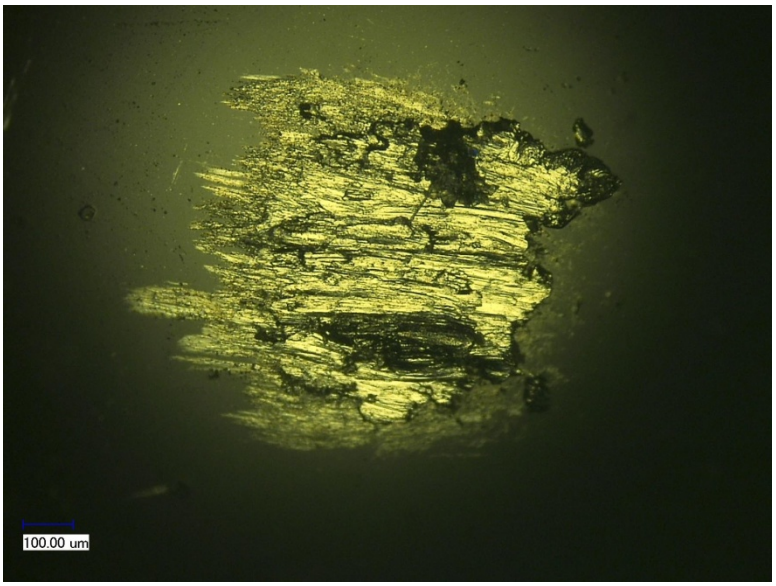


Figure 57: Pin  10 at 200 times magnification.

Disk 5 Inner

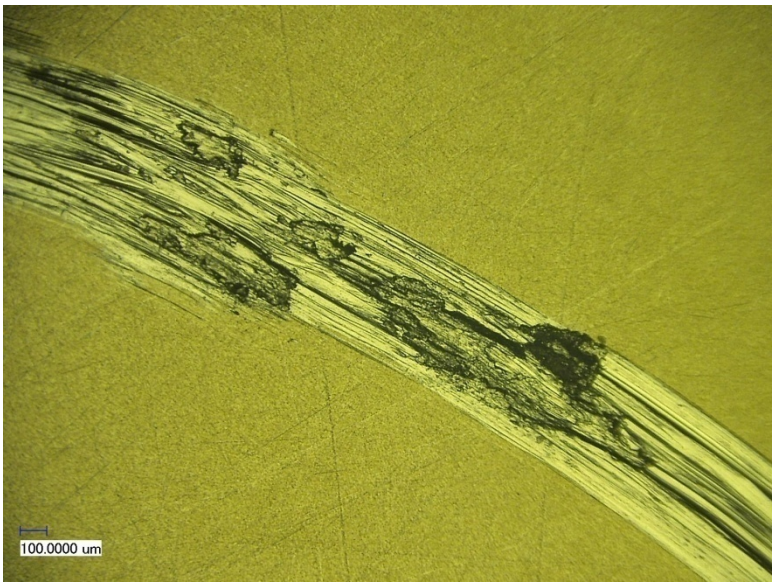


Figure 58: Disk 5 inner track, 10 N load at 100 times magnification with adhesion.

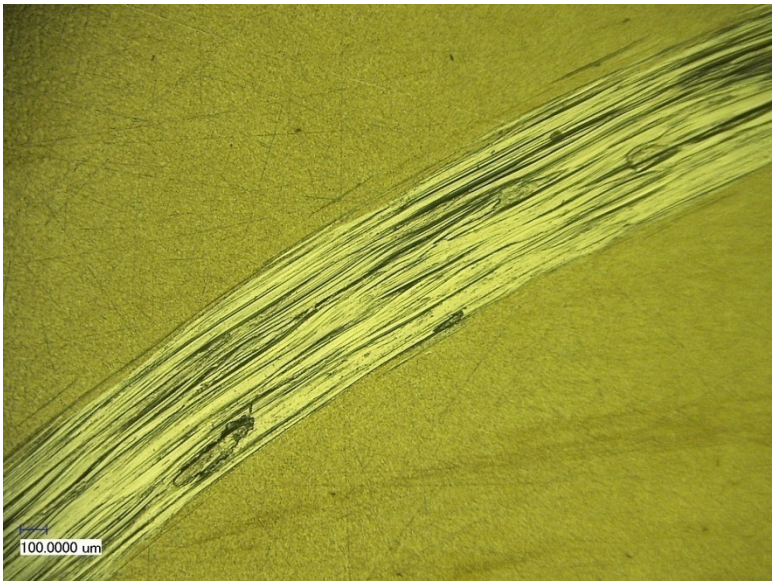


Figure 59: Disk 5 inner track, 10 N load at 100 times magnification typical wavy surface with adhesion.

Pin 8

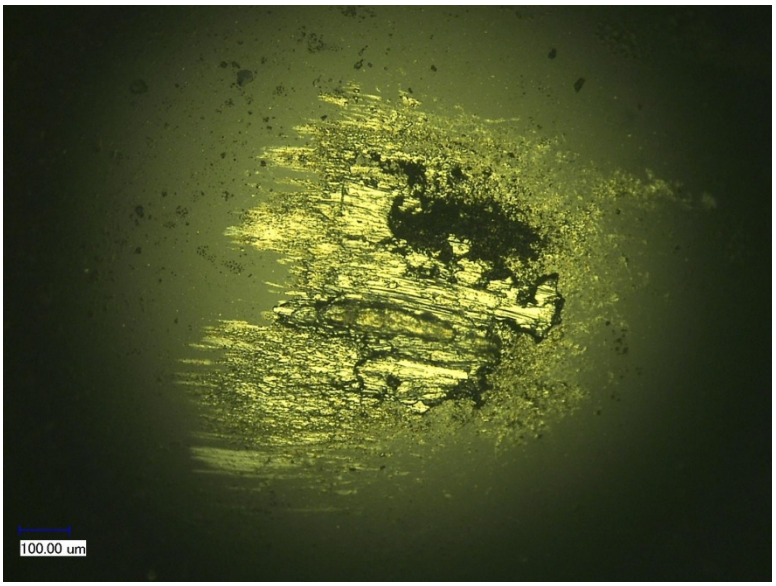


Figure 60: Pin 8 at 200 times magnification.

Disk 5 Outer

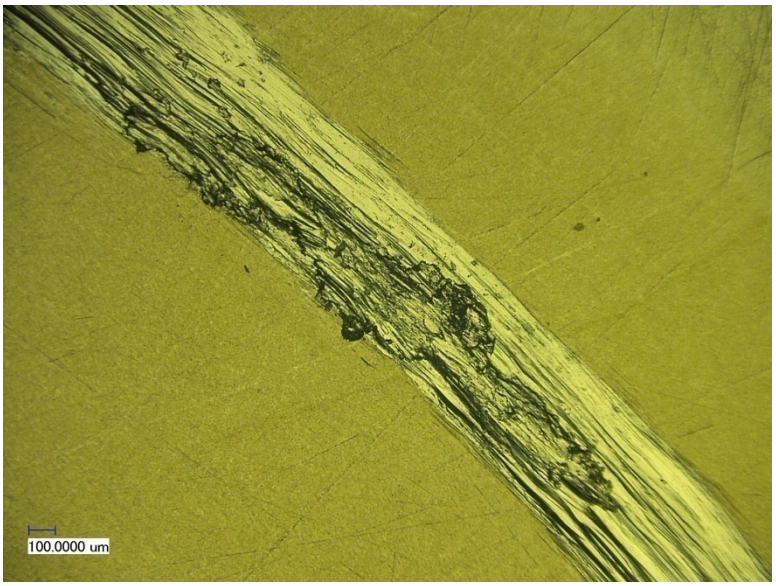


Figure 61: Disk 5 outer track, 20 N load at 100 times magnification with adhesion.

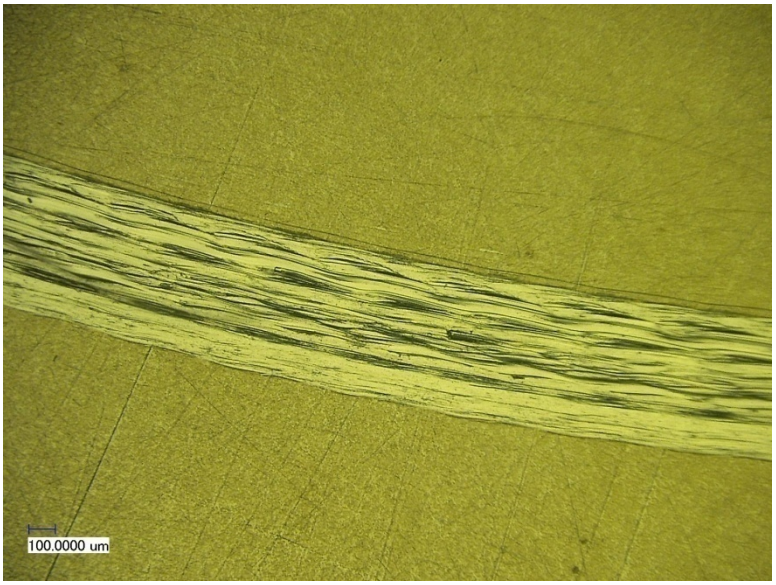


Figure 62: Disk 5 outer track, 20 N load at 100 times magnification wavy surface.

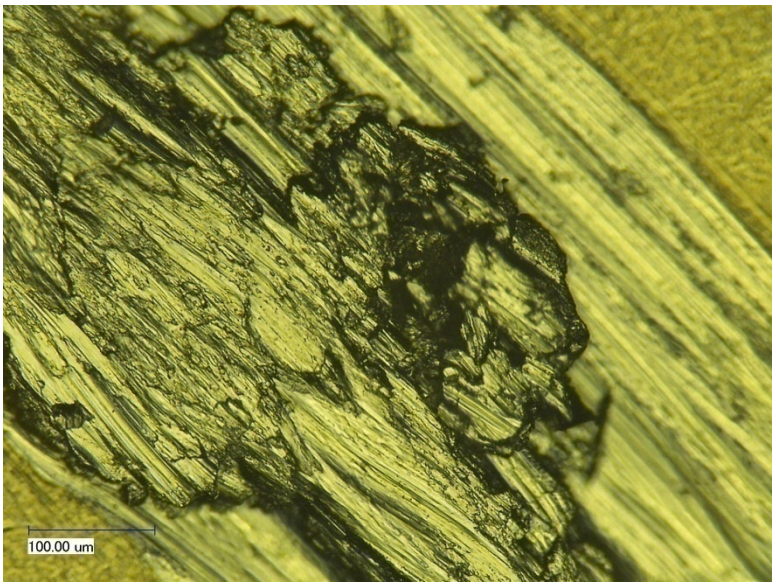


Figure 63: Disk 5 outer track, 20 N load at 500 times magnification with adhesion.

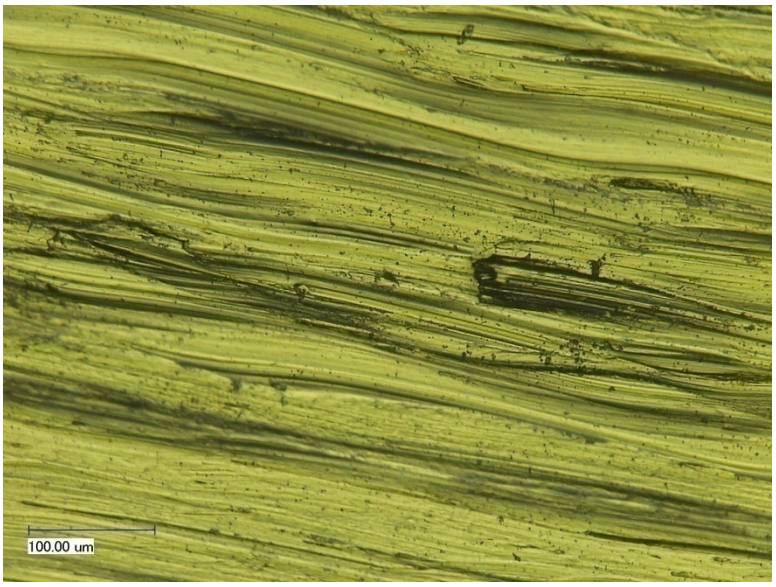


Figure 64: Disk 5 outer track, 20 N load at 500 times magnification wavy surface.

Pin 11

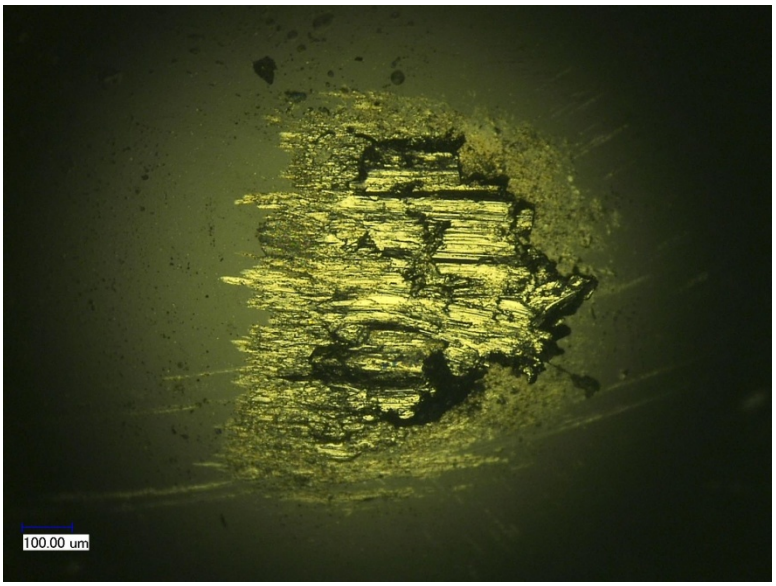


Figure 65: Pin 11 at 200 times magnification.

Disk 6 Inner

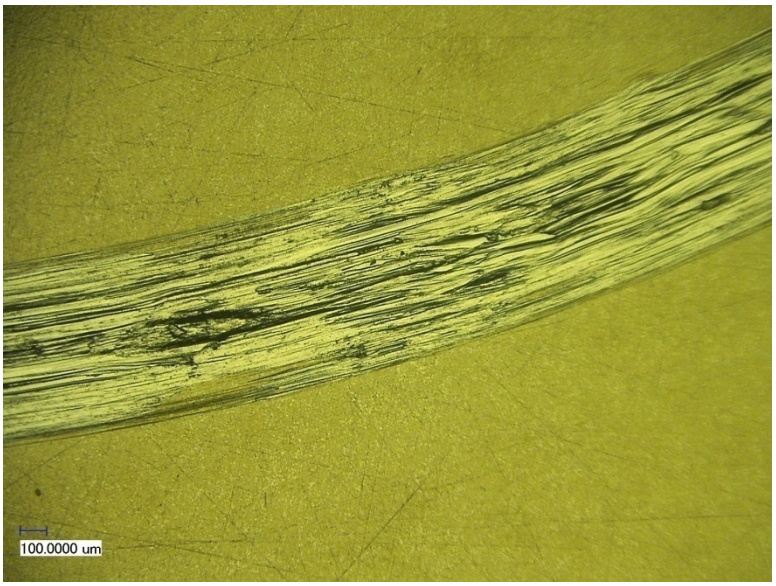


Figure 66: Disk 6 inner track, 10 N load at 100 times magnification with adhesion and wavy surface.

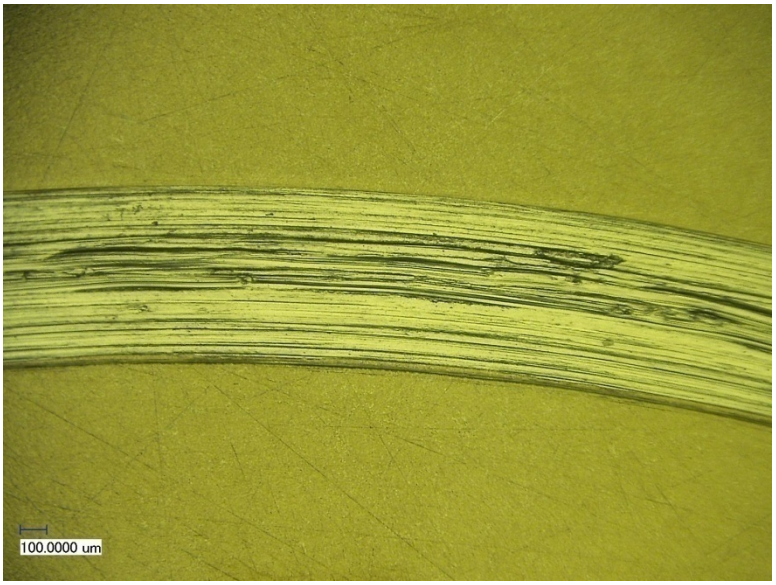


Figure 67: Disk 6 inner track, 10 N load at 100 times magnification typical with small adhesive areas.

Pin 9

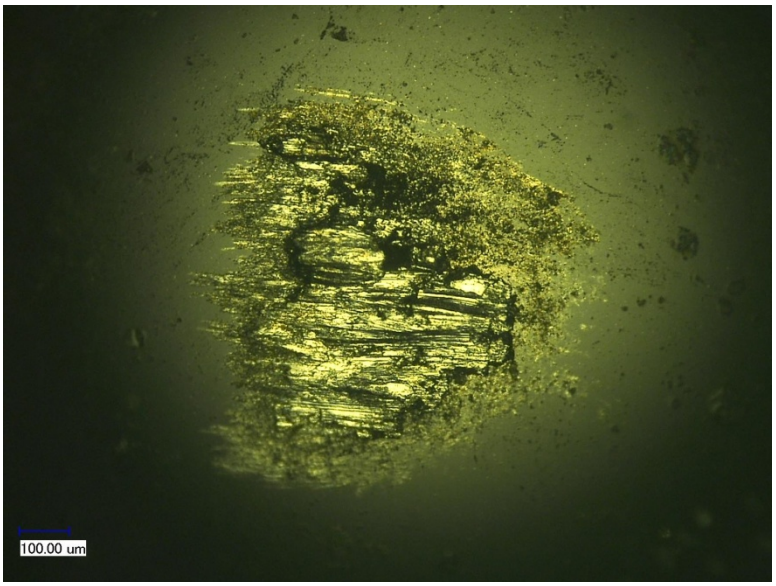


Figure 68: Pin 9 at 200 times magnification.

Disk 6 Outer

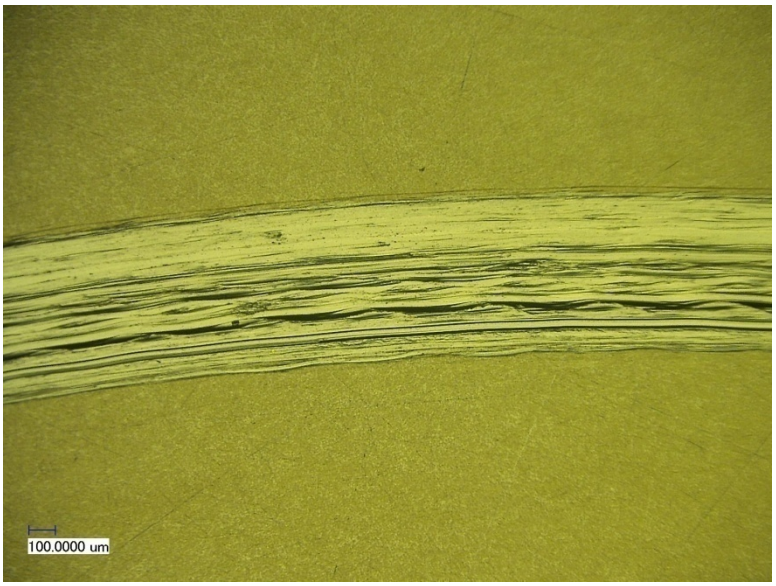


Figure 69: Disk 6 outer track, 20 N load at 100 times magnification typical surface.

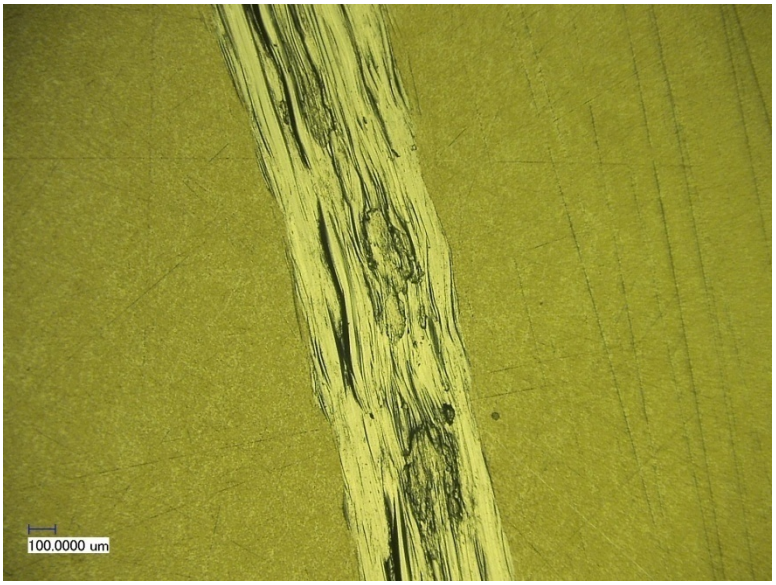


Figure 70: Disk 6 outer track, 20 N load at 100 times magnification with adhesion.

Pin 12

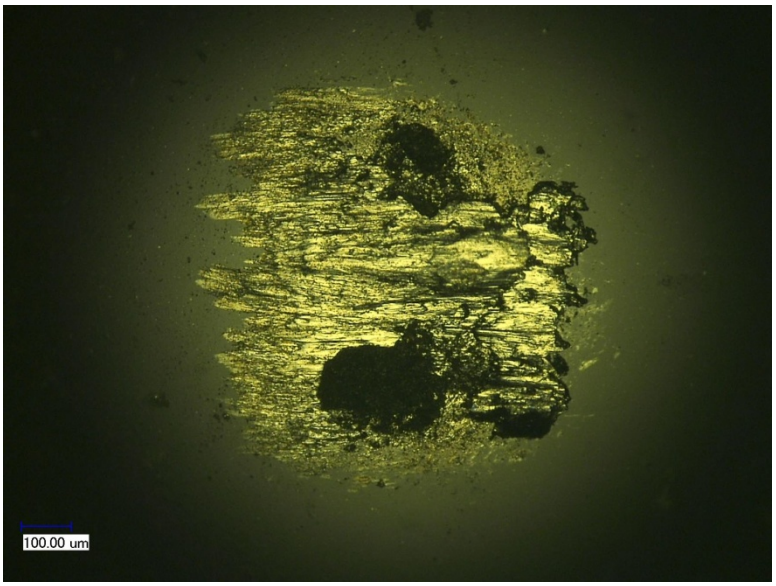


Figure 71: Pin 12 at 200 times magnification.

## Group 3 – Room Temperature, Exposed, Disks 7-9

### Disk 7 Inner

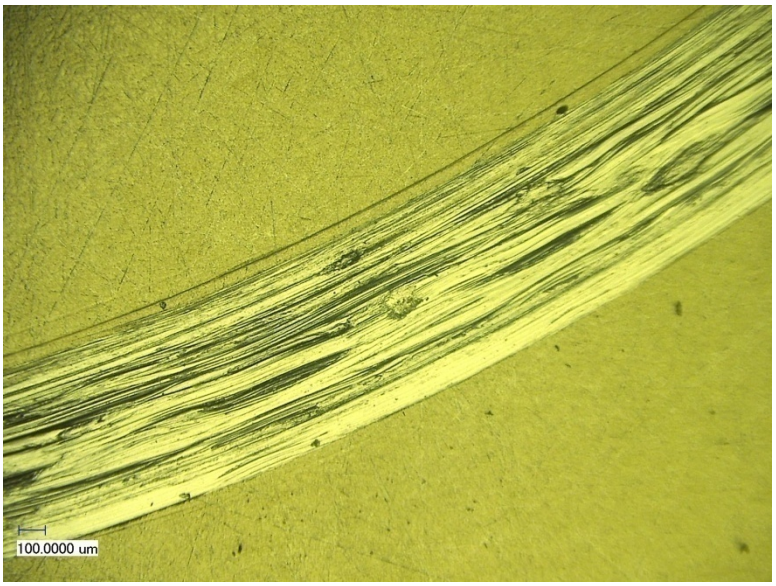


Figure 72: Disk 7 inner track, 10 N load at 100 times magnification typical surface.

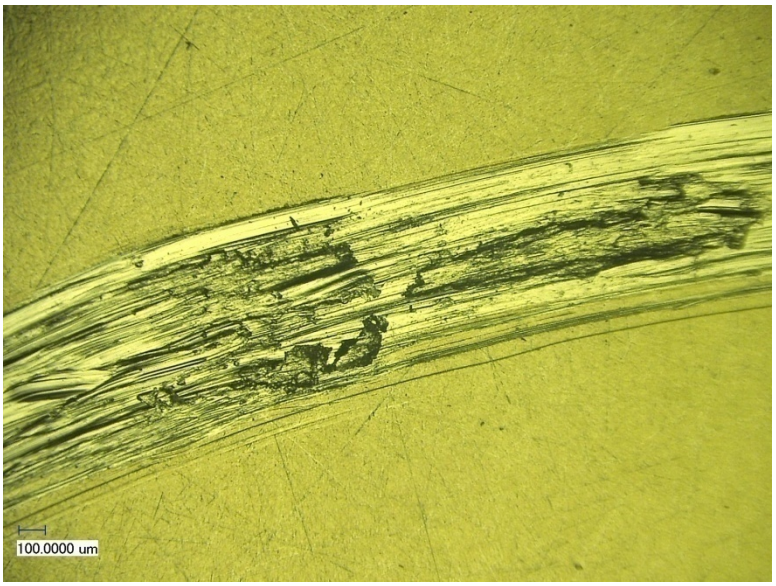


Figure 73: Disk 7 inner track, 10 N load at 100 times magnification with adhesion.

Pin 13

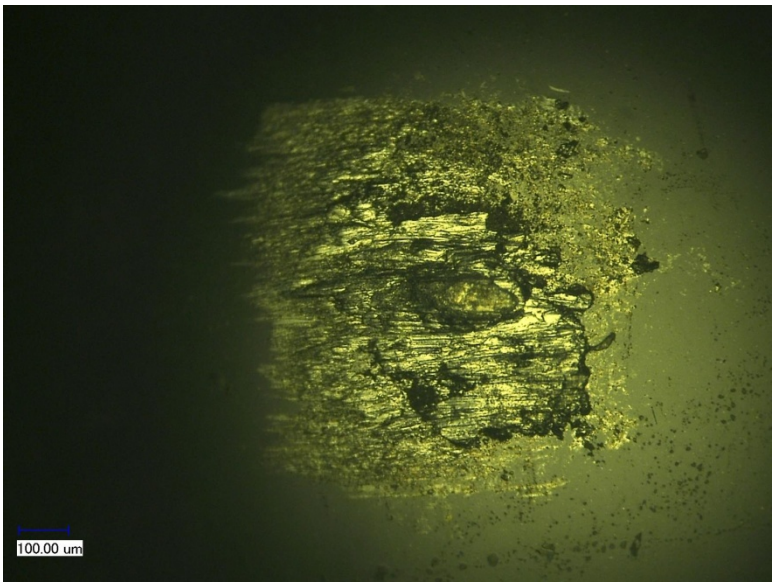


Figure 74: Pin 13 at 200 times magnification.

Disk 7 Outer

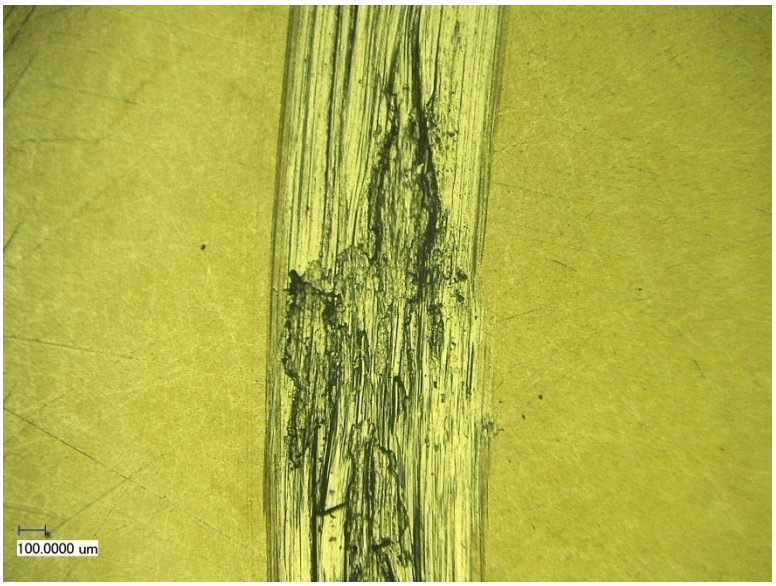


Figure 75: Disk 7 outer track, 20 N load at 100 times magnification with adhesion.

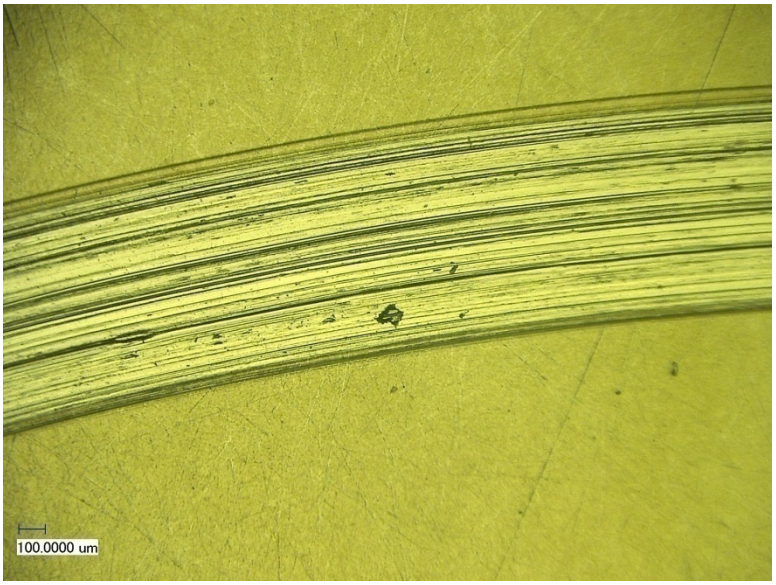


Figure 76: Disk 7 outer track, 20 N load at 100 times magnification typical surface with adhesive areas.

Pin 16

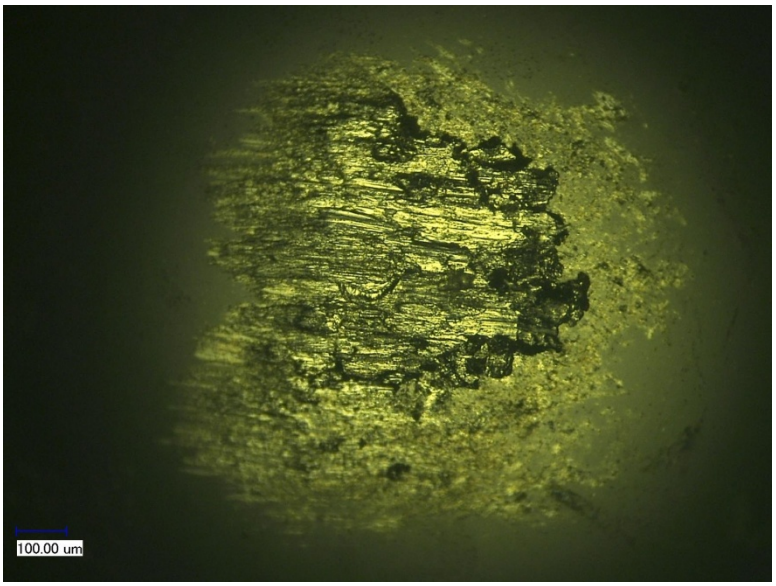


Figure 77: Pin 16 at 200 times magnification.

Disk 8 Inner

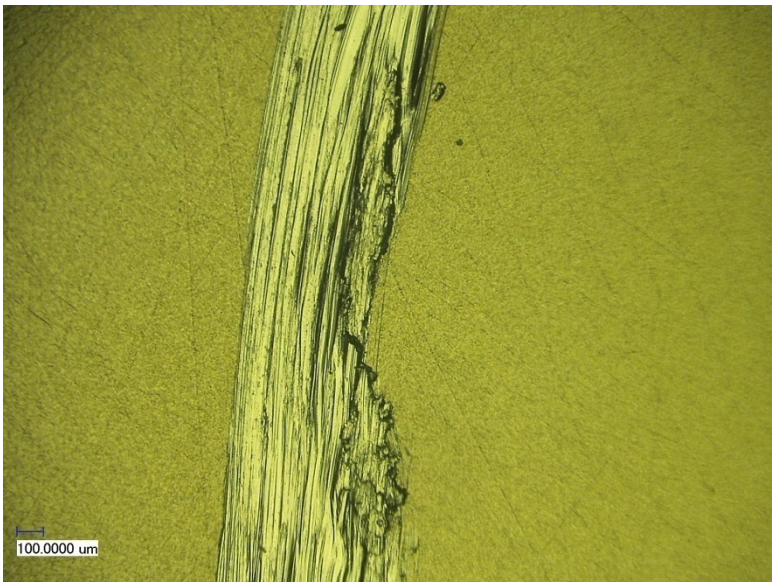


Figure 78: Disk 8 inner track, 10 N load at 100 times magnification with adhesion.

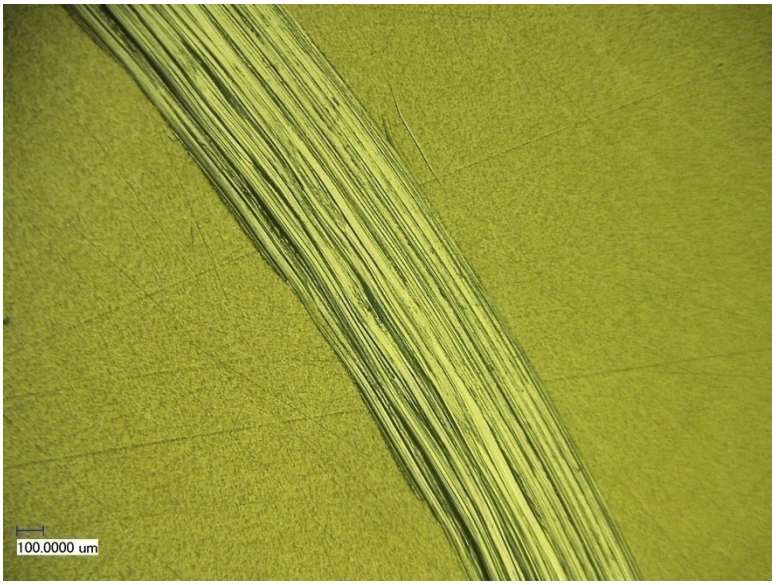


Figure 79: Disk 8 inner track, 10 N load at 100 times magnification typical surface.

Pin 14

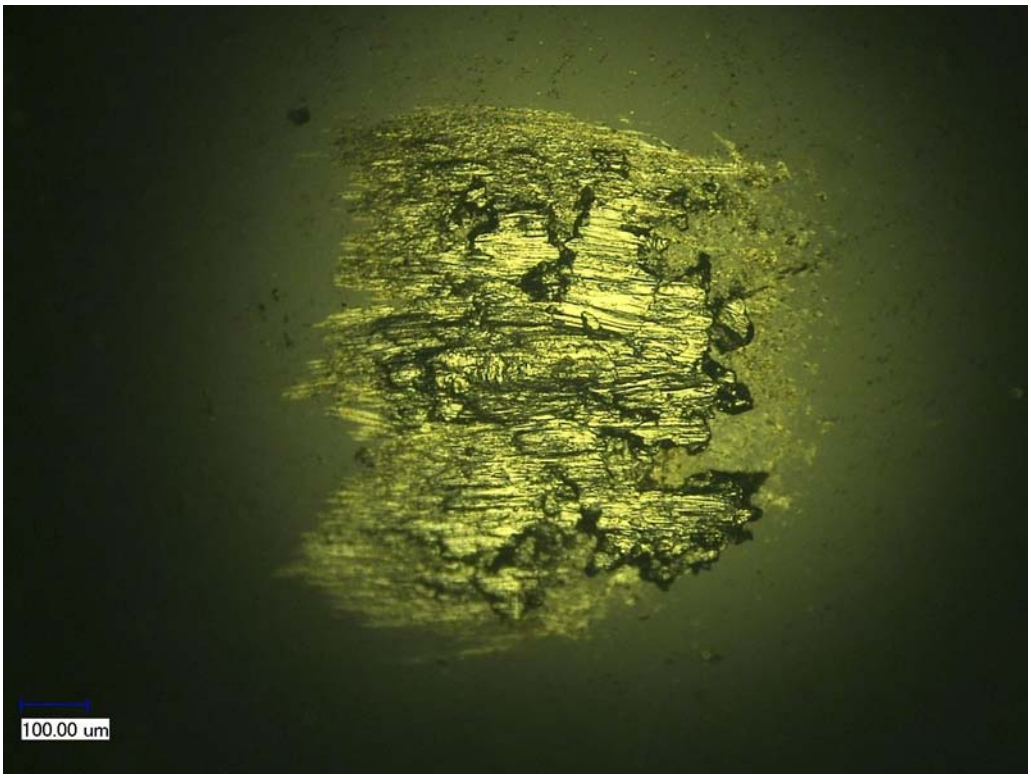


Figure 80: Pin 14 at 200 times magnification.

Disk 8 Outer

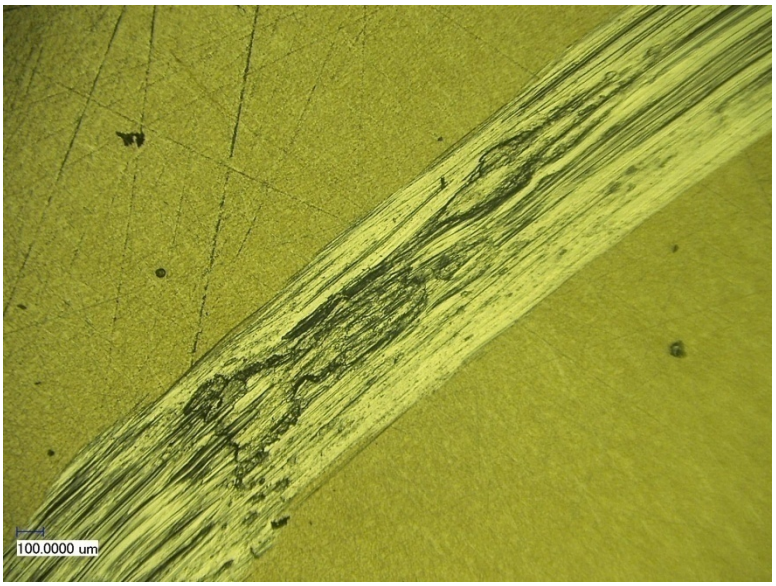


Figure 81: Disk 8 outer track, 20 N load at 100 times magnification with adhesion.

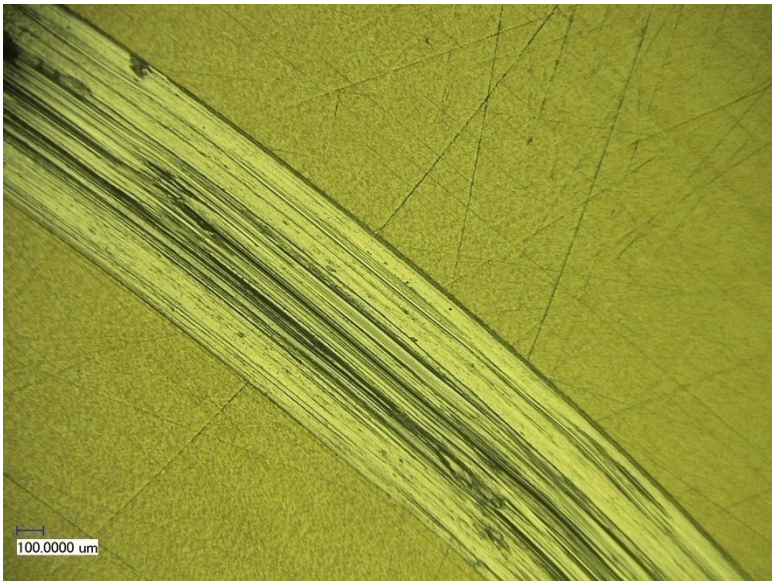


Figure 82: Disk 8 outer track, 20 N load at 100 times magnification typical surface with adhesion.

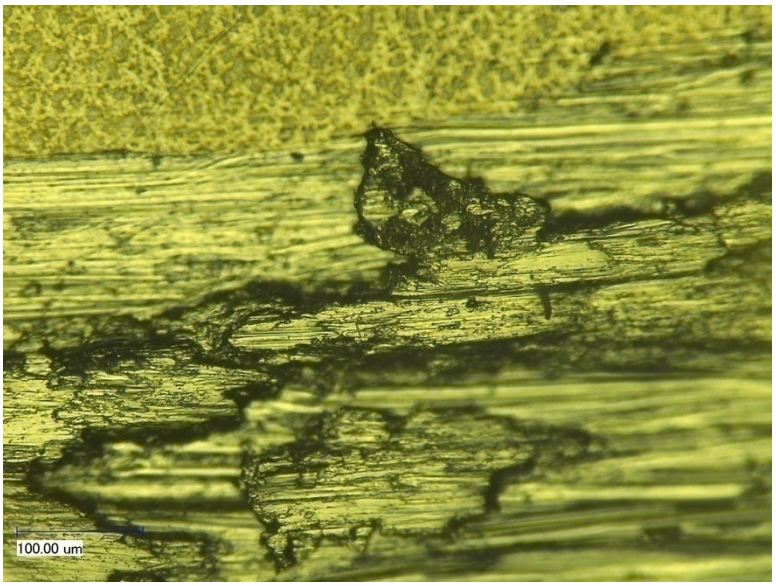


Figure 83: Disk 8 outer track, 20 N load at 500 times magnification adhesive area.

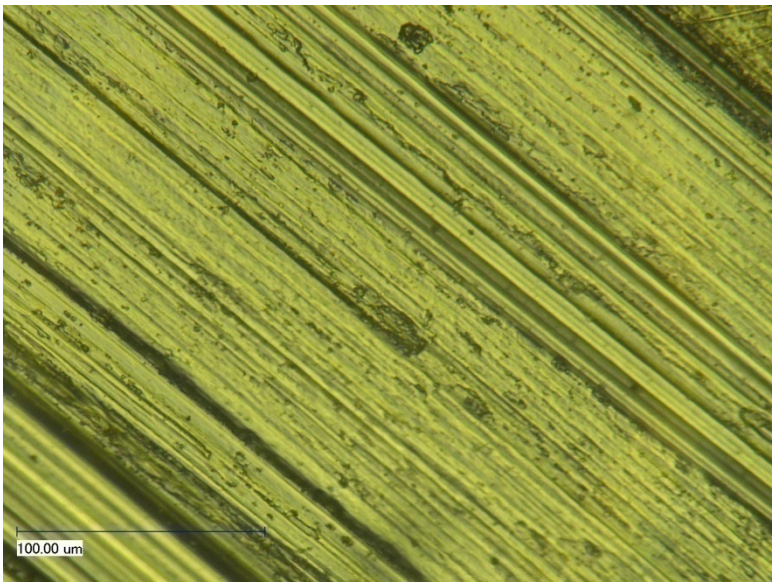


Figure 84: Disk 8 outer track, 20 N load at 1000 times magnification typical surface with adhesion.

Pin 17

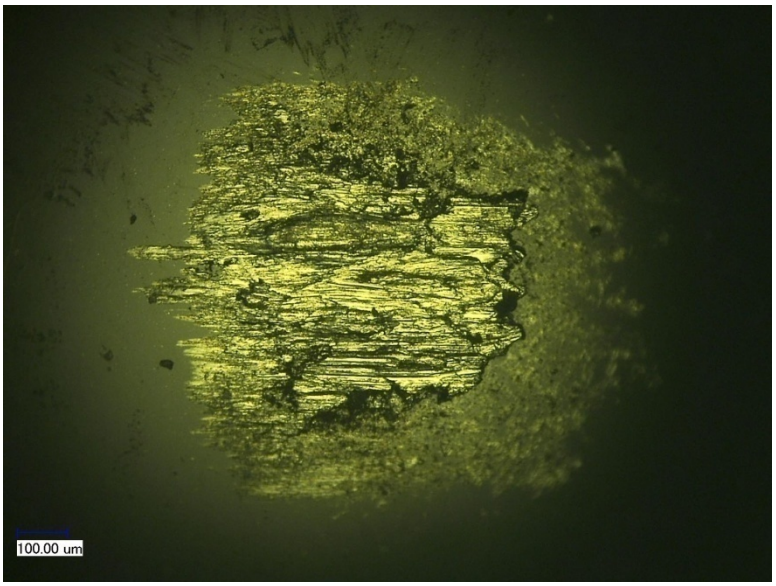


Figure 85: Pin 17 at 200 times magnification.

Disk 9 Inner

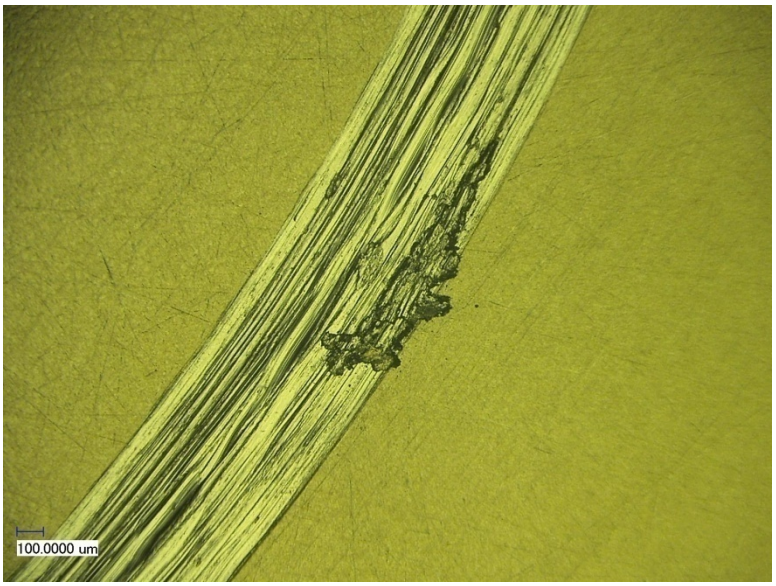


Figure 86: Disk 9 inner track, 10 N load at 100 times magnification typical surface with adhesion.

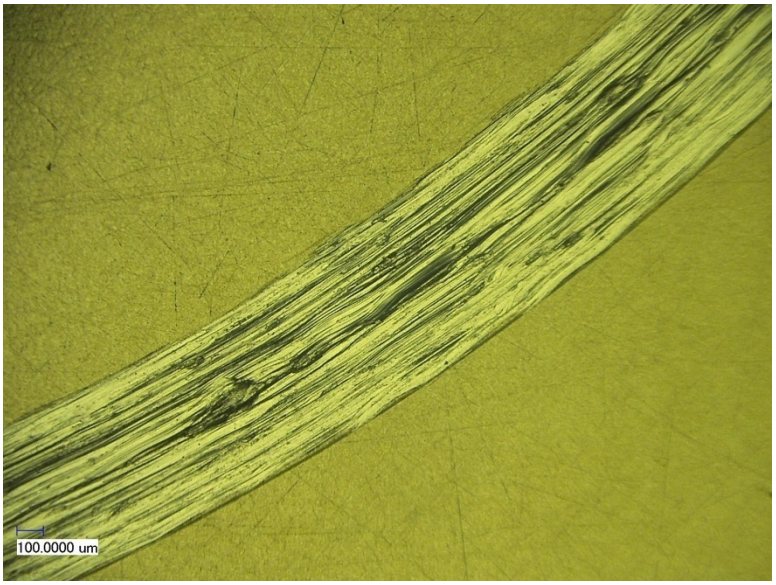


Figure 87: Disk 9 inner track, 10 N load at 100 times magnification typical wavy surface with adhesion.

Pin 15

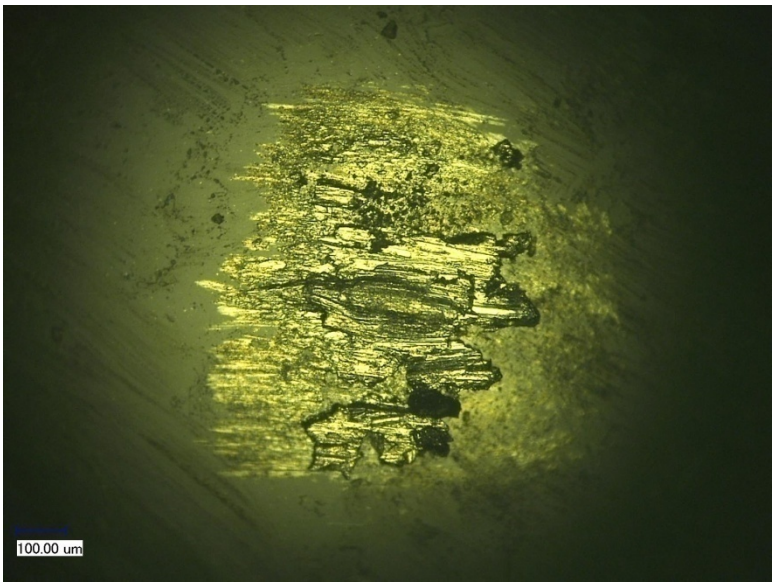


Figure 88: Pin 15 at 200 times magnification.

Disk 9 Outer

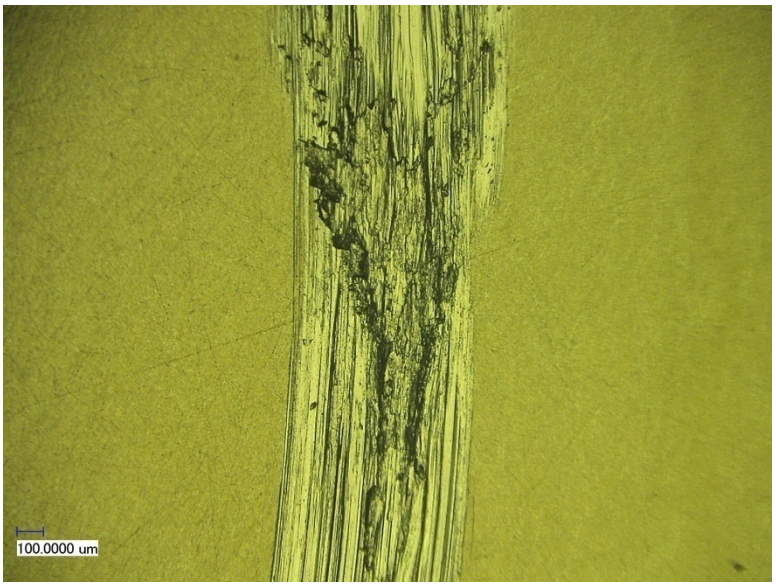


Figure 89: Disk 9 outer track, 20 N load at 100 times magnification with adhesion.

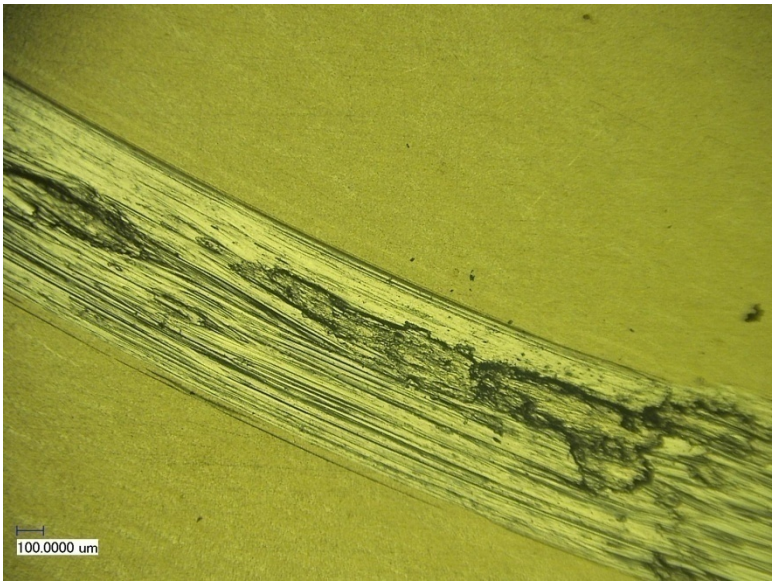


Figure 90: Disk 9 outer track, 20 N load at 100 times magnification typical surface with adhesion.

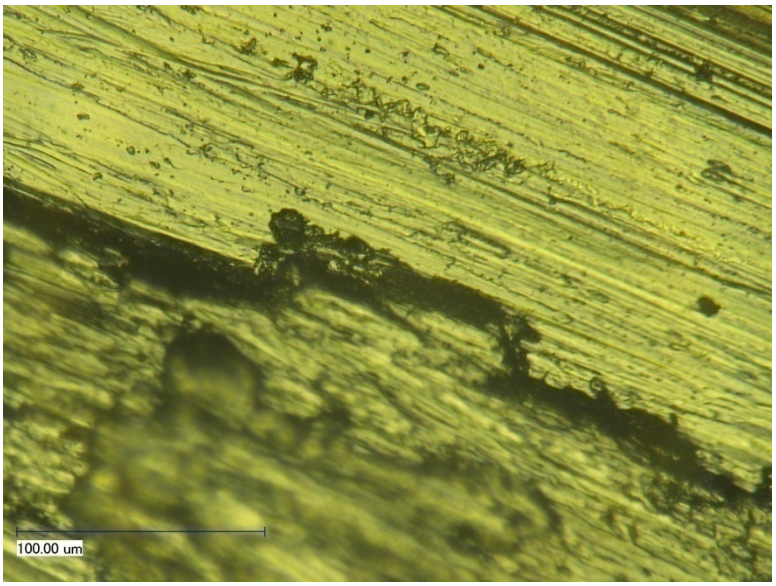


Figure 91: Disk 9 outer track, 20 N load at 1000 times magnification with adhesive area with cleaved edges.

Pin 18

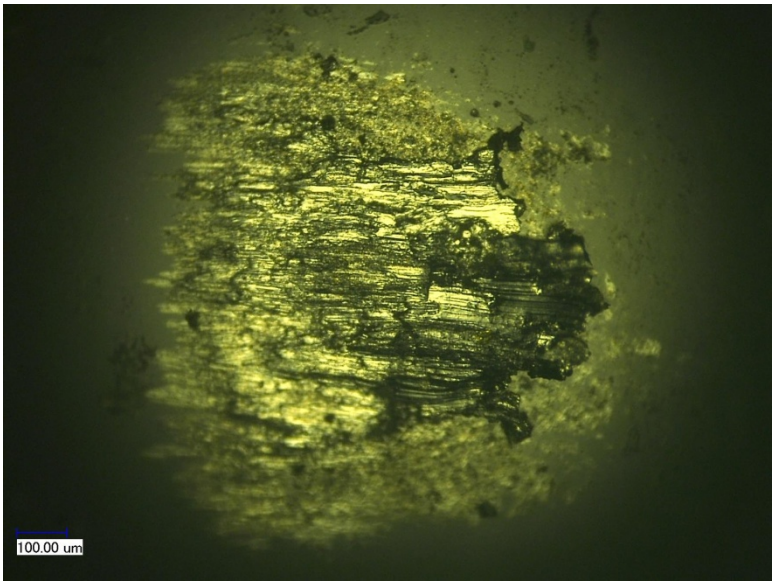


Figure 92: Pin 18 at 200 times magnification.

## Group 4 – Low Temperature, Exposed, Disks 10-12

Disk 10 Inner

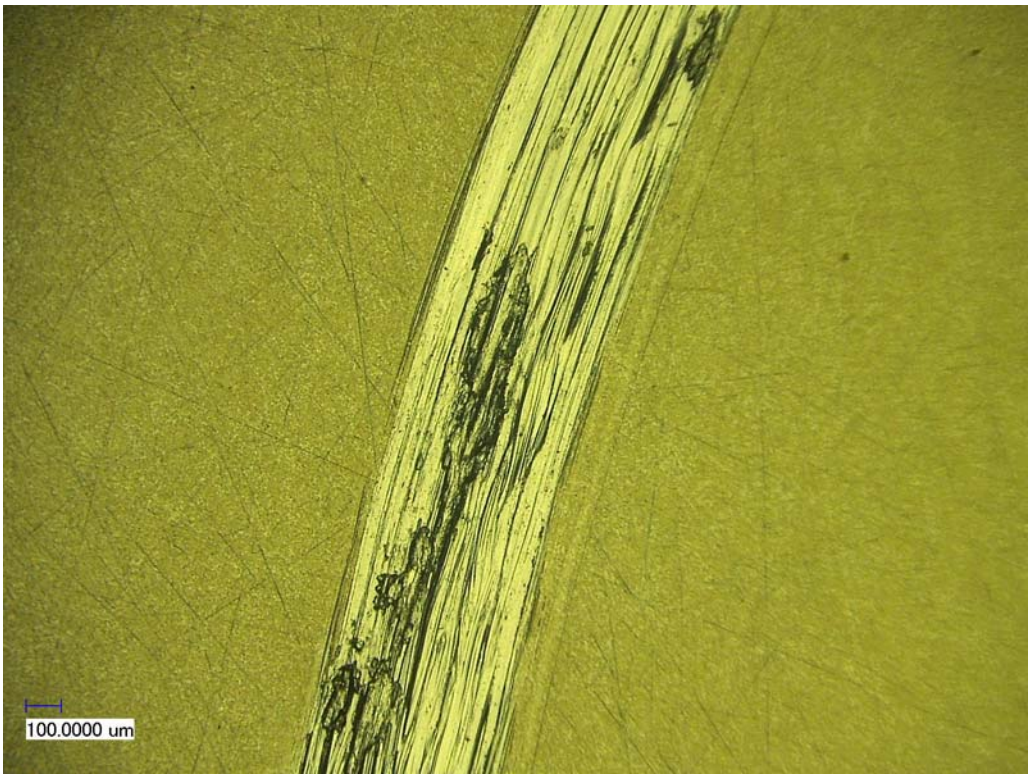


Figure 93: Disk 10 inner track, 10 N load at 100 times magnification with adhesion.

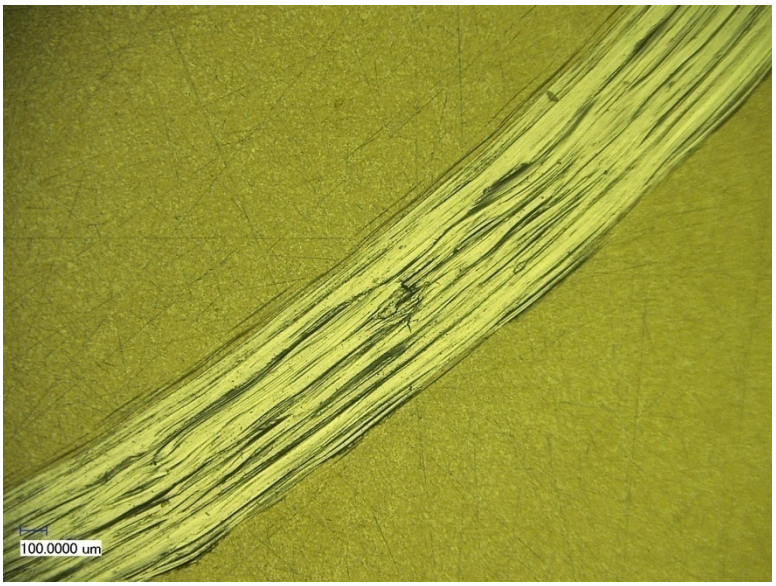


Figure 94: Disk 10 inner track, 10 N load at 100 times magnification typical surface.

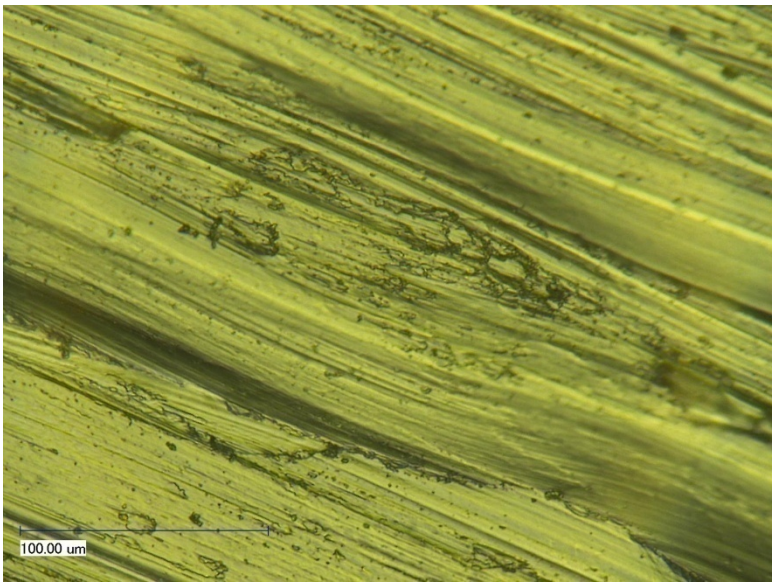


Figure 95: Disk 10 inner track, 10 N load at 1000 times magnification with wavy surface.

Pin 19

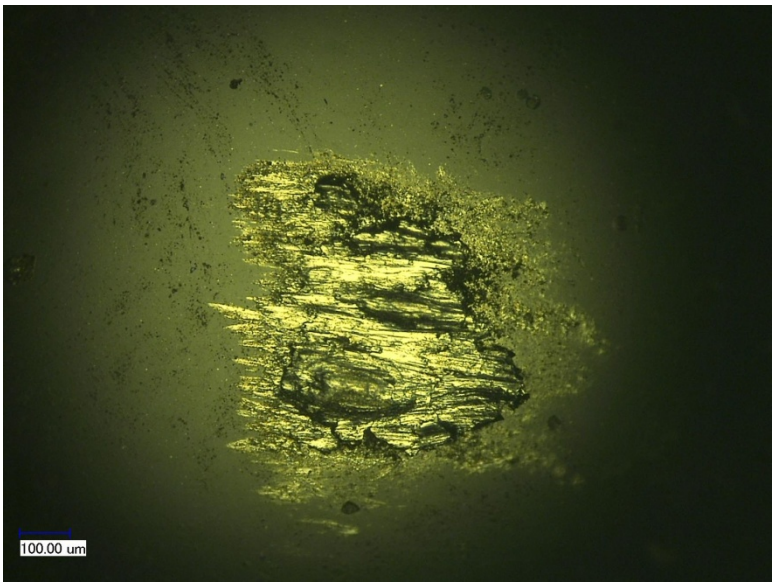


Figure 96: Pin 19 at 200 times magnification.

Disk 10 Outer

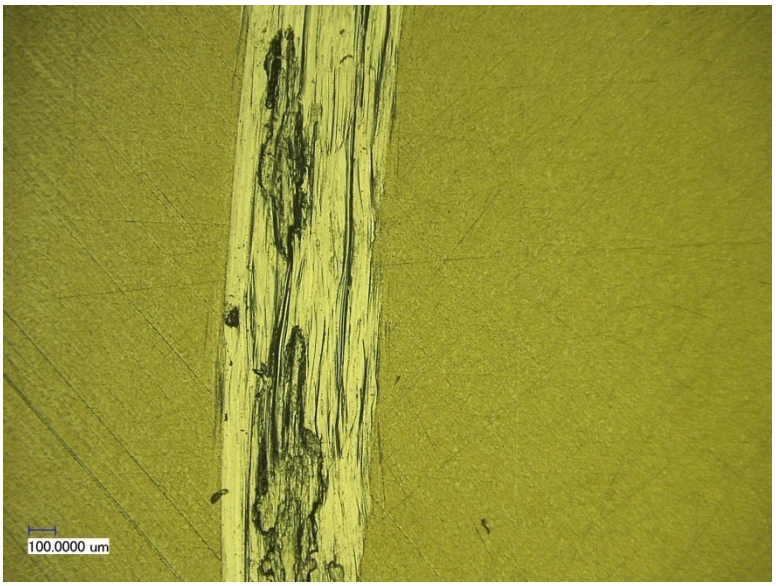


Figure 97: Disk 10 outer track, 20 N load at 100 times magnification with adhesion.

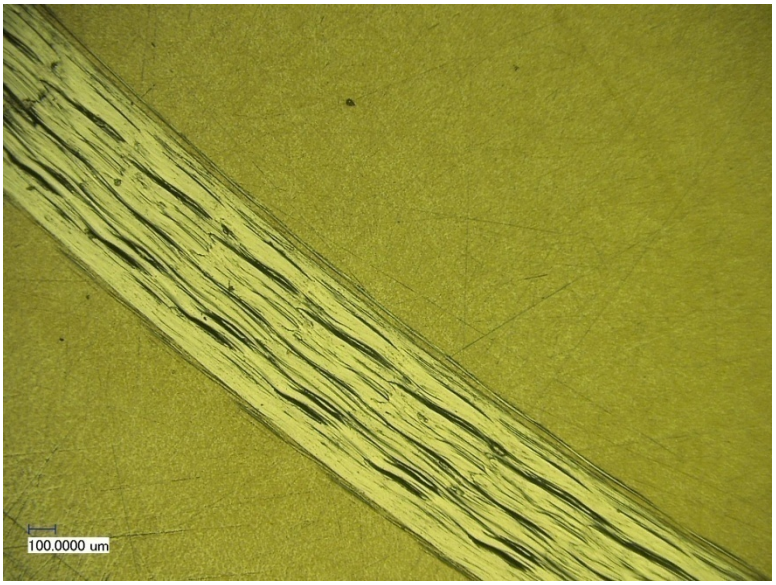


Figure 98: Disk 10 outer track, 20 N at 100 times magnification load wavy surface

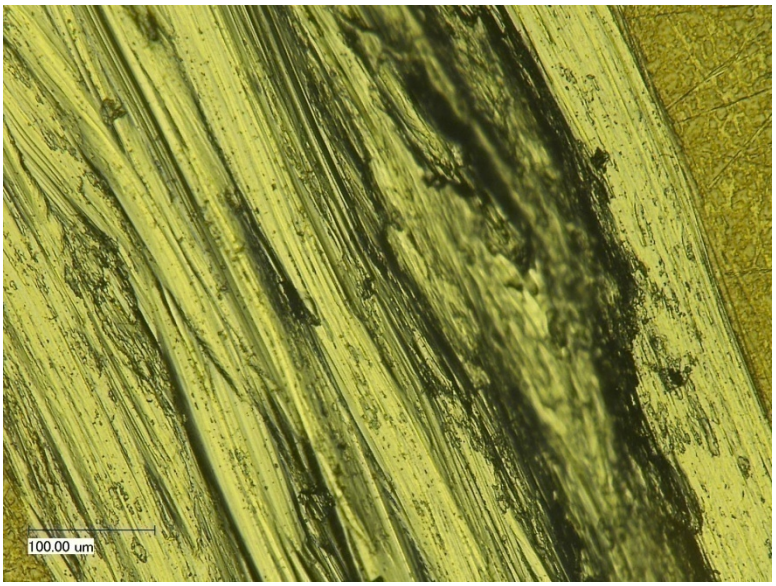


Figure 99: Disk 10 outer track, 20 N load at 500 times magnification with adhesion.

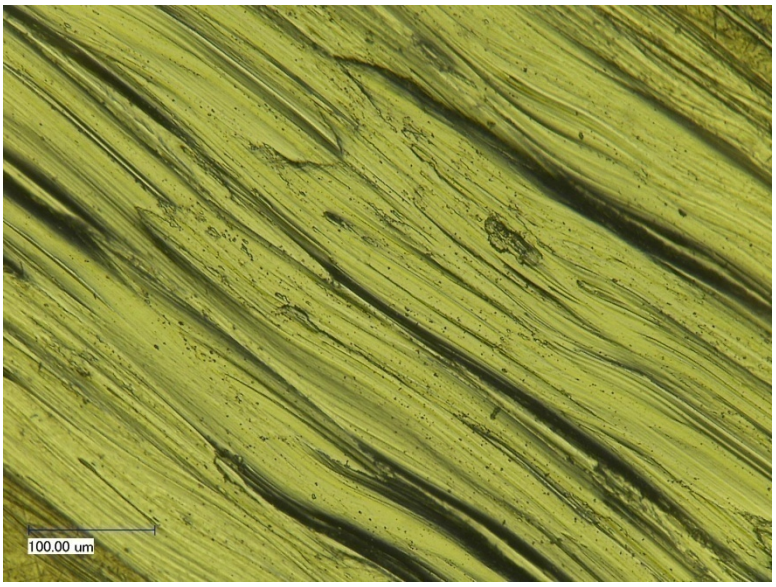


Figure 100: Disk 10 outer track, 20 N load at 500 times magnification with wavy surface.

Pin 22

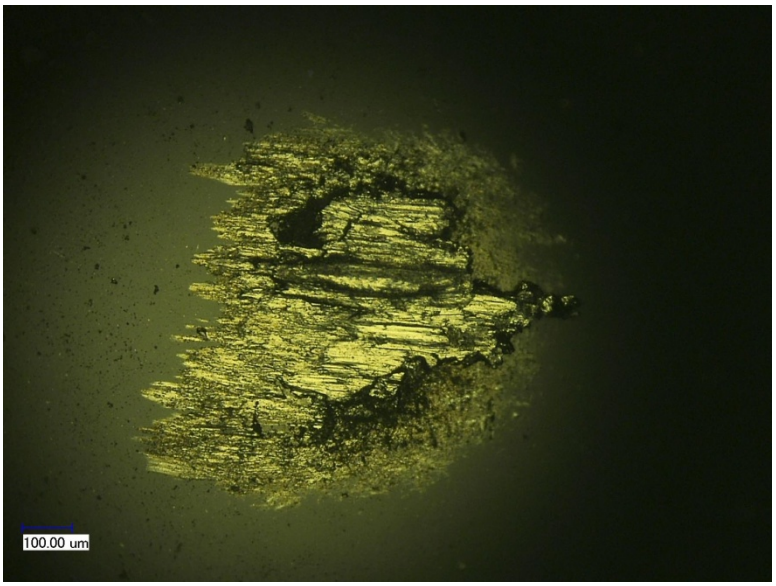


Figure 101: Pin 22 at 200 times magnification.

Disk 11 Inner

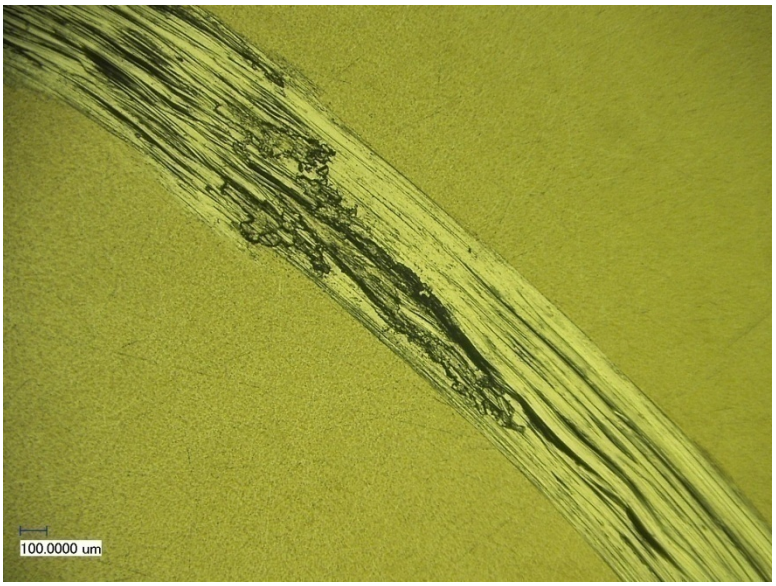


Figure 102: Disk 11 inner track, 10 N load at 100 times magnification with adhesion.

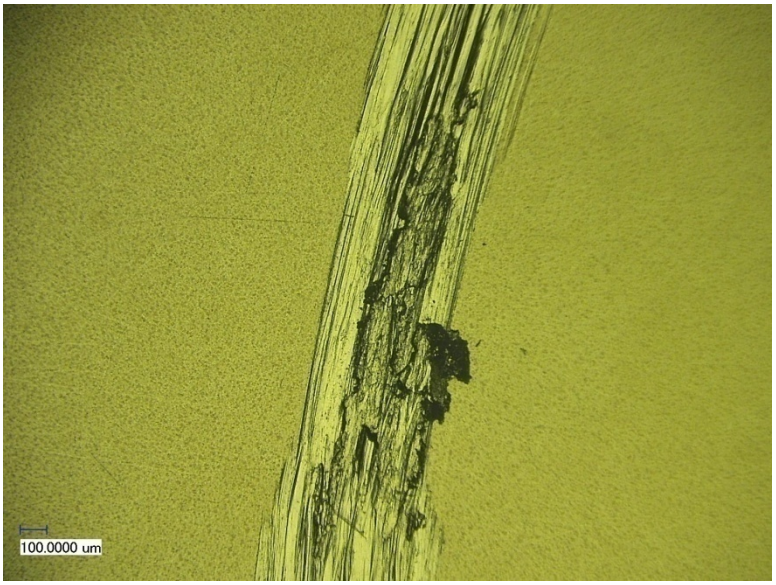


Figure 103: Disk 11 inner track, 10 N load at 100 times magnification with adhesive areas.

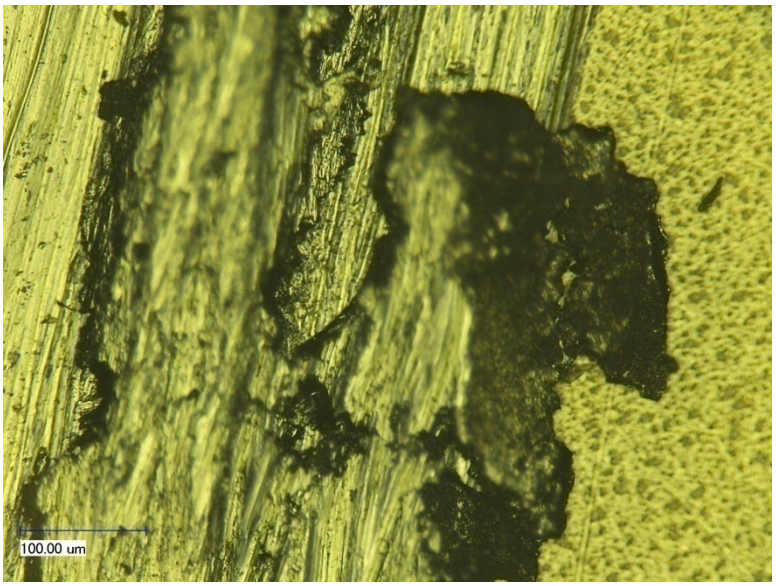


Figure 104: Disk 11 inner track, 10 N load at 500 times magnification with adhesive area.

Pin 20

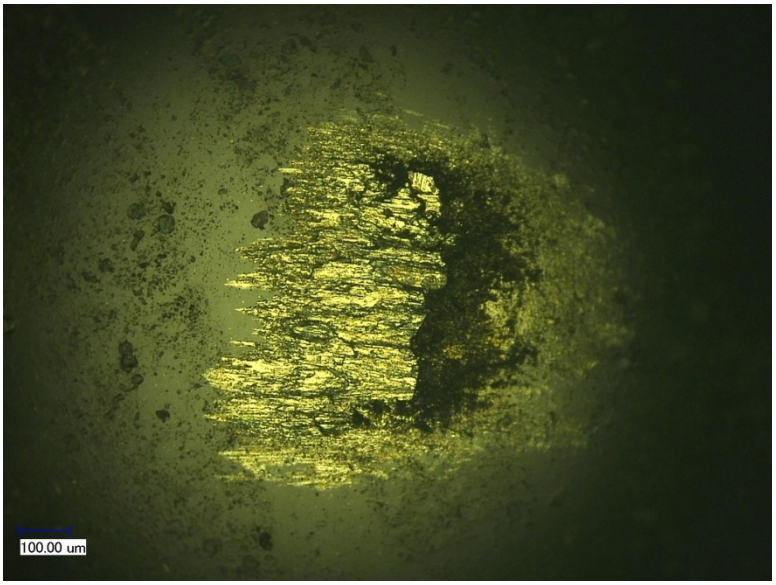


Figure 105: Pin 20 at 200 times magnification.

Disk 11 Outer

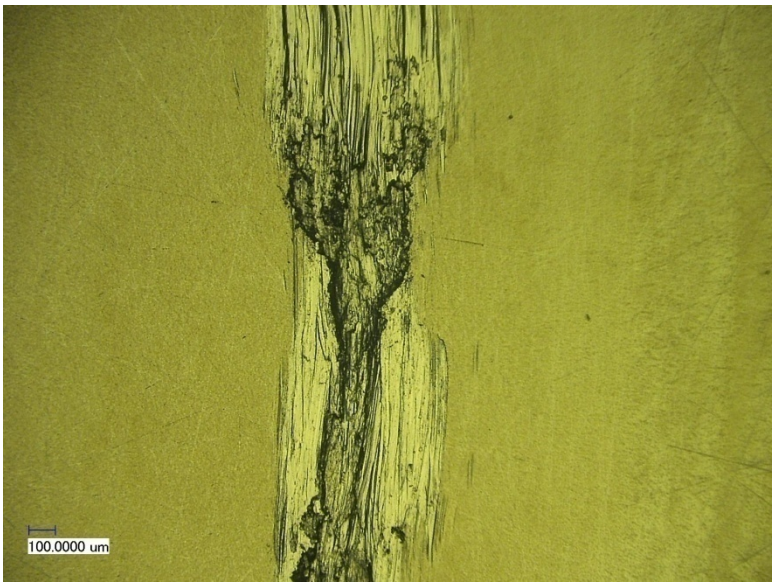


Figure 106: Disk 11 outer track, 20 N load at 100 times magnification with large adhesive area.

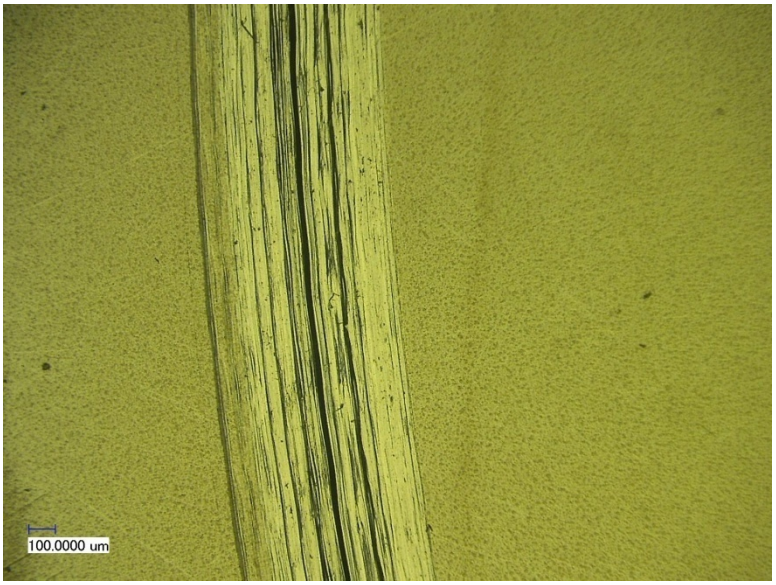


Figure 107: Disk 11 outer track, 20 N load at 100 times magnification typical wavy surface.

Pin 23

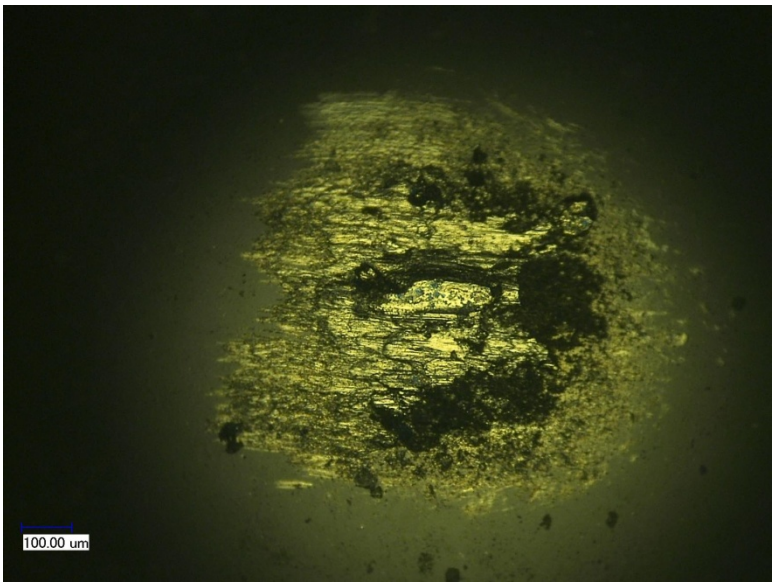


Figure 108: Pin 23 at 200 times magnification.

Disk 12 Inner

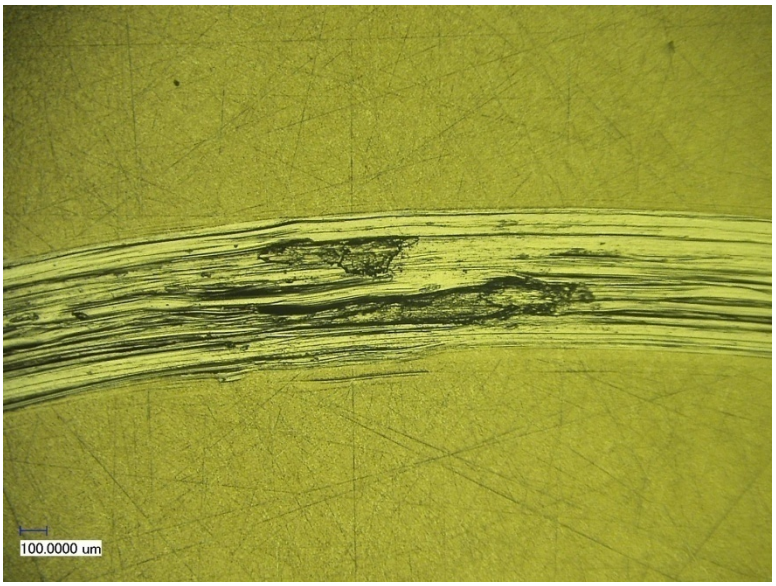


Figure 109: Disk 12 inner track, 10 N load at 100 times magnification with adhesion.

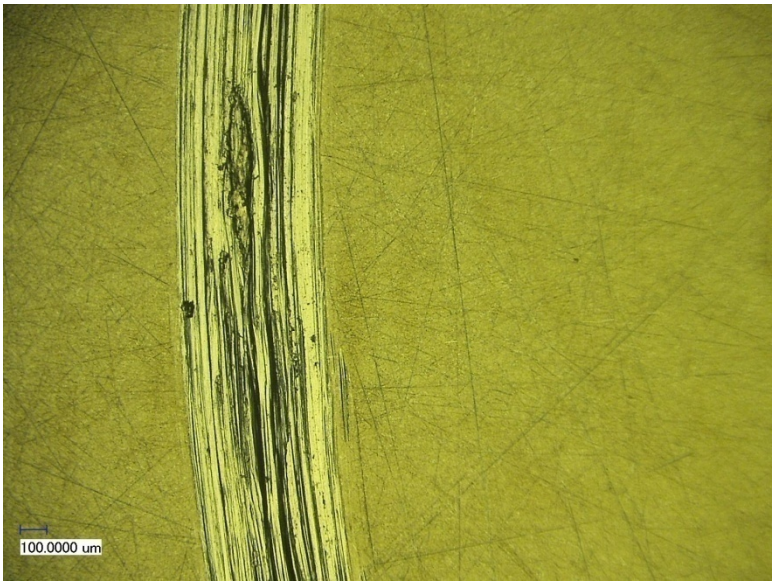


Figure 110: Disk 12 Inner track, 10 N load at 100 times magnification typical surface with adhesive areas.

Pin 21

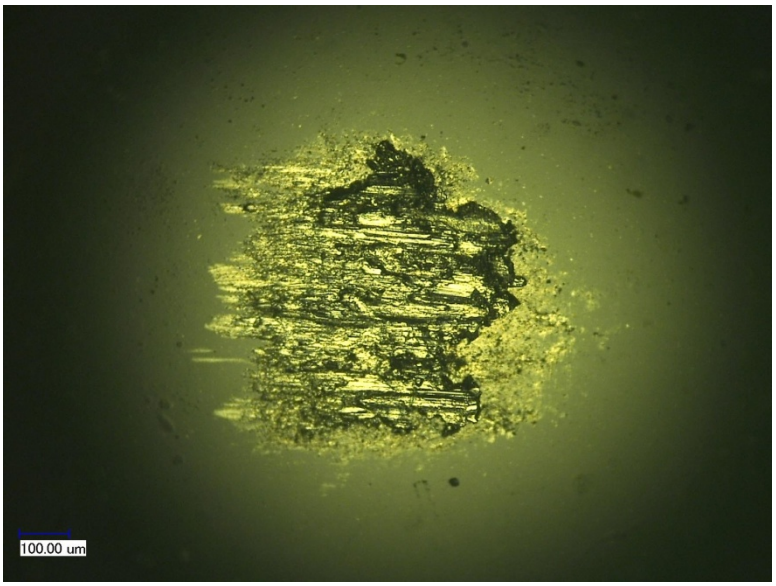


Figure 111: Pin 21 at 200 times magnification.

Disk 12 Outer

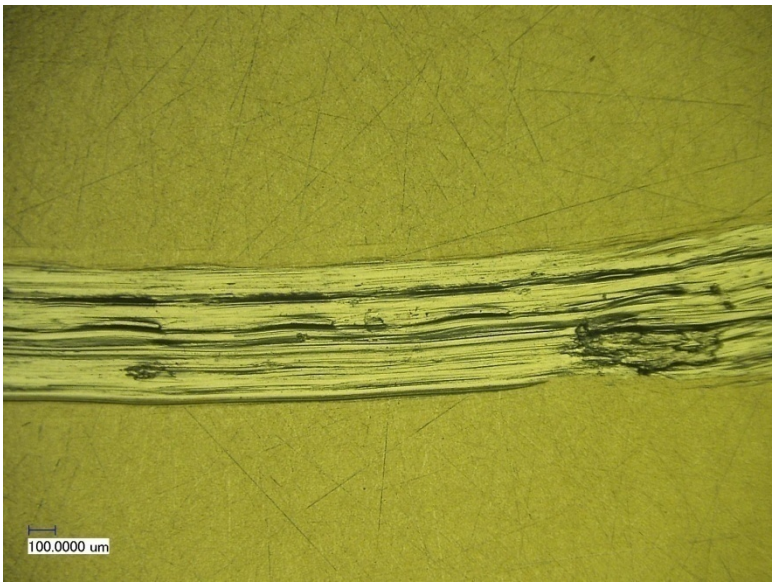


Figure 112: Disk 12 outer track, 20 N load at 100 times magnification wavy surface with adhesive area.

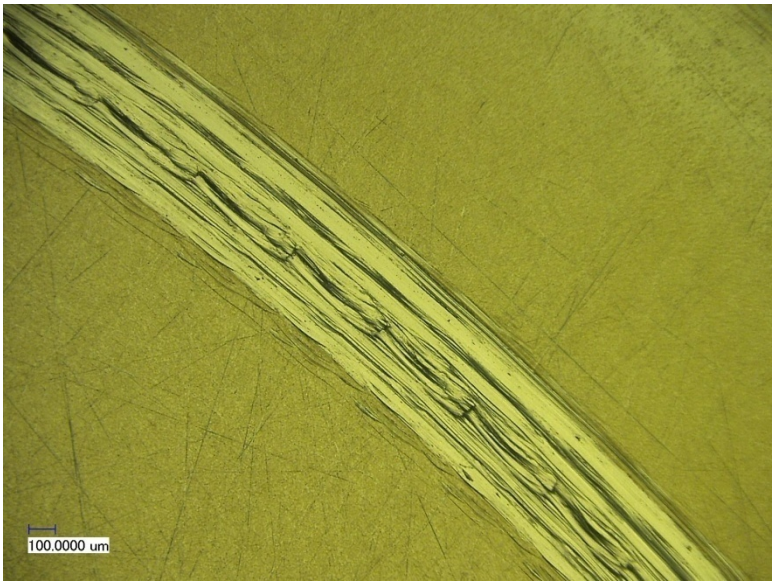


Figure 113: Disk 12 outer track, 20 N load at 100 times magnification wavy surface resembling stick slip.

Pin 24

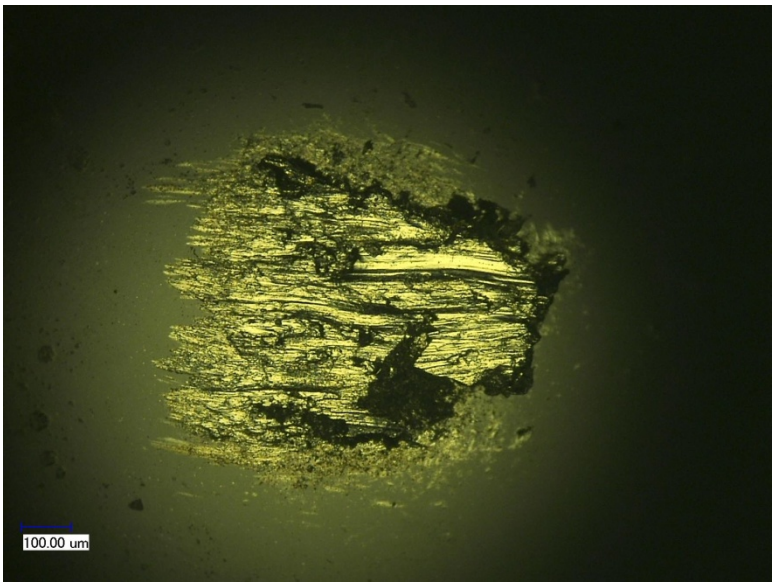


Figure 114: Pin 24 at 200 times magnification.

# VITA

Name: Ryan Travis Gola

Address: Department of Mechanical Engineering, Texas A&M University

College Station, Texas 77845. Mail stop: 3123

Email Address: ryangola@gmail.com

Education: B.S., Mechanical Engineering, Texas A&M University, 2004

M.S., Mechanical Engineering, Texas A&M University, 2008